

PALAEOPROTEROZOIC PROGRADE METASOMATIC-METAMORPHIC OVERPRINT ZONES IN ARCHAEOAN TONALITIC GNEISSES, EASTERN FINLAND

MATTI PAJUNEN and MATTI POUTIAINEN

PAJUNEN, M. and POUTIAINEN, M. 1999. Palaeoproterozoic prograde metasomatic-metamorphic overprint zones in Archaean tonalitic gneisses, eastern Finland. *Bulletin of the Geological Society of Finland* 71, Part 1, 73–132.

Several occurrences of coarse-grained kyanite rocks are exposed in the Archaean area of eastern Finland in zones trending predominantly northwest–southeast that crosscut all the Archaean structures and, locally, the Palaeoproterozoic metadiabase dykes, too. Their metamorphic history illustrates vividly Palaeoproterozoic reactivation of the Archaean craton.

The early-stage kyanite rocks were formed within the framework of ductile shearing or by penetrative metasomatism in zones of mobile brecciation. Static-state coarse-grained mineral growth during the ongoing fluid activity covered the early foliated fabrics, and metasomatic zoning developed. The early-stage metasomatism was characterized by Si, Ca and alkali leaching. The late-stage structures are dilatational semi-brittle faults and fractures with unstrained, coarse-grained fabrics often formed by metasomatic reactions displaying Mg enrichment along grain boundaries. Metamorphism proceeded from the low-T early-stage Chl-Ms-Qtz, Ky/And-St, eventually leading to the high-T late-stage Crd-Sil assemblages. The thermal peak, at 600–620°C/4–5 kbar, of the process is dated to 1852±2 Ma (U-Pb) on xenotime. Al-silicate growth successions in different locations record small variations in the Palaeoproterozoic clockwise P-T paths. Pressure decreased by c. 1 kbar between the early and late stage, i.e. some exhumation had occurred. Fluid composition also changed during the progression, from saline H₂O to CO₂ rich. Weak retrograde features of high-T phases indicate a rapid cooling stage and termination of fluid activity.

The early-stage Ky-St assemblages resemble those described from nearby Palaeoproterozoic metasediments in the Kainuu and North Karelia Schist Belts, where the metamorphic peak was achieved late with respect to Palaeoproterozoic structures. The static Ky-St metamorphism in kyanite rocks was generated by fluid-induced leaching processes at elevated T during the post-orogenic stage after collision of the Palaeoproterozoic island arc complex with the Archaean craton in Palaeoproterozoic and/or reactivated Neoarchaean zones of weakness. The distribution of late-stage Crd-Sil metasomatism-metamorphism indicates that the corresponding thermal event was widespread in the Nurmes–Sotkamo area. Isotopic studies on Archaean granitoids and greenstone belts also indicate such late heating. According to pressure determinations, the Archaean±Palaeoproterozoic crust has been uplifted and exhumed about 15–20 km since 1850 Ma. Contemporaneous magmatic activation occurred in the North Karelia Schist Belt, too. The seismic deep structure of the crust, particularly the thick high-velocity layer in the lower crust, postulates some kind of disturbance in the lower crust

and lithospheric mantle. The dilatational late-stage heat flow, CO₂-rich fluidization and Mg metasomatism, and exhumation are connected with this disturbance. It is suggested that they were related to magmatic underplating into the lower crust after the Svecofennian-Archaean collision.

Key words: Archean, Paleoproterozoic, tectonics, reactivation, overprint, metamorphism, metasomatism, P-T path, mineral reaction, fluids, fluid inclusions, kyanite, cordierite, xenotime, U/Pb age, eastern Finland

Matti Pajunen: Geological Survey of Finland, P.O. Box 96, FIN-02151 Espoo, Finland.

E-mail: matti.pajunen@gsf.fi

Matti Poutiainen: Department of Geology, P.O. Box 11, FIN-00014 University of Helsinki, Finland.

E-mail: matti.poutiainen@helsinki.fi

INTRODUCTION

The Meso- to Neoarchaeon craton of eastern Finland, the western part of the large Archaean domain of the Fennoscandian Shield, consists of tonalitic-trondhjemitic-granodioritic migmatites and granitoids (TTG) and Neoarchaeon greenstone and paragneiss belts (Simonen 1980, Kontinen 1991, Luukkonen 1992). It is bordered by the Palaeoproterozoic Svecofennian Domain along a suture zone in the southwest (Koistinen 1981). The southwestern margin of the craton is partly covered by overthrust allochthonous and autochthonous Palaeoproterozoic sequences (Koistinen 1981, Huhma 1986) (Fig. 1). A detailed structural analysis of the craton in the Kuhmo area and its evolutionary history were presented by Luukkonen (1992, see also references therein). The few metamorphic studies conducted show that amphibolite- and, locally, granulite-facies conditions were achieved in the TTG areas and greenschist- to amphibolite-facies conditions in the greenstone belts. Widespread low-grade retrogression characterizes both associations (Taipale 1982, Paavola 1984, Tuisku & Sivonen 1984, Hölttä & Paavola 1989, Blais & Auvray 1990, Gruau et al. 1992).

The Palaeoproterozoic overprint on the Archaean craton has aroused increasing interest in recent years. The Palaeoproterozoic extensional rifting stages are recorded by several mafic magma pulses between 2.44 and 1.97 Ga ago (Aro & Laitakari 1987, Alapieti & Lahtinen 1989, Vuollo 1994).

About 1.9–1.875 Ga ago the Svecofennian island arc complex collided with the passive Archaean craton margin (Vaasjoki & Sakko 1988). The effects of this collision, seen in the nappes and overthrusts northeast of the suture zone, were discussed first by Wegmann (1928) and Väyrynen (1939). Park and Bowes (1983) and Park (1988) studied the basement-cover relations during Palaeoproterozoic polyphase deformation in the contact area of the North Karelia Schist Belt and the Archaean craton, noting the sliced structure of the Archaean basement owing to Palaeoproterozoic tectonism but preservation of Archaean structures further away from the thrust zones. Recent studies have confirmed that the Svecofennian orogeny gave rise to the formation of a block structure in the Archaean area, too (e.g. Kohonen et al. 1991, Kohonen 1995). Jegouzo and Blais (1993) observed that a continuation of some Palaeoproterozoic structures of the Kainuu Schist Belt overprints the Archaean basement in the Sotkamo area, and that Palaeoproterozoic diabase dykes are overprinted by metamorphic schistosity near the Kuhmo Greenstone Belt. The steeply foliated Palaeoproterozoic sequences within the Archaean in central Russian Karelia, east of the Finnish border, demonstrate the considerable extent of the Palaeoproterozoic reconstructive structures in the eastern Archaean area (see Ward 1993). To the west, however, only a weak Palaeoproterozoic deformation in the Lentiira and Ilomantsi areas has been described (Luukkonen 1985, 1988, 1989a, Ward

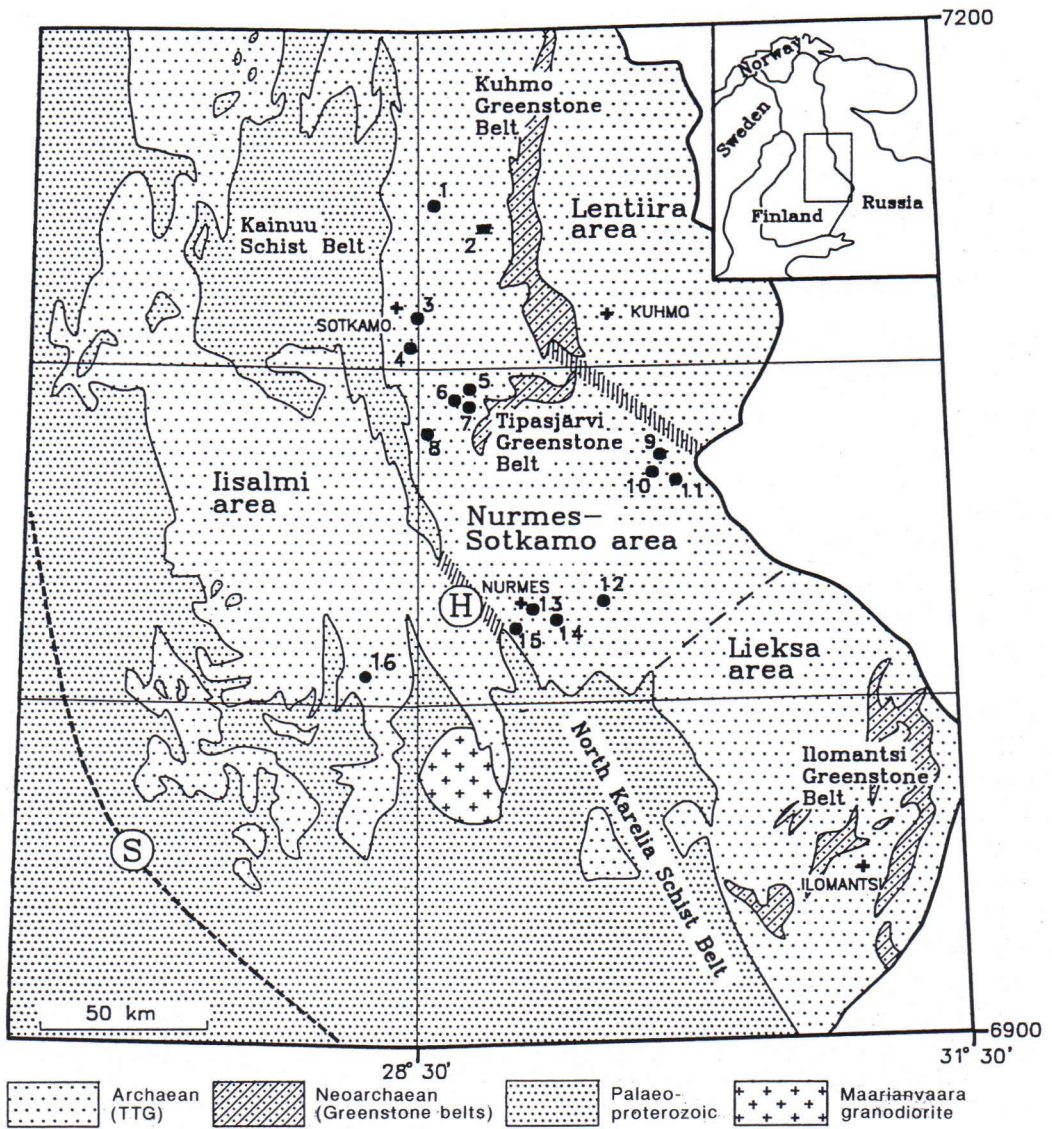


Fig. 1. Kyanite rock occurrences (black dots = exposed; boulder = local boulders) in eastern Finland: 1 = Tuomaanvaara, 2 = Turkkivaara, 3 = Kallioniemi, 4 = Varisniemi, 5 = Korpilampi, 6 = Kauhealampi, 7 = Havukkalammit and east Havukkalammit, 8 = Matovaara, 9 = Levävaara, 10 = Hiltuspuro, 11 = Teljo, 12 = Egyptinkorpi, 13 = Lehtovaara (not studied), 14 = Tetrilampi, 15 = Kynsiniemi (not studied), 16 = Nilsä (not studied). Hatched lines = tectonic boundaries: (H) = Nunnanlahti-Holinmäki Shear Zone and (S) = approximate location of the suture zone between Svecofennian island arc complex and Archaean complexes; thin dashed line = border between the Nurmes-Sotkamo and Lieksa areas, defined on basis of geophysical data.

1993). On the basis of geophysical data, Korja et al. (1993) suggested that the lower crust and Moho of the westernmost Archaean was also reformed during Palaeoproterozoic time.

Isotopic resetting is recorded in the K-Ar isotopic compositions of TTG biotite and hornblende, which show late heating to temperatures exceeding the biotite and hornblende K-Ar closure tem-

peratures, that is, about 300°C and 500°C, respectively, over a large area of the Archaean. Biotites were reset, on average, 1795±21 Ma ago and hornblendes 1851±41 Ma ago (Kontinen et al. 1992). O'Brien et al. (1993) determined K-Ar ages of 1811–1707 Ma on biotites in the Ilomantsi area, and attributed them to Palaeoproterozoic metamorphism; Karhu et al. (1993) made a similar suggestion on the basis of the large variation in the oxygen isotope composition of carbonates in that area. According to Gruau et al. (1992), the Nd and O isotopic and REE compositions of the southern Kuhmo Greenstone Belt komatiites were modified by regional metamorphism and CO₂ fluidization about 1.8 Ga ago. Medium-pressure kyanite-sillimanite metamorphism is widespread in the eastern Archaean terrain (Korsman 1982, Russian Academy of Science et al. 1993). Belyaev et al. (1993) and Petrov (1993) among others, attributed it to Palaeoproterozoic reactivation.

The main constraint on metamorphic studies in the Archaean area is the scarcity of appropriate mineral parageneses for conventional thermobarometric studies. In several locations, however, kyanite-bearing rocks have served as valuable indicators of metamorphic crystallization conditions. Here, we focus on the zones of spectacular, coarse-grained kyanite rocks that occur in the TTG environment. These rocks have a wide diversity of composition and fabric. Previous investigations concentrated on kyanite and U-Th prospecting, without much emphasis on the origin of these kyanite-bearing rocks (Rask 1979, Pekkala 1982, Äikäs 1989, Horneman & Hyvärinen 1987, 1989).

Our study is based on observations made at several kyanite rock sites – the term *kyanite rock* refers to the rock association in a general sense – in the Nurmes–Sotkamo area (Fig. 1). We describe kyanite rocks in detail and examine their tectonic-metamorphic evolution and genesis and their relation to the Palaeoproterozoic reactivation of the Archaean crust. Petrological study is supported by fluid inclusion data. The tectonic-metamorphic succession was dated with structural and isotopic methods.

This research is part of the “*Global Geoscience Transects*” project of the Geological Survey of

Finland. The fluid inclusion determinations, comprising microthermometry and studies of composition and morphology, were made by Matti Poutiainen. Matti Pajunen is responsible for all the rest including the interpretations presented here.

GEOLOGICAL OUTLINE

The Archaean craton of eastern Finland can be divided into the Iisalmi granitoid-migmatite area to the west of the Palaeoproterozoic Kainuu Schist Belt with its structural extension in the Nunnalahti–Holinmäki Shear Zone (Kohonen et al. 1991), and the eastern Archaean area. Eastwards the thickness of the crust decreases dramatically, from 56 to 46 km, in the vicinity of the Kuhmo Greenstone Belt (Yliniemi et al. 1993). This decline in crustal thickness is due to the thinning of the high-velocity layer of the lower crust east of the Kuhmo Greenstone Belt (Korja et al. 1993, Korja et al. 1994). The granitoid-migmatite area between the Kainuu Schist Belt and the Kuhmo Greenstone Belt is called the Nurmes–Sotkamo area and the area of thin crust to the east of the Kuhmo Greenstone Belt, the Lentiira area. The Lieksa area (Fig. 1) is defined on the basis of its characteristic magnetic and gravimetric pattern only.

There are several records of rocks over 3.0 Ga old (e.g. Paavola 1986, Kozhevnikov et al. 1987, Sorjonen-Ward & Claué-Long 1993) from the Archaean area of eastern Finland and Russian Karelia. According to structural observations of Luukkonen (1988, 1992), the oldest remnants of the Archaean crust in eastern Finland are the highly deformed amphibolites in trondhjemitic-tonalitic migmatites. The early mafic to intermediate crust was deformed by D₁ and D₂, and was subject to dynamothermal medium- to high-grade metamorphism about 2843±18 Ma ago (Luukkonen 1985).

Intracontinental rifting about 2.79–2.7 Ga ago produced ultramafic to felsic metavolcanics and volcanoclastic metasediments of the greenstone belts (Luukkonen 1992). Widespread paragneisses in the Nurmes–Sotkamo area have a calc-alkaline volcanic-plutonic provenance (Kontinen 1991).

The rocks of the early TTG crust and greenstones were tightly to isoclinally folded, overthrust, fragmented by D_3 and intruded by felsic D_3 magmas. Luukkonen (1992) connects the thermal event with magmatic underplating. Unlike the amphibolite or greenschist facies metamorphism present in most of the terrain, granulite facies Archaean metamorphism is restricted to sharply defined areas, e.g. in the Iisalmi (Paavola 1984, Hölttä & Paavola 1989) and Lieksa areas (Kontinen & Paavola 1996), and in Russian Karelia near the Finnish-Russian border (Kozhevnikov et al. 1987, Belyaev et al. 1991).

Late Neoarchaeon structures record cratonization of the crust. D_4 structures, northwest-southeast and conjugate northeast-southwest-trending faulting and folding, indicate diminishing ductility under retrograde conditions. Aplogranitic neosome in F_4 axial planes has been dated to 2657 ± 32 Ma. The latest Neoarchaeon D_5 and D_6 structures appear as open folds. Felsic intrusives in D_6 fractures have been dated to c. 2642–2575 Ma (Luukkonen 1985).

The 2.44-Ga mafic layered intrusions and dykes (Alapieti & Lahtinen 1989, Vuollo 1994) and 2.2–1.97-Ga diabase magmatism (Aro & Laitakari 1987, Vuollo 1994) imply tensional early Palaeoproterozoic conditions resulting in break-up of the Archaean “supercontinent” (see Lahtinen 1994). Most of the diabase dykes trend east-west and northwest-southeast (Luukkonen 1985, Aro & Laitakari 1987) and, according to Luukkonen (1985), were often intruded along reactivated Archaean zones of weakness. The Archaean structures are crosscut by anorogenic 2435 ± 12 Ma (Luukkonen 1989b) to 2352 ± 25 Ma (Horneman 1990) old granites. These earliest Palaeoproterozoic processes were followed by collision of the Svecofennian domain with the Archaean craton from the south and southwest (Koistinen 1981). The collisional and post-collisional events were outlined in section “Introduction”

KYANITE ROCKS

The majority of the known kyanite rock occur-

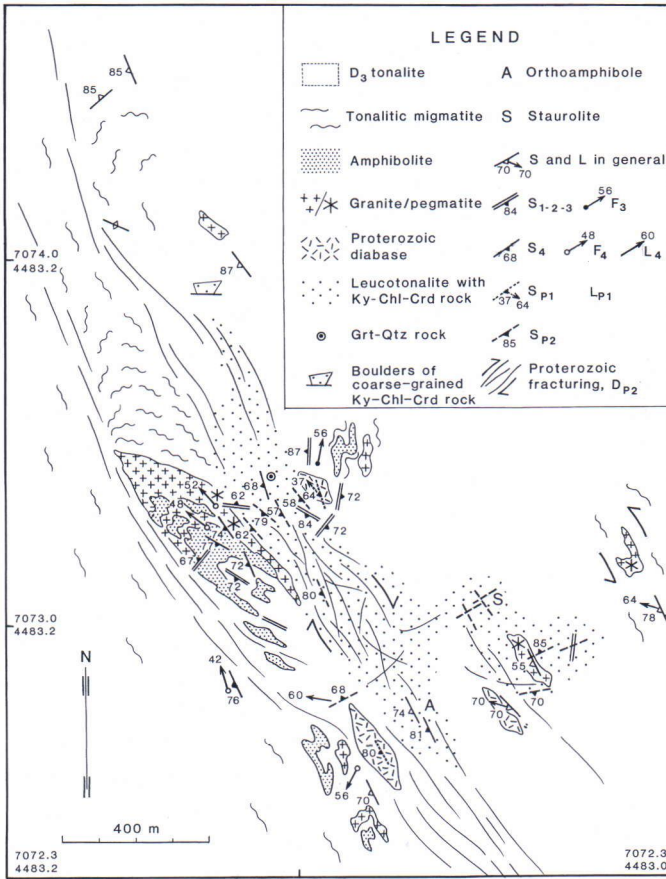
rences in the eastern Archaean area are in the Nurmes–Sotkamo area (Fig. 1). Similar rocks are exposed in a zone trending north–south through Nilsä in the Iisalmi area. Despite detailed geological mapping north of Kuhmo, no corresponding occurrences have been found there; nor have such rocks been encountered in the Lieksa area. At most of the sites studied, the contact between the kyanite rock and its host is well exposed. The structures and mineral growth history are particularly well exposed at Hiltuspuro, Nurmes, which is why this site was chosen for detailed study.

Hiltuspuro

Country rocks

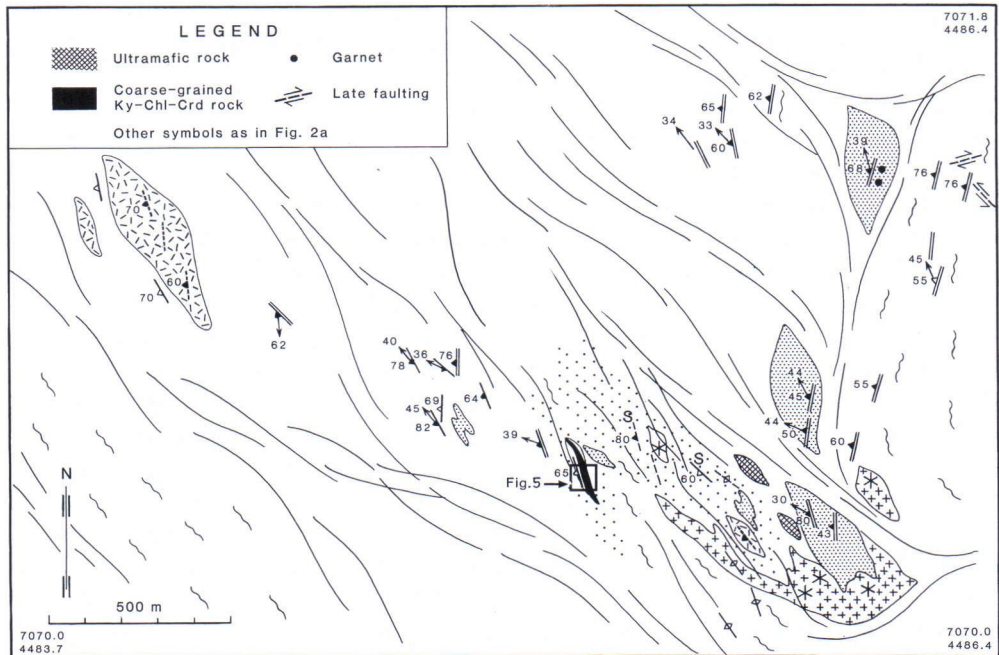
At Hiltuspuro the kyanite rock is exposed in a 4×0.5 km² area associated with a lineament trending northwest–southeast on the low-altitude aeromagnetic map and a long valley on the topographic map. The country rocks are tonalites and tonalitic migmatites with amphibolitic and mica gneissic remnants (Figs. 2a and b). Amphibolite has a regional metamorphic assemblage of Pl-Hbl±Qtz±Grt (mineral abbreviations in Appendix 1); only tiny garnets are found in the Hiltuspuro area. Structurally, the tonalites are comparable to the D_3 granitoids of Luukkonen (1992); they are homogeneous and medium grained with a metamorphic microstructure and the mineral assemblage, Pl-Qtz-Bt±Hbl±Ksf (Appendix 2). Medium-grained and pegmatitic potassic granite dykes crosscut the other rock types. Small retrograde and sheared ultramafic bodies occur in the southeastern part of the area. In northwest Hiltuspuro a coarse-grained garnet-quartz rock is associated with a kyanite rock. The rotated internal structure of some garnet grains suggests growth under simple shear conditions. A few small garnets are partly altered to chlorite and rimmed by a younger-generation garnet.

Diabase dykes up to 100×500 m² in size (see Fig. 2b), similar to the dated Palaeoproterozoic dykes, are weakly to moderately foliated. The mineral lineation is well developed in narrow dykes although, a blasto-ophitic microstructure is



a

Fig. 2. Lithology and tectonic features in the Hiltuspuro area: a) northwest Hiltuspuro, b) southeast Hiltuspuro.



b

often still visible. The primary mineral assemblage has completely recrystallized as an amphibolite facies assemblage, Hbl-Pl-Ilm/Mag. Epidotization and biotitization are distinct in some strongly foliated dykes.

Deformation

The earliest Archaean structure identified at Hiltuspuro (Figs. 2a and b) is a penetrative S_{1-2} mineral foliation in amphibolitic remnants that has been folded by tight to isoclinal F_3 plunging moderately northwards. The composite foliation is often the only detectable structure in amphibolites. In tonalites the penetrative mineral foliation is northerly to northeasterly S_3 . This foliation has been zonally reoriented by open to tight F_4 folds plunging moderately northwestwards or, rarely, to southeast. Weak S_4 dips steeply or moderately to southwest. The sheared limbs of F_4 folds are characterized by pegmatitic granite and biotitization of amphibolite. These structures broadly correspond to those described by Luukkonen (1988) from further north.

The observed contacts of the Palaeoproterozoic metadiabase dykes trend northwest-southeast and are sheared. Lineation L_{P1} ($P1$ = Palaeoproterozoic structure in metadiabase) plunges moderately northwestwards, and mineral foliation S_{P1} is subvertical, dipping steeply southwestwards. Thus, there is no marked difference between the trends of the regional Neoproterozoic D_4 (see Luukkonen 1988) and D_{P1} . In fact, exact identification of the Neoproterozoic D_4 and the Palaeoproterozoic D_{P1} in the tonalitic country rocks is difficult except near the dyke contacts, where S_{P1} may occasionally be traced to the country rock.

The penetrative Neoproterozoic structures of tonalites are crosscut by breccia, fault and fracture zones. The breccia zones consist of a coarse-grained, strongly recrystallized rock with indistinct mica foliation shown by later static mineral overgrowth. The breccia zones have weakly sheared, gradual or even "intrusive" replacement contacts (see a corresponding structure in Fig. 12 from Levävaara) with tonalite. Tonalitic fragments are corroded and assimilated by coarse-grained brec-

cia matrix. Weak northwest-southeast crenulation deforms the zones. The surroundings of the breccia zones are characterized by semi-brittle, curved fractures and faults, up to 10 cm wide, that penetrate the Neoproterozoic structures from northwest to southeast and locally from northeast to southwest and north to south. This structure dips steeply or moderately to southwest. A predominantly dextral strike slip component is evident in the northwest-southeast-trending faults, but the existence of an opposite displacement, too, makes interpretation of the sense of displacement difficult, as good vertical sections for displacement observations are rare. Indeed, the shear sense can be seen only along the contact zones; their interior, however, is characterized by unoriented, static mineral growth, as in the coarse-grained zones described above.

The orientation of the semi-brittle structure is close to that of the regional Neoproterozoic D_4 . However, D_4 is compressional/transcompressional folding and ductile in character, whereas the semi-brittle zones typically show dilatational features such as filled fractures. The semi-brittle zones crosscut the syn- D_4 pegmatitic granite dykes and the Palaeoproterozoic metadiabase dykes, in which the metamorphic assemblage, Hbl-Pl-Ilm/Mag, has altered to Hbl-Ep-Ab-Qtz. Accordingly, the semi-brittle deformation is younger than the Palaeoproterozoic D_{P1} , and is named here D_{P2} (= deformation later than D_{P1}).

Kyanite rock

In the late breccia and semi-brittle D_{P2} zones, the Archaean tonalites have altered to heterogeneous kyanite rocks. The changes in mineral composition involve differential mobility of the primary rock-forming components and a metasomatic alteration process (cf. Korzhinskii 1970). Close to the kyanite rock the primary mineral assemblage of tonalite has altered to Pl-Qtz-Chl-Bt-Rt through decomposition of biotite to chlorite and rutile. Hornblende, K-feldspar and sphene are absent. Thus, the tonalite is leucotonalitic in appearance and is characterized by narrow fractures filled with chlorite and quartz and by irregular chlorite-rich patches. Plagioclase is often coarser within chlo-



Fig. 3. Coarse-grained kyanite-chlorite-cordierite rock at Hiltuspuro. Gradual metasomatic zoning is expressed by kyanite- (centre), plagioclase- and chlorite-biotite-rich (left) portions. The photograph is from the outcrop shown in Fig. 2b and sketched in Fig. 5. Photo by M. Pajunen.



Fig. 4. Kyanite-cordierite association in semi-brittle dilatational fractures, D_{P2} , in tonalite at Hiltuspuro. Biotite aggregates form spots, and tonalite is enriched in felsic components in vicinity of fractures. Photo by M. Pajunen.

ritized portions of the rock than in unaltered tonalite.

The altered rocks are either (1) coarse-grained kyanite-chlorite-cordierite rocks in breccia zones (Fig. 3), (2) kyanite-cordierite rocks in semi-brittle fracture/fault zones (Fig. 4) or (3) irregular cordierite-rich patches replacing the tonalite without distinct deformation on outcrop scale.

(1) The ultimate metasomatism of tonalite is expressed by a coarse-grained kyanite-chlorite-cordierite rock that crops out in southeast Hiltuspuro (Fig. 2b). A boulder, a few cubic metres in size, in northwest Hiltuspuro (Fig. 2a) implies more extensive distribution of this

penetrative process. The chlorite- and biotite-rich groundmass of the rock is overgrown by unoriented kyanite laths (average 5.5–6.5% kyanite in some outcrops, Rask 1979), up to 15–20 cm long, scattered grains of staurolite, 1 cm across, fresh, blue cordierite and scarce fibrous sillimanite. This quartz-free rock shows coarse, irregular metasomatic zoning (Fig. 5).

A coarse-grained, entirely recrystallized chlorite-staurolite-plagioclase rock with staurolite porphyroblasts, 1–3 cm across, in southeast Hiltuspuro replaces the tonalite with irregular contacts. It is similar to the kyanite-chlorite-cordierite rock in appearance, and con-

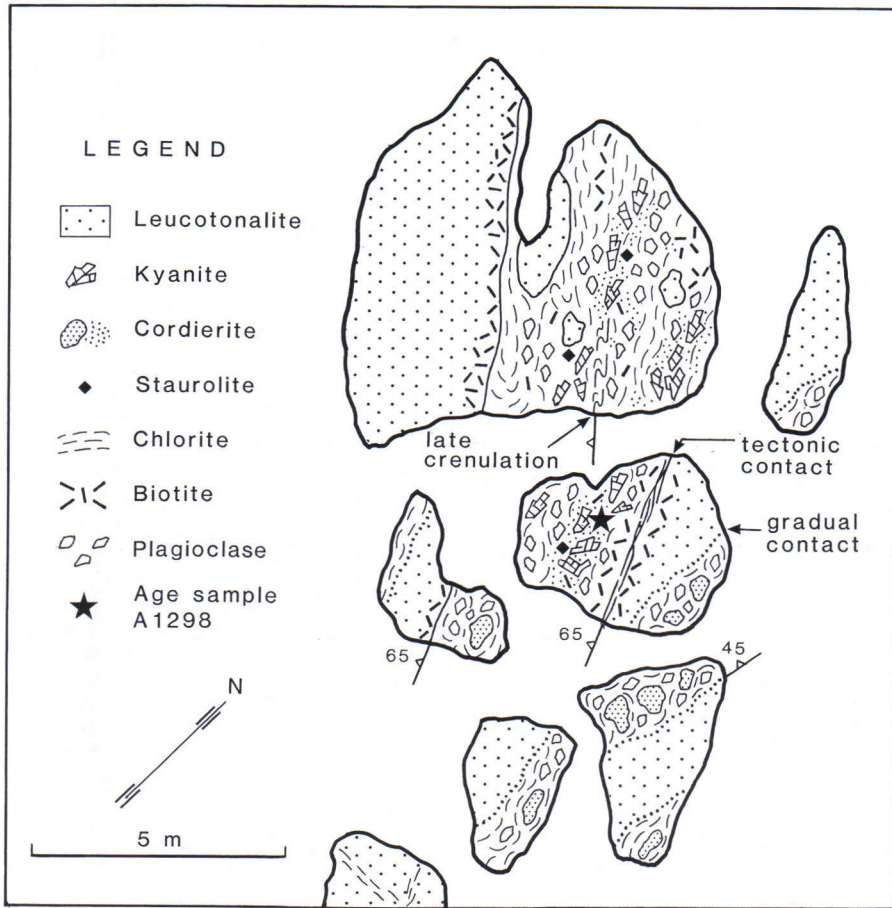


Fig. 5. Field sketch of coarse-grained kyanite-chlorite-cordierite rock with metasomatic zoning at Hiltuspuro. Location of outcrop shown in Fig. 2b.

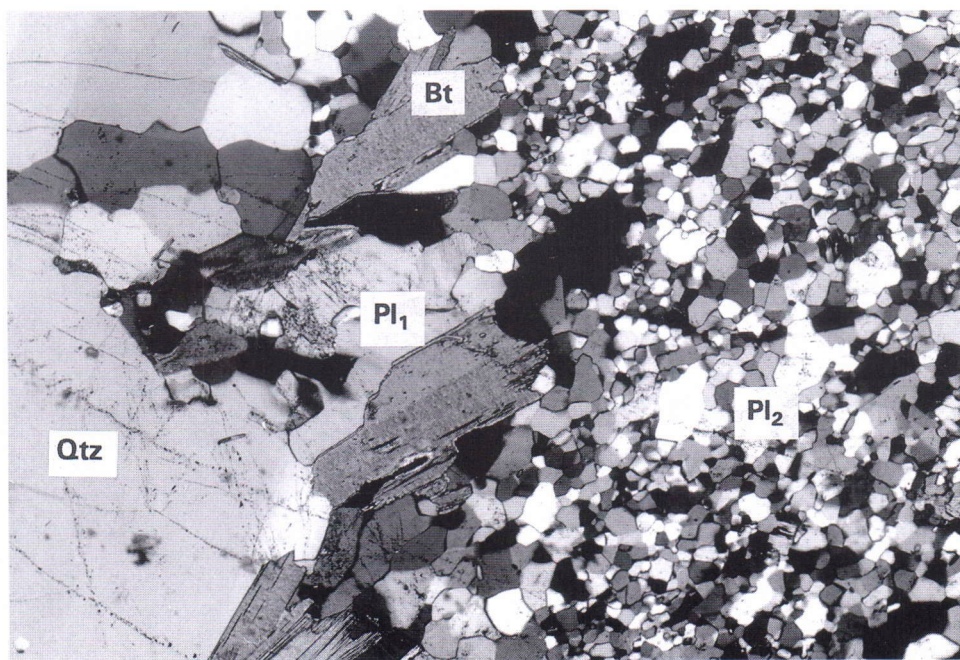


Fig. 6. Annealed plagioclase, Pl_2 , and quartz showing crystallization in unstrained state in semi-brittle fracture (to the right) at Hiltuspuro. Bt and Pl_1 represent relics of "primary" minerals in tonalite. Field of view c. 4 mm wide. Crossed nicols. Photo by M. Pajunen.

tains irregular staurolite-, chlorite- and plagioclase-rich portions.

- (2) The Archaean foliation in tonalite was reoriented by D_{P2} close to the semi-brittle kyanite-cordierite rock zones. Plagioclase recrystallized and biotite accumulated into spots. In the margin of the zone, the plagioclase and quartz are smaller and poorly annealed (Fig. 6). In the central part of the zones, metasomatic neomineralization took place under static conditions as evidenced by the undeformed fabric. Random grains of kyanite 1–5 cm in diameter, and of staurolite, up to 0.5 cm in diameter, are surrounded by cordierite and fine-grained sillimanite. Chlorite is a minor phase in these zones.
- (3) Cordierite-rich patches, 5–30 cm in diameter, and irregular zones, up to 2–3 m wide, replace the tonalite without a clear link to deformation on outcrop scale. In places, however, the zones follow the direction of the earlier foliation – Neoarchaean S_4 or Palaeoproterozoic

D_{P1} . Under the microscope the overall replacement of the previous phases by cordierite±sillimanite and quartz is pronounced, and the early phases are preserved only as small relics in large cordierite porphyroblasts (Fig. 7). In northwest Hiltuspuro, fibrous, radial orthoamphibole aggregates, a few millimetres in diameter, occur in cordierite. Coarse-grained biotite and chlorite form large aggregations, especially within cordierite-rich rocks.

The succession of mineral growth is remarkably systematic in the altered rocks. The metamorphic-metasomatic textures are described in greater detail in section "Metasomatic-metamorphic reaction history" (pp. 93–104). Various, dominantly quartz-free biotite-, chlorite- and plagioclase-bearing early parageneses are well preserved in the coarse-grained kyanite-chlorite-cordierite rock. The mica-rich assemblage is overgrown by static kyanite and staurolite that were crystallized contemporaneously.

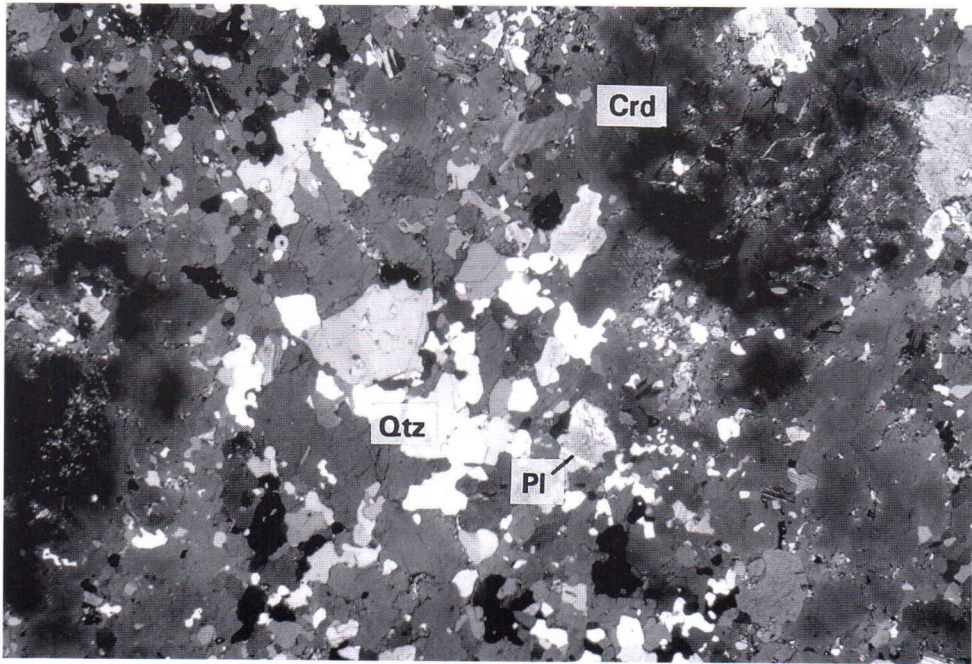


Fig. 7. Detail of cordierite-rich patch including remnants of “primary” plagioclase and recrystallized quartz at Hiltuspuro. Field of view c. 4 mm wide. Crossed nicols. Photo by M. Pajunen.

The early, “low-T” kyanite-staurolite paragenesis is overprinted by later, “high-T” cordierite and contemporaneous sillimanite, with the result that kyanite and staurolite occur as corroded relics in cordierite (Fig. 8). Biotite has decomposed into cordierite in contact with kyanite. Cordierite replaces the other phases, even plagioclase, in kyanite rocks. Fibrous sillimanite was formed by, for instance, polymorphic transformation of kyanite. Orthoamphibole crystallized after chlorite and biotite. In general, the semi-brittle zones and cordierite-rich patches show mineral assemblages representing more advanced metasomatism under late “high-T” conditions.

Retrogressive metamorphic reactions, e.g. pin- itization of cordierite, muscovitization of aluminium silicates, muscovitization and chloritization of staurolite, and carbonatization of orthoamphibole, were so weak that prograde parageneses are always dominant. These reactions are often restricted to the surroundings of late fractures.

Other targets

The kyanite rocks close to the Kainuu Schist Belt (Fig. 1) are connected with the shear zones trending northwest–southeast and dipping southwest. Early features are well preserved at *Kallioniemi* and *Kauhealampi*, because the late, “high-T” cordierite-sillimanite assemblage (cf. Hiltuspuro) is absent (Appendix 2). Decomposition of primary biotite and plagioclase into chlorite and muscovite has proceeded with increasing deformation from the margins towards the centre of zones. The central part of the zone has, however, been neomineralized to coarse-grained kyanite rock with unoriented kyanite laths, up to 10–15 cm in diameter, caused by static mineral growth. Kyanite replaces mainly muscovite. A sequence of metasomatic zones from tonalitic Pl-Qtz-Bt to Chl-Ky- Ms-Qtz±Pl was formed. Segregation of mica- and quartz±plagioclase-rich domains is common.

At *Turkkivaara* (local boulders only) relics of early shearing structures, e.g. bending of Archaean

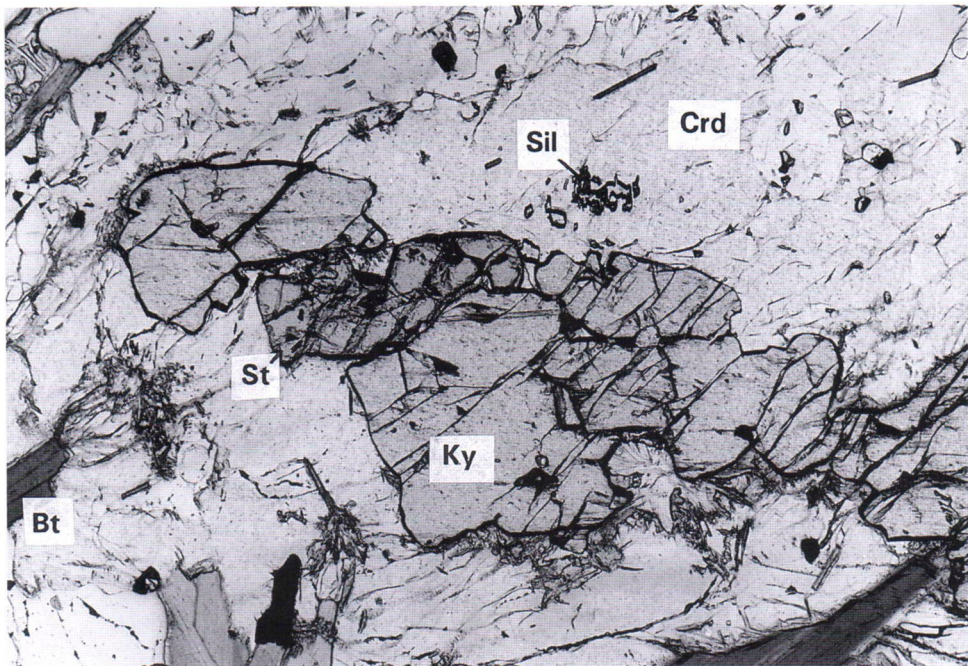


Fig. 8. Kyanite-staurolite paragenesis surrounded by later cordierite and sillimanite in a narrow D_{P_2} zone at Hiltuspuro. Field of view c. 4 mm wide. Plane polarized light. Photo by M. Pajunen.

foliation, are well preserved (Fig. 9). The oldest product of shearing and concomitant metasomatism is a foliated biotite-plagioclase rock – kidney-shaped plagioclase porphyroblasts in biotite mass – overgrown by static kyanite and staurolite. The kyanite is rimmed by later andalusite, which also occurs as large subidioblastic porphyroblasts. Cordierite and scarce fibrous sillimanite are the most recent phases. Cordierite rims and corrodes kyanite and andalusite (Fig. 10), and has locally altered into muscovite and chlorite.

The mineral growth succession in the kyanite rock about one kilometre east of Havukkalammit, east Havukkalammit, is much the same as that at Turkkivaara. The relation of the rock to its surroundings is unknown. Andalusite, which rims kyanite and is itself surrounded by cordierite, is xenoblastic and corroded, but exists in equilibrium with cordierite. There is metasomatic segregation of nearly monomineralic muscovite and biotite rocks. Micas have been replaced isovolumetrically by cordierite (Fig. 11).

At Korpilampi, Havukkalammit and Levävaara the relation between the coarse-grained, weakly oriented kyanite rocks and shearing is not as clear as at the westernmost sites described above. The kyanite rocks have irregular, sharp or gradual, or breccia-like replacement contacts with the variably altered tonalitic country rocks. The breccia fragments are strongly assimilated and rather mobile in appearance, suggesting brecciation in a ductile state (Fig. 12). At Levävaara, a Palaeoproterozoic metadiabase dyke shows well-developed amphibolite-facies mineral schistosity, and the country-rock tonalite is blastomylonitic-mylonite gneissic in fabric. The mica-rich kyanite rock is undeformed; it has only local late crenulations (cf. Hiltuspuro), due to which the large kyanite crystals were broken and altered into muscovite. Metadiabase shows alteration that occurred after the formation of the peak metamorphic assemblages in its contact zone, indicating that the alteration process postdated the amphibolite facies parageneses and deformation of metadiabase.



Fig. 9. Metasomatic kyanite-andalusite-cordierite rock penetrating tonalite (in upper right corner) at Turkkiivaara. The foliation in tonalite is bent in the direction of early shearing, and the foliation is still visible in the zone itself. The early biotite-plagioclase paragenesis (Bt = black and Pl = white, in lower left corner) covered by static mineral growth of cordierite (grey, biotite foliation as relic) and Al-silicates (white prisms in middle of photograph). Photo by M. Pajunen.

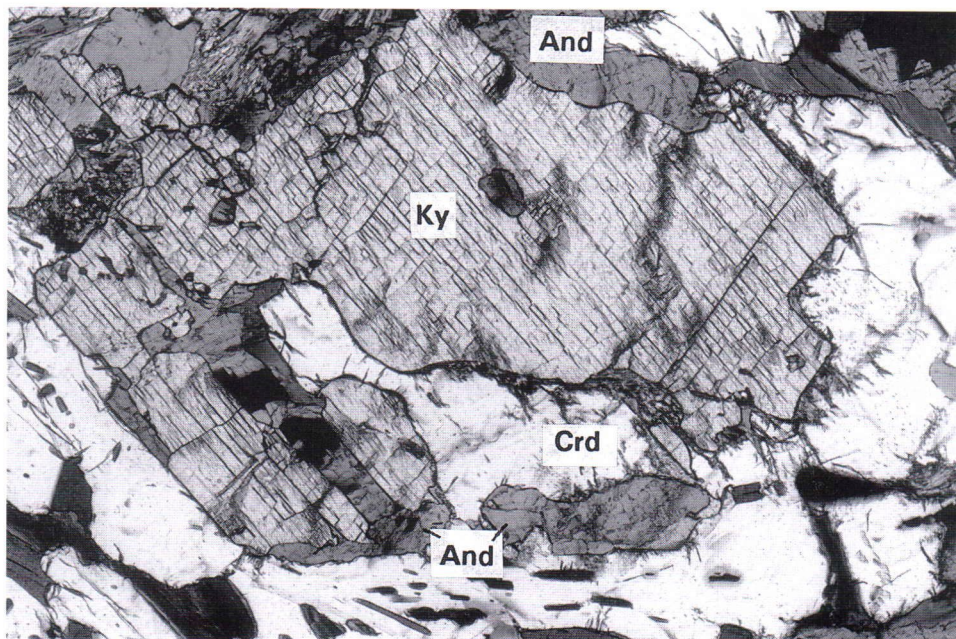


Fig. 10. Kyanite rimmed by later andalusite and cordierite at Turkkiivaara. Field of view c. 4 mm wide. Crossed nicols. Photo by M. Pajunen.

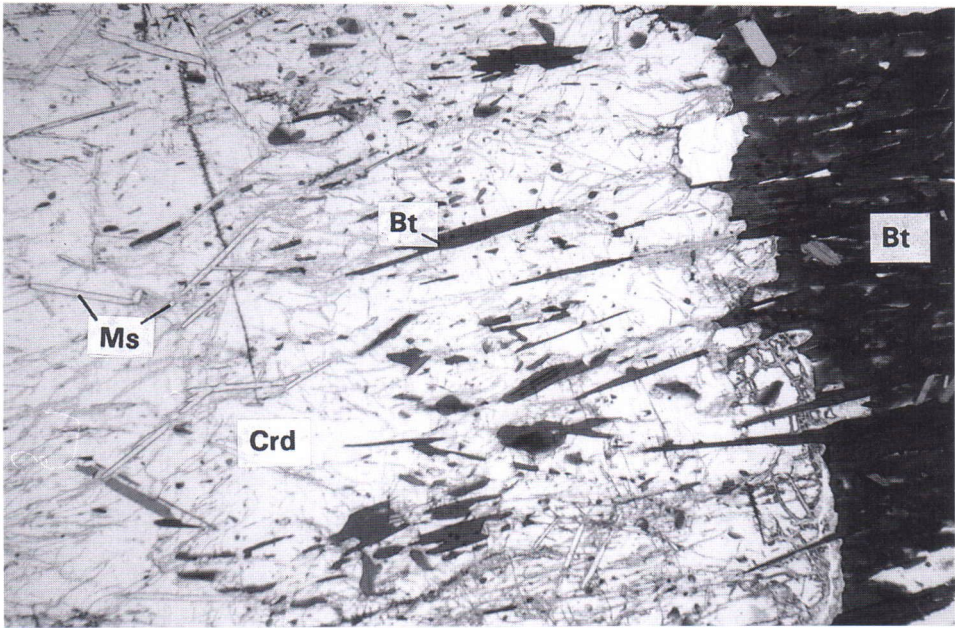


Fig. 11. Foliated, monomineralic biotite rock (cf. Fig. 9) overgrown by cordierite at east Havukkalammit. Biotite foliation is preserved as relic in internal structure of cordierite. In the middle of the cordierite porphyroblast new, more randomly oriented muscovite has crystallized instead of biotite. Field of view c. 4 mm wide. Plane polarized light. Photo by M. Pajunen.



Fig. 12. Mobile, brecciated replacement contact of coarse-grained kyanite rock and tonalite at Levävaara. Metasomatic zoning, for example, a zone rich in tourmaline (black patches in upper-left corner), is well developed. Photo by M. Pajunen.



Fig. 13. Metasomatic biotite-plagioclase (black), plagioclase-magnetite-biotite (white) and epidote-clinoamphibole (darkish grey) zones at Havukkalammit. Photo by M. Pajunen.

Compositional variation is pronounced. Extremely well-developed metasomatic zoning exists at Havukkalammit, where zones from the tonalitic assemblage, $Pl-Qtz-Bt \pm Hbl$, to quartz-free, medium-grained $Pl-Mag-Bt$ and $Ep-Cam$ (Fig. 13) and also to coarse-grained $Bt-Pl$, $Bt-Ky-Pl$ and $Bt-Ky$ assemblages were formed. At Havukkalammit and Korpilampi the late “high-T” cordierite-sillimanite assemblages are absent, and the kyanite-biotite pair is stable, although fresh, exceptionally anorthite-rich and irregularly, even oscillatory, zoned plagioclase rims (see later) exist between biotite and kyanite. Kyanite occurs as fresh and uncorroded laths, up to 50 cm long, which in places are surrounded by fibrous kyanite of a later generation (Fig. 14). At Levävaara a late cordierite-sillimanite assemblage, albeit weaker than at Hiltuspuro, developed. The texture of kyanite and andalusite indicates that they crystallized more or less concurrently, and that there is a progression from chlorite-muscovite to kyanite-staurolite (Fig. 15).

At *Varpuniemi* and *Matovaara* (Appendix 2) a fully recrystallized granoblastic fabric formed in northwest-southeast-trending shear zones cross-cutting the Archaean tonalite. At *Varpuniemi*, staurolite grains, about 1 cm in size, and rare kyanite porphyroblasts occur in a quartz-free assemblage, and at *Matovaara* there is an exceptional orthoamphibole-bearing rock with unoriented amphibole laths, 2–4 cm long.

At *Tuomaanvaara*, irregular cordierite-chlorite rock patches, corresponding to the cordierite-rich patches at Hiltuspuro, overprint the Archaean tonalite without distinct deformation (Fig. 16). The early $Chl-Ms-Qtz$ and $Ky/And-St$ assemblages (see above) are absent.

The kyanite rock at *Teljo* (one outcrop) is fully comparable to the narrow zones and cordierite-rich patches at Hiltuspuro. Locally, cordierite grains replace plagioclase along grain boundaries (Fig. 17).

The kyanite rock at *Tettilampi* differs from that at Hiltuspuro in its more intense sillimanitization;

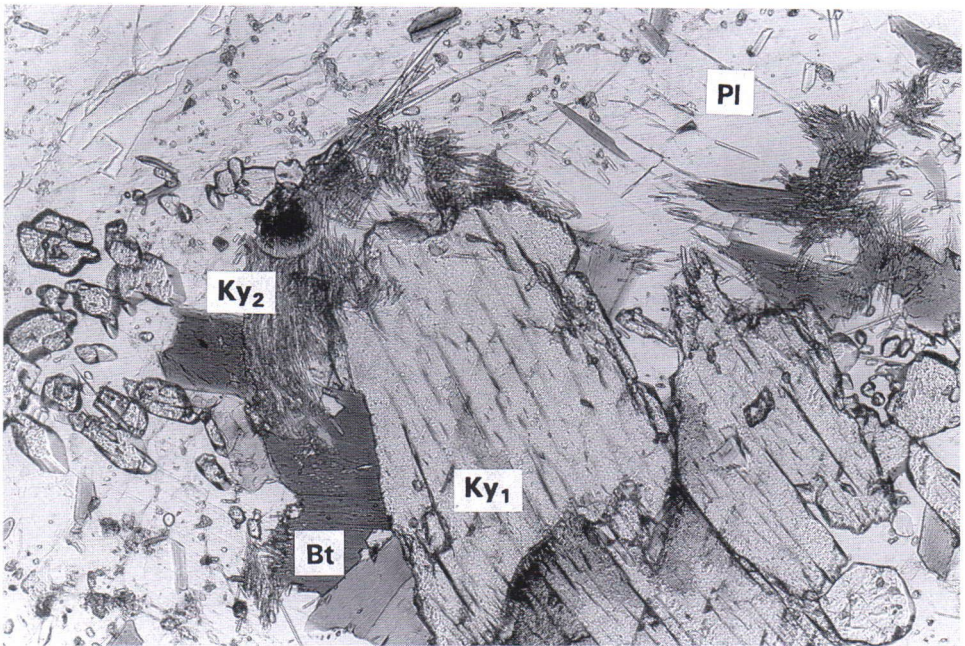


Fig. 14. Coarse-grained kyanite (Ky₁) and fibrous kyanite (Ky₂) generations at Havukkalammit. Fibrous kyanite phase was identified by X-ray methods, and it has inclined extinction along c -axis. Field of view c. 2 mm wide. Plane polarized light. Photo by M. Pajunen.

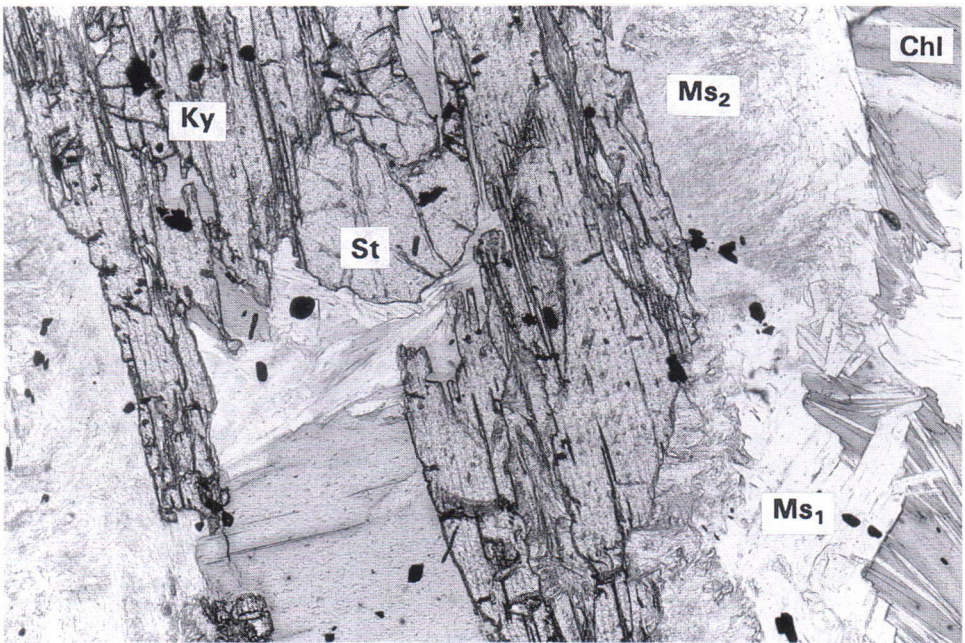


Fig. 15. Kyanite-staurolite paragenesis overgrowing coarse-grained chlorite-muscovite (Ms₁) paragenesis at Levävaara. Retrograde fine-grained muscovite (Ms₂) rimming kyanite. Field of view c. 4 mm wide. Plane polarized light. Photo by M. Pajunen.

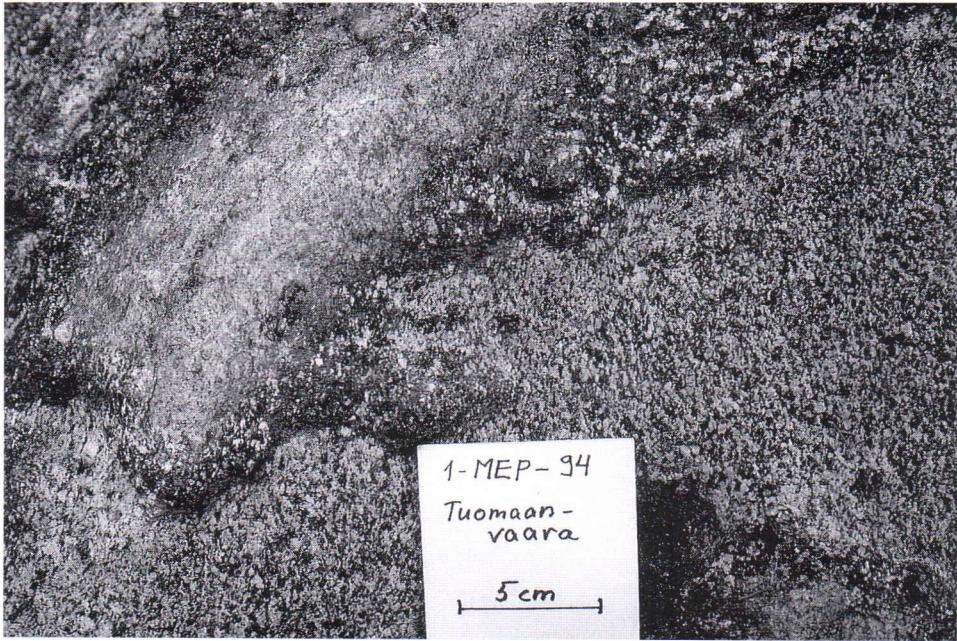


Fig. 16. Cordierite-rich patch, surrounded by chlorite-rich zone, has grown isovolumetrically on foliated and folded Archaean structure of gneissic tonalite at Tuomaanvaara. Photo by M. Pajunen.

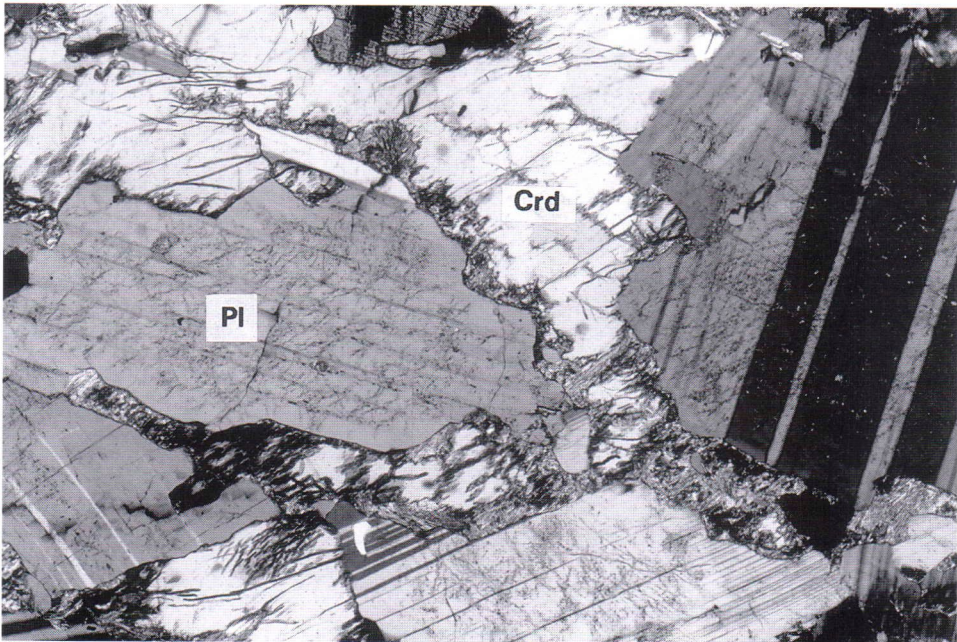


Fig. 17. Cordierite replacing plagioclase along grain boundaries at Teljo. The replacement is locally total, and only small relics of previous phases are preserved (cf. Fig 7). Field of view is c. 4 mm wide. Crossed nicols. Photo by M. Pajunen.

sillimanite even forms narrow monomineralic zones overgrowing kyanite. Some kyanite grains follow the grain boundaries of earlier plagioclase, indicating alteration along grain boundaries in the same manner as the cordierite at Teljo. Muscovite is a significant by-product of cordierite after kyanite and biotite.

Notes on accessory minerals of kyanite rocks

Some features regarding accessory phases need to be emphasized (see Appendix 2). Abundant rutile crystallized in chloritization and/or sericitization of biotite at most of the sites and was stable during metasomatism. Ilmenite is scarce in staurolite- and orthoamphibole-bearing assemblages. Apatite occurs regularly and abundantly, especially in altered rocks rich in cordierite, indicating phosphorus mobility during metasomatism. Fresh xenotime inclusions in cordierite in the southern occurrences imply phosphorus enrichment and rearrangement of radioactive components and yttrium (see section "Isotope geology", pp. 110–112). REE mobility during the alteration is shown by local allanite crystallization. Radioactive minerals in chlorite-rich assemblages, not affected by the late-stage event, are often metamictic. Local enrichment of boron is manifested in crystallization of tourmaline porphyroblasts, up to 10 cm in diameter, at Levävaara (Fig. 12).

MINERAL CHEMISTRY

The chemical compositions of minerals were analysed on polished thin sections at the Geological Survey of Finland in Espoo using the wave-length dispersive technique and a Jeol Jcxa – 733 Superprobe. The acceleration voltage was 15 kV. The electron beam current was 15 nA for cordierite, plagioclase and muscovite and 25 nA for other phases; the beam diameter was 1 µm for garnet and 10 µm for other minerals. Natural mineral standards were employed for all elements except Al, for which synthetic corundum was used. ZAF procedures were applied to correct the analytical data. The results confirmed by several analyses are shown as averages of n analyses in Appendices 3–10. Ring number refers to the local mineral assemblage analysed within each thin section.

Kyanite

Kyanite is, in general, pure Al_2SiO_5 , but minor impurities

of iron (0.45–0.54 wt% FeO) were found in the kyanite from a narrow zone at Hiltuspuro. The coarse-grained kyanite from Havukkalammit contains small amounts of iron (0.05–0.51 wt% FeO; analyses 1–3 on p. 13 in Horneman & Hyvärinen 1987).

Cordierite

Cordierite is fresh, as only weak pinitization along grain boundaries and fractures is sometimes observed. The cordierites $[(\text{Mg},\text{Fe})_2^{\text{M}}(\text{Al},\text{Fe})_4^{\text{T1}}(\text{Si},\text{Al})_5^{\text{T2}}\text{O}_{18}]$ analysed from Hiltuspuro and Tetrilampi vary slightly in composition (Appendix 3, analyses 1–14). That at Tetrilampi is richest in Mg: $X_{\text{Mg}}^{\text{Crd}} = \text{Mg}/(\text{Fe}+\text{Mn}+\text{Mg})$ is 0.84–0.85 (analyses 13–14). At Hiltuspuro, the highest $X_{\text{Mg}}^{\text{Crd}} = 0.84$ was analysed from a coarse-grained kyanite-chlorite-cordierite rock (analyses 11–12). In orthoamphibole-bearing assemblages (analyses 1–7), $X_{\text{Mg}}^{\text{Crd}}$ varies in the range 0.81–0.83 and the cordierite richest in iron, $X_{\text{Mg}}^{\text{Crd}} = 0.77$ –0.79, is in staurolite-bearing assemblages (analyses 8–10). The compositional zoning in cordierite is small. Trace element Na_2O has a slight variation; the coarse-grained kyanite-chlorite-cordierite rocks have the highest values.

Staurolite

The composition of staurolite $[(\text{Fe},\text{Mg})_2^{\text{M4+M6}}(\text{Al},\text{Fe})_9^{\text{M6}}(\text{Si},\text{Al})_4^{\text{T}}\text{O}_{23}(\text{OH})]$ with yellow pleochroism varies very little in samples analysed from the narrow alteration zones of Hiltuspuro. The $X_{\text{Mg}}^{\text{St}} = \text{Mg}/(\text{Fe}+\text{Mn}+\text{Mg})$ values range from 0.26 to 0.28 (Appendix 4, analyses 15–18). Analysis 15, which has the lowest $X_{\text{Mg}}^{\text{St}}$, is of a small, younger idiomorphic grain in cordierite, and analysis 16 is of a corroded, xenoblastic grain in the same paragenesis.

Garnet

The garnet-quartz rock at Hiltuspuro has various garnet $[(\text{Ca},\text{Fe},\text{Mg},\text{Mn})_3(\text{Al},\text{Cr})_2(\text{Si},\text{Ti})_3\text{O}_{12}]$ parageneses, even in one sample: (1) Grt-Bt-Chl-Qtz (Appendix 5, analyses 19–22) and (2) Grt-Pl-Ms-Qtz (analyses 23–25). The garnet is poor in Mg, $X_{\text{Mg}}^{\text{Grt}}$ ranging from 0.04 to 0.09. Paragenesis (1) shows two generations of garnet: the older core ($X_{\text{Alm}} = 0.60$ and $X_{\text{Sps}} = 0.21$, analysis 20), which has altered into chlorite, and the younger rim generation ($X_{\text{Alm}} = 0.60$ –0.62 and $X_{\text{Sps}} = 0.22$ –0.23, analyses 19 and 21–22) enveloping chlorite. X_{Grs} is low (0.09–0.11). Syntectonic garnet in the muscovite-bearing paragenesis (2) (analyses 23–25, a grain about 6 mm in diameter), with weak zoning in composition from core to rim, has X_{Alm} ranging from 0.77 to 0.82. Mn and Ca contents are lower than in paragenesis (1): $X_{\text{Sps}} = 0.10$ –0.13 and $X_{\text{Grs}} = 0.03$ –0.04.

Orthoamphibole

Orthoamphibole was found in one outcrop at Hiltuspuro and at Matovaara (not analysed). Complex substitutions and the impossibility of analysing Fe^{2+} and Fe^{3+} separately by

microprobe complicates determination of the amphibole formula $[(\text{Vac}, \text{Na}, \text{K})^{\text{A}}(\text{Na}, \text{K}, \text{Ca}, \text{Mn}, \text{Mg}, \text{Fe})_2^{\text{M4}}(\text{Fe}, \text{Mg}, \text{Mn}, \text{Ca})_2^{\text{M1+M3}}(\text{Al}, \text{Ti}, \text{Fe}, \text{Mg})_2^{\text{M2}}(\text{Si})_4^{\text{T1}}(\text{Si}, \text{Al}, \text{Ti})_4^{\text{T2}}\text{O}_{22}(\text{OH})_2]$ (Vac = vacancy) (Robinson et al. 1982). The mineral formulae were normalized to 15 cations and all Fe was considered as Fe^{2+} . Mg and Fe were divided between M4, M1+M3 and M2 sites according to the molecular portion, $X_{\text{Mg}}^{\text{Oam}} = \text{Mg}/(\text{Fe}+\text{Mg})$ (Appendix 6, analyses 26–34). According to the classification of Leake (1978), all the orthoamphiboles are anthophyllitic except that of analysis 27, which is gedritic in composition. As products of the same chlorite breakdown reaction, coexisting gedrite and anthophyllite (analyses 27 and 28) occur as separate grains in the paragenesis, Ged-Ath-Crd-Chl-Qtz. Gedrite has lower $X_{\text{Mg}} = 0.61$ and higher Na = 0.43 p.f.u. (p.f.u. = atoms per formula unit) than coexisting anthophyllite, 0.65 and 0.07, respectively. Al^{tot} in gedrite is 2.28 p.f.u. as against 0.55 p.f.u. in coexisting anthophyllite. The substitutions of Na and Al in gedrite are due to edenitic ($\text{Vac}, \text{Si}=\text{Na}, \text{Al}^{\text{IV}}$) and tschermakitic ($\text{Mg}^{\text{VI}}, \text{Si}^{\text{IV}}=\text{Al}^{\text{VI}}, \text{Al}^{\text{IV}}$) substitutions (cf. Robinson et al. 1982). The other orthoamphiboles of the same rock are anthophyllites, with X_{Mg} between 0.67 and 0.69 and Al^{tot} ranging from 0.62 p.f.u. in the complex assemblage, Ath-Crd-Pl-Bt-Chl-Qtz-Ky (analysis 26), to 0.24–0.44 in the assemblage, Ath-Crd-Qtz±Pl (analyses 32–34). Anthophyllites 29–30 with $X_{\text{Mg}} = 0.68$ and $\text{Al}^{\text{tot}} = 0.47$ –0.39 replace biotite in the paragenesis, Ath-Bt-Crd.

Plagioclase

Plagioclase is albitic, $X_{\text{Ab}} = 0.90$ –0.98, in kyanite-chlorite-cordierite rocks at Hiltuspuro (analyses 41–43 and 45–47) and Tetrilampi (analysis 50) (Appendix 7). It is weakly zonal. The kyanite rock at Havukkalammit (analyses 35–40) is exceptional in having plagioclase rich in anorthite component, ranging from 0.57 to 0.86 (analyses 35–37) in older grains rich in inclusions and from 0.59 to 0.75 (analyses 38–40) in plagioclase reaction rims between kyanite and biotite. Its heterogeneous optical extinction properties indicate irregular variation in composition. The plagioclase of the garnet-quartz rock (analyses 48–49) at Hiltuspuro generally contains somewhat more anorthite component than the other rocks of the area. The potassium content is low in all samples.

Biotite

Biotites $[(\text{Vac}, \text{K}, \text{Na})^{\text{A}}(\text{Mg}, \text{Fe}, \text{Ca})^{\text{M1}}(\text{Mg}, \text{Fe}, \text{Mn}, \text{Ti}, \text{Al})_2^{\text{M2}}(\text{Si})_2^{\text{T1}}(\text{Si}, \text{Al})_2^{\text{T2}}\text{O}_{10}(\text{OH})_2]$ at Havukkalammit, Hiltuspuro and Tetrilampi (Appendix 8) are intermediate in Al-Si/octahedral cation substitution. At Hiltuspuro, the staurolite-bearing parageneses have lower $X_{\text{Mg}}^{\text{Bt}} = \text{Mg}/(\text{Mg}+\text{Fe})$ values, 0.60–0.64 (analyses 70–74), than the other altered parageneses. $X_{\text{Mg}}^{\text{Bt}}$ is 0.71–0.73 (analyses 63–68) in orthoamphibole-bearing parageneses, 0.73–0.74 (analyses 75–76) in the coarse-grained assemblage, Bt-Chl-Crd-Chl-Pl-Qtz, and high, 0.76 (analysis 77), in Bt-Chl-Crd aggregates. The $X_{\text{Mg}}^{\text{Bt}}$ values of the biotite in the narrow zones are higher

(0.72–0.75) at Tetrilampi (analyses 59–62) than in corresponding zones at Hiltuspuro. In the coarse-grained Bt-Ky-Pl paragenesis at Havukkalammit, $X_{\text{Mg}}^{\text{Bt}}$ ranges from 0.67 to 0.72 (analyses 51–58) and is low, 0.32–0.36 (analyses 78–79), in the garnet-quartz rock at Hiltuspuro. The Ti content is evidently buffered by rutile to 0.05–0.07 p.f.u. except at Havukkalammit, where it is 0.03–0.05 p.f.u. (Fig. 18).

Chlorite

Chlorite $[(\text{Mg}, \text{Fe}, \text{Mn})_4^{\text{M1}}(\text{Al}, \text{Mg}, \text{Fe}, \text{Mn})_2^{\text{M2}}(\text{Si}, \text{Al})_2^{\text{T2}}(\text{Si})_2^{\text{T1}}\text{O}_{10}(\text{OH})_2]$ (Appendix 9) exists in various assemblages, but its composition varies only slightly. At Hiltuspuro, the $X_{\text{Mg}}^{\text{Chl}} = \text{Mg}/(\text{Fe}+\text{Mn}+\text{Mg})$ values are high, from 0.75 to 0.80 in altered rocks (analyses 83–90), being highest in the Chl-Bt-Crd aggregate (analysis 90), where biotite, too, is richest in Mg. At Havukkalammit, $X_{\text{Mg}}^{\text{Chl}}$ is between 0.70 and 0.75 (analyses 84–86). In the garnet-quartz rock, $X_{\text{Mg}}^{\text{Chl}}$ is 0.34–0.36 (analyses 91–93).

White micas

Early muscovite $[(\text{Vac}, \text{K}, \text{Na})^{\text{A}}(\text{Mg}, \text{Fe}^{2+}, \text{Mn})^{\text{M1}}(\text{Al}, \text{Fe}^{3+}, \text{Ti})_2^{\text{M2}}(\text{Al}_{1-x}, \text{Si}_{3+x})_4^{\text{T1+T2}}\text{O}_{10}(\text{OH})_2]$ with chlorite occurs as inclusions in kyanite at Havukkalammit (analyses 94–95) (Appendix 10). At Tetrilampi the muscovite is in the paragenesis, Ms-Crd-Ky/Sil-Bt-Qtz±Pl (analyses 99–103). $X_{\text{Na}} = \text{Na}/(\text{Na}+\text{K})$ is 0.18–0.19 at Havukkalammit and 0.25–0.29 at Tetrilampi. There is slight substitution of celadonite component in muscovite. The small mica grains at Hiltuspuro generated by the alteration of albitic plagioclase in the plagioclase-cordierite reaction rim are paragonitic in composition, with $X_{\text{Na}} = 0.85$ –0.88 (analyses 96–97) and a high Mg content, 0.14–0.58 p.f.u. In the garnet-quartz rock at Hiltuspuro X_{Na} is 0.13 (analysis 98).

FLUID INCLUSIONS

To shed light on fluid composition during metasomatism, a fluid inclusion study was made on carefully gathered samples. The likelihood of finding representative fluid inclusions was good, because the rocks are coarse grained, and generally well preserved from late deformations.

Fluid inclusions in 0.3-mm-thick, doubly-polished plates cut from kyanite-chlorite-cordierite rock (from the outcrop shown in Figs. 2b, 3 and 5) from southeast Hiltuspuro were investigated using a Linkam THMSG 600 programmable heating/freezing stage attached to a Leitz Ortholux Pol transmitted light microscope (see Shepherd et al. 1985). The stage was calibrated with a set of syn-

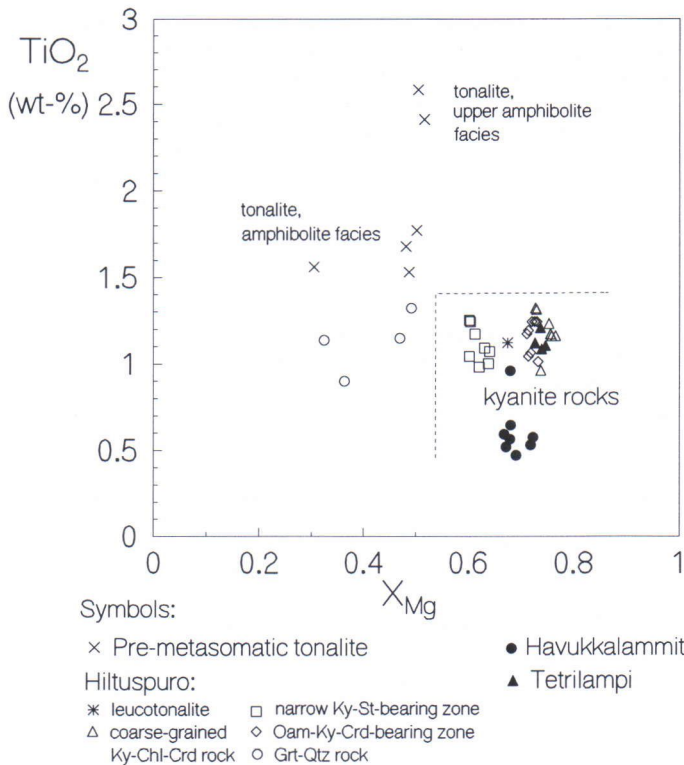


Fig. 18. Biotite compositions in kyanite rocks and pre-metasomatic Archean tonalites on TiO_2 vs. X_{Mg} diagram.

thetic fluid inclusion standards (see Sterner & Bodnar 1984). At a temperature interval of -60° to 300°C , the recorded temperatures of phase transitions have a precision of $\pm 0.2^\circ$ to 2.0°C . Analytical errors are thus insignificant in terms of geological interpretation.

The data obtained from 60 carefully selected fluid inclusions (c. 5 to 70 μm in the longest dimension) in kyanite and cordierite are summarized in Table 1. No fluid inclusions were found in andalusite from Levävaara. Two types of fluid inclusion were identified: (1) aqueous, two-phase inclusions with moderate salinity and (2) monophasic, apparently pure liquid CO_2 inclusions without a visible amount of water. The salinities and densities of the aqueous and carbonic inclusions were calculated from the last ice melting temperatures and homogenization temperatures to liquid and were modelled in binary ($\text{H}_2\text{O}-\text{NaCl}$) and unary (CO_2) systems in the equations of Bottinga and Richet (1981) and Brown and Lamb

(1989), respectively, using the FLINCOR program (Brown 1989). The isochore slopes presented in Fig. 31 were calculated using the above equation of states and FLINCOR. The relevant data for constructing isochores are listed in Table 1.

The fluid inclusions were further subdivided into primary, pseudosecondary and secondary inclusions (Table 1) using criteria given by Roedder (1984). Their mode of occurrence is shown in Fig. 19. In kyanite, primary aqueous inclusions are tubular in shape and aligned parallel to the c -axis of the crystal (Figs. 19 and 20). In cordierite, pseudosecondary carbonic inclusions occur in small groups and their shape is usually of negative crystals. Secondary carbonic inclusions in cordierite, and aqueous inclusions in kyanite and cordierite occur in healed fractures with rounded to irregular shapes. The mutual cross-cutting features of these secondary inclusion trails in cordierite suggest that the carbonic inclusions pre-date the aqueous inclusions. It is assumed that the

Table 1. Summary of fluid types, microthermometric data and paragenetic classification of fluid inclusions in kyanite and cordierite of kyanite-chlorite-cordierite rock at Hiltuspuro ($x=7070.51$, $y=4485.25$).

Inclusion type/mineral	T_h H ₂ O T°C	T_m H ₂ O T°C	Salinity eq.wt % NaCl	T_h CO ₂ T°C	T_m CO ₂ T°C	Density g/cm ³	Paragenetic classification
H ₂ O/kyanite	251 to 264	-9.5 to -11	13 to 15	-	-	0.92	primary
H ₂ O/kyanite and cordierite	227 to 245	-7.5 to -13	11 to 17	-	-	0.93 to 0.95	secondary
CO ₂ /cordierite pseudosecondary	-	-	-	8.5 to 13.5	-56.6	0.83 to 0.87	
CO ₂ /cordierite	-	-	-	21 to 29	-56.6	0.63 to 0.7	secondary

T_h = temperature of total homogenization of inclusion contents into liquid

T_m = melting temperature of ice and carbon dioxide

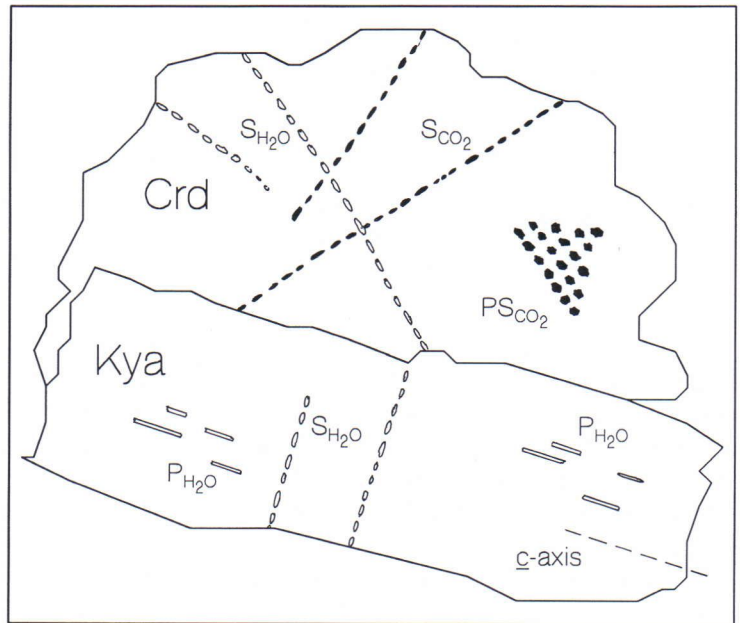


Fig. 19. Schematic illustration of mode of occurrence of primary (P), pseudosecondary (PS) and secondary (S) fluid inclusions in cordierite and kyanite.

primary and pseudosecondary inclusions provide information on fluids passing through the rock during crystallization of the mineral involved.

METASOMATIC-METAMORPHIC REACTION HISTORY

Metasomatism, the mass transfer and reorganization of rock-forming components, occurs whenever a moving fluid is out of equilibrium with the

local rock (Korzhinskii 1970, Thompson 1988). The process is maintained by infiltration and/or diffusion processes in solid rock (e.g. Korzhinskii 1970, McCaigh & Knipe 1990). Both processes have a tendency to develop monomineralic metasomatic zoning. In infiltration metasomatism, components are transported by migrating pore solutions, and the zones that are formed have homogeneous phase compositions. In diffusion metasomatism, in contrast, the components migrate by diffusion through pore solution film, and phase

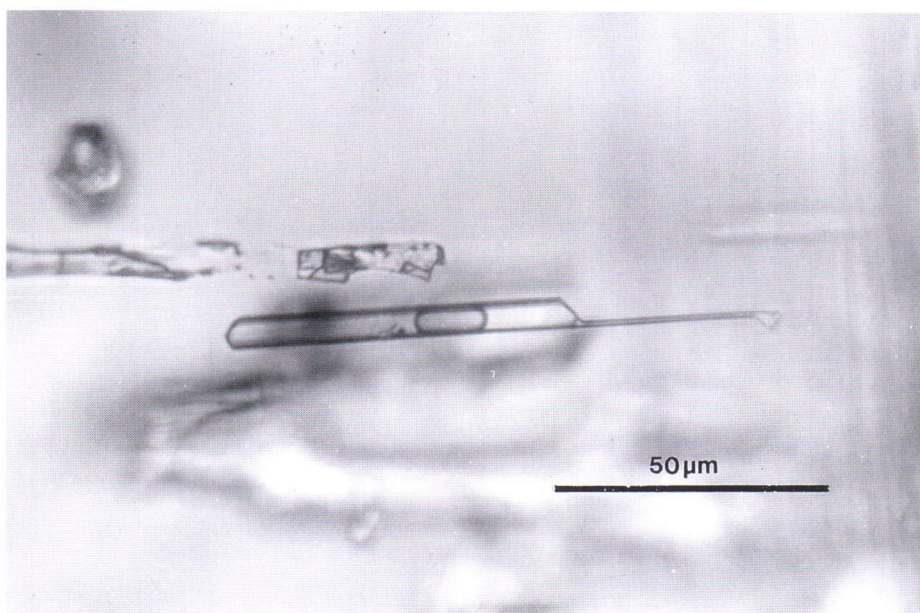


Fig. 20. Primary H_2O inclusion in kyanite at Hiltuspuro ($x=7070.51$, $y=4485.25$) from the outcrop shown in Figs. 2b, 3 and 5. Photo by M. Poutiainen.

compositions may vary within zones. Metasomatic zones formed simultaneously have sharp boundaries in which one component becomes perfectly mobile and the number of inert components decreases by one, one phase then being totally replaced by a new one. Thus, the fluid composition, especially its pH-Eh states and the character of dissolved components, vary from one zone to another. Diffusion may change the boundaries, making them gradual. Generally, both processes act concurrently in metasomatism. In nature, metasomatic zoning is seldom systematic, and the zones constitute a complex mixture (Korzhinskii 1970).

The metasomatic-metamorphic reaction history of the kyanite rocks can be established by combining the information available on their common features. The metasomatic-metamorphic succession can be divided into early, late and cooling stages. In the westernmost targets, the earliest stage was connected with shearing (Fig. 9). This was overprinted by static-state metasomatism in the centre of the zone, which was the part most susceptible to fluid flow. Further east, the fluid action of the early stage gave rise to mobile breccia-like replacement structures (Fig. 12) and well-developed metasomatic zoning (Fig. 13).

During the late stage, fluid-induced metasomatism occurred along semi-brittle fractures and mineral grain boundaries under unstrained conditions (Figs. 4 and 17). The cooling stage was associated with weak fracturing and static retrogression.

Early stage

Metasomatic zoning and mineral assemblages

Early parageneses or their relics are preserved in the coarse-grained kyanite rocks at Hiltuspuro and to the northwest of it, but in the south they are more or less overprinted by later processes or, as at Tuomaanvaara, were not formed at all. Characteristic mineral growth successions and metasomatic zones during progressive metasomatism are compiled in Table 2.

Large changes in volume, even losses of up to 60%, have been described from shear zones (e.g. Selverstone et al. 1991). The estimation of volume changes and the amount of chemical mass trans-

Table 2. Metasomatic zoning and mineral growth succession in kyanite rocks. Uncertain crystallization stages are shown by arrows.

Occurrence (in Fig. 1)	Pre-metasomatic stage		Metasomatic stages					Cooling stage
	Primary assemblages		Early-stage mineral growth			Late-stage mineral growth		
	Rock type	Original assemblage	Initial assemblages and metasomatic zones	Successive mineral growth	Transitional or unknown stage	Assemblage in alteration front	Final assemblage	
Tuomaanvaara (1)	tonalite	Pl-Bt-Qtz	not developed			Chl-Qtz and Bt in cordieritization front	Crd	pinitization
Turkkivaara (2)	tonalite	Pl-Bt-Qtz	Bt-Pl ± Ms1 Chl1-Ms Bt	Ky ± St	And		Crd-Ms Crd ± Sil	Ms2 Chl2
Kallioniemi (3)	tonalite	Pl-Bt-Qtz	Ms-Chl-Pl-Qtz	Ky			not developed	
Varisniemi (4)	tonalite	Pl-Bt-Qtz	Chl-Pl	St ± Ky			not developed	Ms
Korpilampi (5)	tonalite	Pl-Bt-Qtz	Bt-Pl-Qtz-Chl ± Ms1	Ky			not developed	Ms2
Kauhealampi (6)	tonalite	Pl-Bt-Qtz	Chl-Qtz ± Ms1 Chl-Pl	Ky			not developed	Ms2
Havukkalammit (7)	tonalite	Pl-Bt-Qtz	Ms-Chl-bearing assemblages	Ky1-Bt ± Pl1 (rich in An) Bt-Chl ± Pl Ep-Pl ± Cam Pl-Mag-Bt	Ky2 Pl2 (rich in An)			
E-Havukkalammit (7)	not known	not known	Bt-Pl Bt-Qtz Ms	Ky	And		Crd	
Matovaara (8)	altered tonalite	Pl-Bt-Qtz	Bt-Pl-Qtz Qtz (veins)				Oam	Chl
Levävaara (9)	tonalite	Pl-Bt-Qtz	Chl-Pl-Bt Chl-Pl-Qtz Chl-Pl Chl-Ms1 Chl-Bt Bt-Pl Chl-Bt-Sph Pl-Chl-Tou Qtz Bt	Ky ± St Ky-And And Crn-Ky Crn			Crd-Sil	Ms2
Hiltuepuro (10)	tonalite	Pl-Bt-Qtz	Chl1-Pl-Bt Chl1-Bt Bt Bt-Pl Qtz (veins)	Ky-St		Chl in cordieritization front(*)	Crd-Sil Crd-Oam Crd-Qtz Crd	Ms Chl2 carbonatization
Teljo (11)	tonalite	Pl-Bt-Qtz		Ky-Bt-Pl relics in Crd		Chl (*) see above	Crd ± Sil	Ms pinitization
Egyptinkorpi (12)	not known	not known	Bt-Ms1 relics in Ky	Pl-Qtz-Ky			Sil	Ms2
Tettilampi (14)	tonalite and migmatite	Pl-Bt-Qtz		Ky			Crd-Ms1 ± Sil Crd Sil (veins)	Ms2 Chl

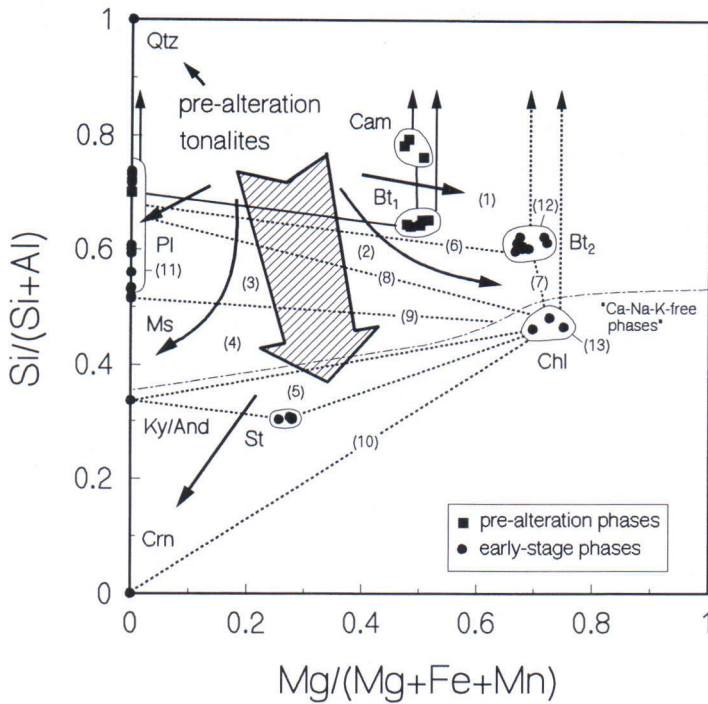


Fig. 21. Compositions of early-stage phases and pre-metamorphic phases in tonalites shown on $Si/(Si+Al)$ vs. $Mg/(Mg+Fe+Mn)$ diagram. The mineral compositions are from Havukkalammit; the compositions of staurolite refer to Hiltuspuro. The directions of metasomatism are shown schematically by arrows and the general trend of alteration by hatched arrow. Typical mineral assemblages are indicated by numbers in parentheses.

fer (cf. Gresens 1967, Grant 1986) during metasomatism is beyond the scope of our study. Thus, only relative changes in composition are shown in the $Si/(Si+Al)$ vs. $Mg/(Mg+Fe+Mn)$ diagram (Fig. 21). The representative mineral assemblages are indicated by the numbers in parentheses. The mineral compositions from Havukkalammit are used; the compositions of staurolite refer to Hiltuspuro, and those of pre-alteration phases in amphibolite facies tonalites are given as "precursor". The early-stage mineral compositions were clearly affected by the later "high-T" conditions, the exchange reactions between phases in particular, and by the late-stage fluid (probably causing the ferromagnesian phases to be enriched in Mg), even though the primary mineral assemblages may have been preserved. Not all the important changes caused by leaching or redeposition during metasomatism can be shown in the diagram. The changes in alkali and calcium contents are characterized only by the line bordering the field of Ca-Na-K-free phases, which descriptively emphasizes the tendency of the system to form Ca-alkali free assemblages in the most altered zones.

It is not possible, for instance, to show the accumulation of calcium-rich phases at Havukkalammit.

In the northwestern targets, that is, Kallionie-mi and Kauhealampi, successive metasomatism accompanied by shearing caused progressive metasomatic zoning towards the centre of the zones. Alteration started with the disappearance of biotite and a decrease in plagioclase content with a concomitant increase in chlorite and muscovite contents. These changes indicate sodium and calcium leaching with a relative increase in $Al/(Al+Si)$ and ferromagnesian components in rock. During advanced metasomatism, when potassium and silica activities diminished and quartz was fully leached out, kyanite and local staurolite were stabilized, replacing muscovite and chlorite. Metasomatism resulted in the compositions characterized by phase fields (4) and (5) in Fig. 21.

Further east, early-stage metasomatic segregation was more extensive and complex metasomatic zoning (Table 2) developed, as illustrated by the arrows in Fig. 21. The early-stage metasomatic zones with gradual or sharp boundaries can be

detected, but at Hiltuspuro and further south they have often been modified, or even destroyed, by later mineral growth. In the southernmost occurrences it is impossible to separate early- and late-stage mineral growths from each other with the aid of microstructures. At Levävaara and Havukkalammit, well-developed and sharply-defined metasomatic zones (Fig. 13) show diverse complex leaching and deposition of components.

The general alteration trend exhibited by the shaded arrow in Fig. 21 led to the disappearance of quartz; locally quartz is concentrated, redeposited, in fractures. An extreme decrease in silica activity occurred at Levävaara, where corundum stabilized with chlorite and aluminium silicates. The decrease in alkalis and Ca and the relative increase in aluminium and Fe-Mg were important processes that changed the mineral compositions towards parageneses rich in chlorite and kyanite/andalusite±staurolite and poor in plagioclase and biotite as silica activity declined. The relative decrease in iron is also shown by the high X_{Mg} of biotite and chlorite compared with that of the less magnesian primary biotite and hornblende, but this change may partly be a result of later fluid activity. Examples of the deposition of leached components are seen in several occurrences. At Havukkalammit the exceptionally high calcium content, e.g. in Ep-Pl-Cam paragenesis, is due to extensive calcium redeposition. Similarly, the patches of monomineralic biotite or chlorite are evidence of the accumulation of components during metasomatism. In the metasomatic zones in kyanite rocks one phase is often enriched at the cost of the others, thus promoting the formation of monomineralic rocks.

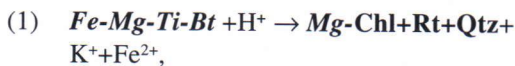
The zones with large tourmaline crystals at Levävaara (Fig. 12) are examples of the deposition of trace elements such as boron.

Mineral reactions

The early-stage reactions were catalysed by saline H_2O fluid as indicated by the fluid inclusions in kyanite (Table 1). Because the fluid inclusion data permit a rough estimation of fluid composition, reactions can be delineated only in simplified forms.

During early-stage metasomatism, silica was a mobile, dominantly consumed component. Above $200^\circ C$, silica is usually released into solution and it combines with water molecules to form a non-tetrahedral $H_4SiO_4^0$ aqueous complex. The dissolution of silica is independent of the concentration of ligands such as chloride or of pH. Under alkaline conditions, silica may dissolve and form alkali silica complexes such as $KH_3SiO_4^-$; silica dissolution then becomes pH dependent. However, the presence of small amounts of chlorine is sufficient to prevent high pH. The solubility of SiO_2 in NaCl solutions increases relative to that in pure water (Sorokin & Dadze 1995, Yardley & Shmulovich 1995). High salinity of fluid during the early stage is indicated by fluid inclusions. Thus, non-alkaline properties during silica leaching are postulated for kyanite rocks. Acid properties of the fluid are also obvious from the mineral assemblages rich in basic components and poor in silica (Korzhinskii 1964). With the exception of reactions producing quartz, silica is not considered in the following formulations.

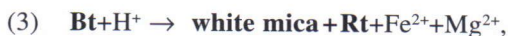
Early-stage shearing was accompanied by decomposition of country rock biotite to chlorite and rutile in the reaction (observed reactants in **bold**)



and formation of muscovite, which, in places, overgrows chlorite. Plagioclase (oligoclase-andesine) has been sericitized; thus, it is likely that the K^+ released in reaction (1) was fixed in muscovite and that especially Na_2O was leached out of the system in the reaction



This process is supported by the increasing quartz content towards the muscovitized part of the shear zones. Locally, white mica (not analysed) was also produced by leaching of ferromagnesian components out of biotite, e.g. in the reaction



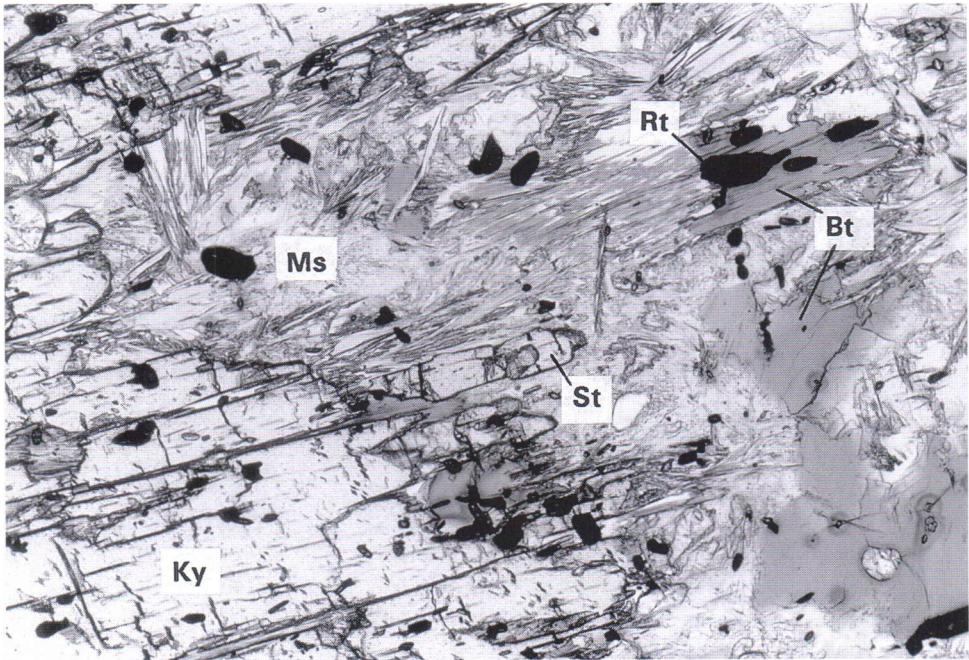


Fig. 22. Leaching of biotite to white mica (seen in upper-right corner) in kyanite-staurolite contact at Levävaara. Later muscovite rims kyanite and staurolite. Field of view c. 4 mm wide. Plane polarized light. Photo by M. Pajunen.

as shown by a sharp alteration front in biotite (Fig. 22).

The microstructures indicate that kyanite and andalusite crystallized more or less simultaneously at Levävaara, whereas at Turkkiavaara and east Havukkalammit andalusite clearly postdates kyanite. Andalusite preceded cordierite, but the exact timing of its crystallization with respect to stage cannot be established. Nevertheless, many reactions are shared by both kyanite and andalusite formation. Kyanite and andalusite with corroded plagioclase (oligoclase-andesine) inclusions (Fig. 23) and kyanite replacing plagioclase along grain boundaries refer to decomposition of plagioclase to aluminium silicate directly in the leaching reaction

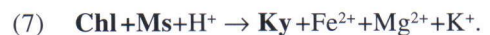


Andalusite-quartz symplectite in the andalusite-plagioclase interface and small quartz grains in the contact of kyanite with plagioclase are interpreted

as products of such a reaction. SiO_2 often dissolved in fluid and deposited elsewhere in dilatational fractures. The kyanite and andalusite frequently contain corroded muscovite inclusions; in such cases Al-silicate formation is attributed to the decomposition of white mica, muscovite and/or paragonite, in reactions (2),



Chlorite and muscovite occur as separate inclusions, often as homoaxial relics after larger grains, in kyanite indicating the leaching reaction



Silica and potassium dissolved in fluid, and/or a new generation of biotite formed, as exemplified by the biotite-kyanite rock at Havukkalammit. Biotite was also decomposed to kyanite in a

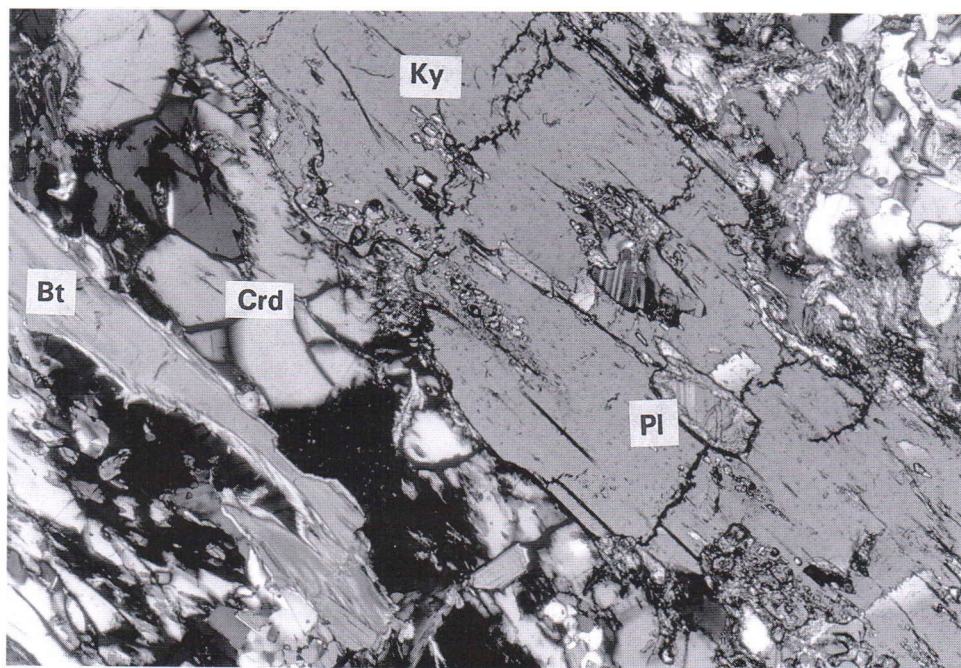
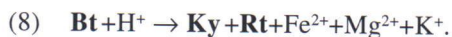
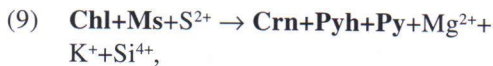


Fig. 23. Corroded plagioclase relics in metasomatic kyanite in narrow zone at Hiltuspuro. Kyanite rimmed by later cordierite, which also replaces biotite. Field of view c. 4 mm wide. Crossed nicols. Photo by M. Pajunen.

metasomatic reaction that released ferromagnesian components and potassium:



At Levävaara, rare sulphurization of intermediate phases has led to corundum formation. Evidence of such a reaction,



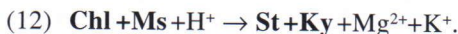
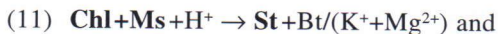
is the sulphide inclusions in corundum. An example of corundum replacing white mica in the leaching reaction,



is shown in Fig. 24. The lack of sulphides or other indications of sulphurization reactions elsewhere in the kyanite rocks suggests their poor sulphide-ore potential. Aluminium is usually considered an

immobile component in metamorphic processes but, as pointed out by Anderson and Burnham (1983), the solubility of aluminium depends on the prevailing conditions – especially on the (KCl, NaCl)/HCl ratio and, thus, on the pH of the fluid. Thus, the relative enrichment of kyanite rock in aluminium may be partly due to the precipitation of Al from solution (cf. Korzhinskii 1964).

Staurolite is a minor phase with kyanite but it is abundant in parageneses St-Chl-Pl and St-Chl-Ms-Pl. Staurolite is free of inclusions and the corroded grains are surrounded by later cordierite or by retrograde muscovite. In the light of the staurolite-bearing assemblages we suggest that staurolite was formed largely in prograde reactions between muscovite and chlorite, e.g.



Staurolite-forming reactions may also be writ-

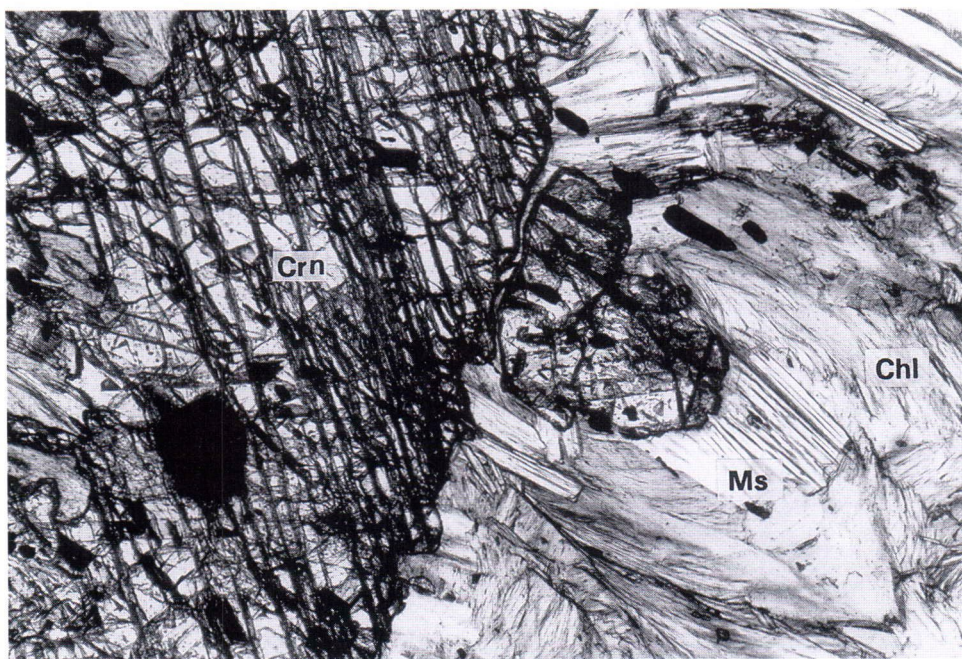


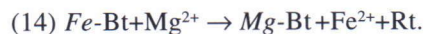
Fig. 24. Corundum replaces muscovite at Levävaara. Field of view c. 4 mm wide. Plane polarized light. Photo by M. Pajunen.

ten as isochemical ones. Staurolite, however, always occurs in quartz-free assemblages, which is not expected in the isochemical reaction after chlorite and muscovite. Thus, according to our interpretation, the more probable staurolite-forming reactions are the metasomatic leaching reactions described above.

It is also impossible to explain the large amounts of chlorite, biotite, plagioclase and kyanite present in certain rock compositions without complex fluid-induced leaching and deposition. The large, zonal albite porphyroblasts in biotite-plagioclase and chlorite-plagioclase rocks at Levävaara and Hiltuspuro record “episodic” re-deposition of sodium. The rim of anorthite-rich plagioclase between biotite and kyanite at Havukalammit (Fig. 25) is difficult to explain without metasomatic deposition of calcium from fluid to replace the ferromagnesian components and potassium in the kyanite-biotite interface. The reaction may be formulated as



Aggregation of coarse-grained biotite and chlorite indicates deposition of potassium and magnesium. The compositions of biotite and chlorite may also have restabilized and homogenized (see Fig. 18 and Appendices 8 and 9) in an exchange reaction with the Mg-rich solution



As stated by Korzhinskii (1970), the metasomatic zones formed through the infiltration process have homogeneous phase compositions (see Fig. 18) and a tendency to form monomineralic zones (Fig. 11). Such features are well displayed in the far-advanced metasomatic zones of the early-stage kyanite rocks.

Late stage

Mineral assemblages

A sharp break between the early-stage and late-stage mineral reactions is not indicated by the

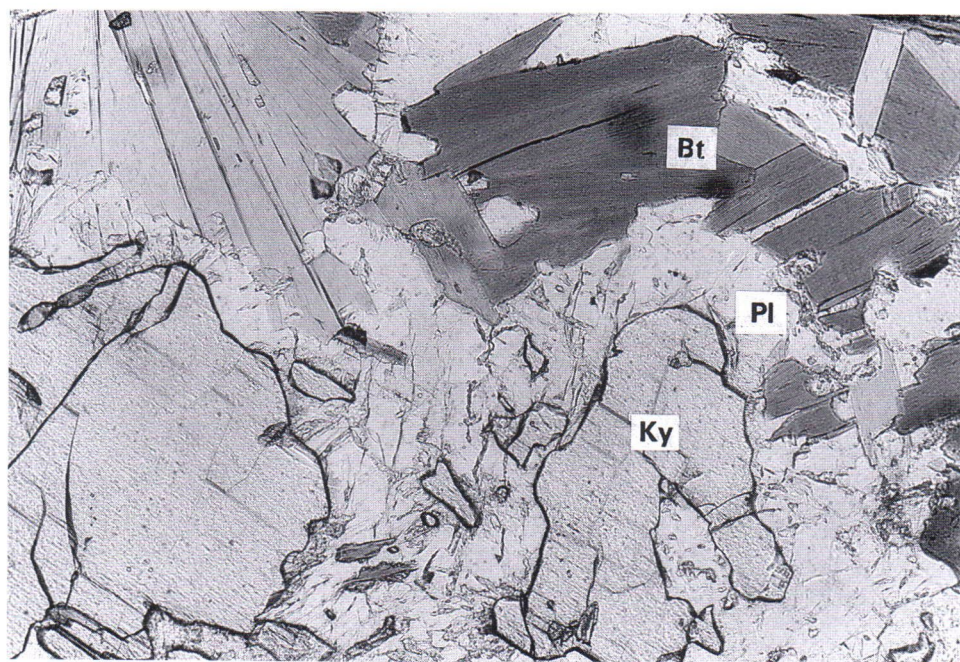


Fig. 25. Metasomatic plagioclase, An_{59-75} , reaction rim between kyanite and biotite at Havukkalammit. Field of view c. 2 mm wide. Plane polarized light. Photo by M. Pajunen.

mineral growth succession alone, because many of the mineral reactions described above continued during the late stage. Differences in structure are, however, striking. The typical late-stage cordierite-sillimanite-bearing parageneses crystallized in dilatational semi-brittle fracture zones (Fig. 4), in patches (Fig. 16) or along fractures in grain boundaries (Fig. 17). The pseudosecondary CO_2 fluid inclusions in cordierite indicate a change in fluid composition after the early stage.

Metasomatic zoning is not as pronounced as that of the early stage (Table 2). The mineral parageneses at Hiltuspuro and Tetrilampi are shown in the $Si/(Si+Al)$ vs. $Mg/(Mg+Fe+Mn)$ diagram (Fig. 26). The late-stage assemblages often occur in dilatational structures replacing earlier phases along their boundaries. The most characteristic feature of this stage is the crystallization of cordierite, which replaces all the other phases in the rock. Plagioclase and biotite are disappearing phases, and alkalis and calcium become mobile components. Biotite has often redeposited in the vicinity of the cordierite-rich portions of altered

rocks. Late-stage metasomatism shifts the mineral compositions towards the Mg edge on the Mg-Fe composition plane, implying the Mg metasomatism was the main alteration process during the late stage as shown by the shaded arrow in Fig. 26. During the early stage, silica leaching was pronounced. In contrast, the late-stage assemblages rich in cordierite and quartz indicate higher silica activity.

Mineral reactions

Progression during the late stage is characterized by metasomatic replacement reactions, but isochemical reactions also occurred. Changes in crystallization conditions, especially in temperature, are evidenced by the polymorphic transformation



Reaction (15), which is typical of the south of the area, and the corresponding kyanite-andalusite \pm sillimanite succession in the north of the area

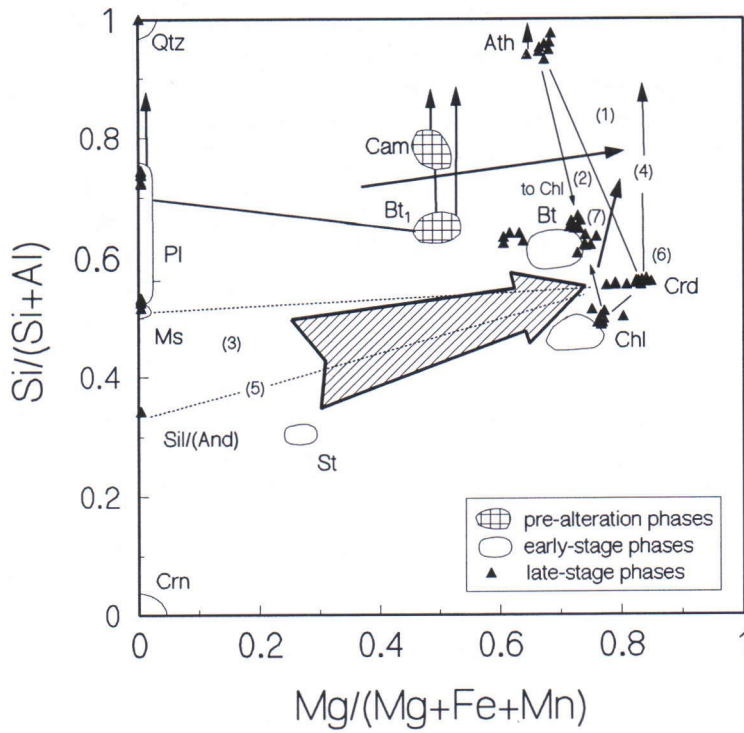


Fig. 26. Compositions of late-stage phases in tonalites shown on Si/(Si+Al) vs. Mg/(Mg+Fe+Mn) diagram. The mineral compositions are from Hiltuspuro and Tetrilampi. The directions of metasomatism are shown schematically by arrows and the general trend of alteration by hatched arrow. Typical mineral assemblages are indicated by numbers in parentheses.

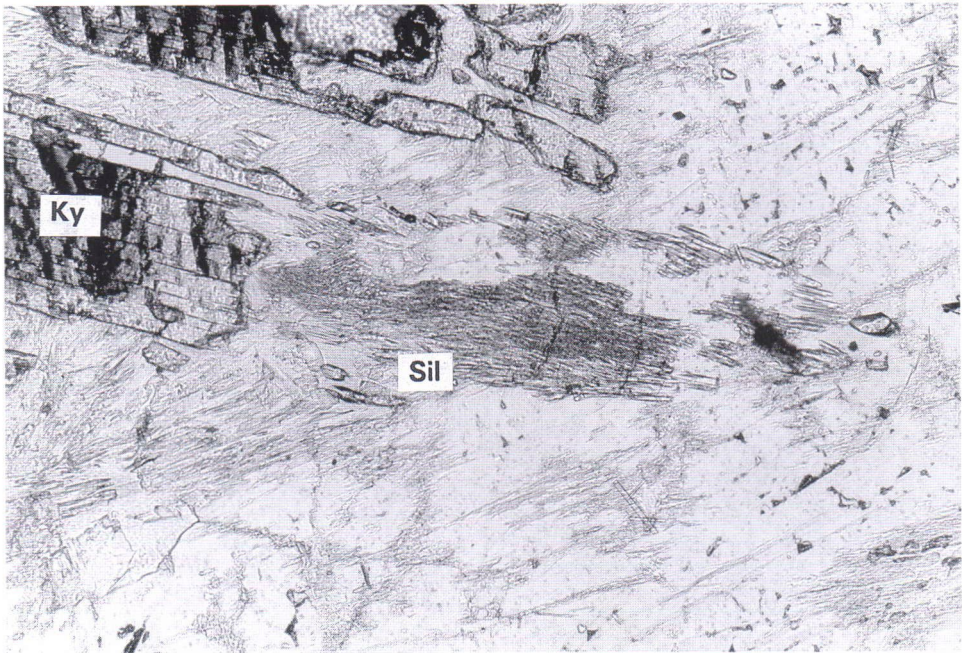
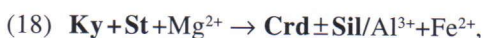
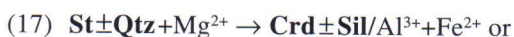


Fig. 27. Kyanite has transformed to sillimanite at Hiltuspuro. Field of view c. 2 mm wide. Plane polarized light. Photo by M. Pajunen.

(cf. Turkkivaara and east Havukkalammit) apparently indicate small variations in local P-T paths (see later). Sillimanite is frequently a by-product of the cordierite-forming reactions. Staurolite and kyanite exist as corroded relics in cordierite (Fig. 8). Staurolite and quartz are not in contact with each other, suggesting the prograde, isochemical reaction



In our opinion, however, it is more plausible that staurolite decomposed in metasomatic reactions with Mg^{2+} in fluid. The reactions could be formulated as



both of which explain, in a simpler way, the observed amounts of phases and the mass balance

of components, e.g. between magnesium and iron. Decomposition of plagioclase rarely produced fibrous sillimanite (cf. reactions 4–6). Sillimanite also formed in narrow shear zones by leaching of biotite and plagioclase (cf. reactions 4 and 8).

Cordierite has grown over all other rock-forming minerals, producing the final paragenesis, Crd-Qtz-Rt-Sil, with corroded relics of pre-existing phases (Fig. 7). Many cordierite-producing reactions are Mg metasomatic and need mobile components for stoichiometry. For example, replacement structures, in which cordierite exploits the earlier phases, such as country-rock plagioclase (Fig. 17), cannot be explained without total rearrangement of the elements, as in the reaction



A narrow rim of paragonitic white mica between the corroded plagioclase and cordierite shows that, at least locally, replacement of plagioclase by cordierite proceeded through a paragonitic mica phase formulated as

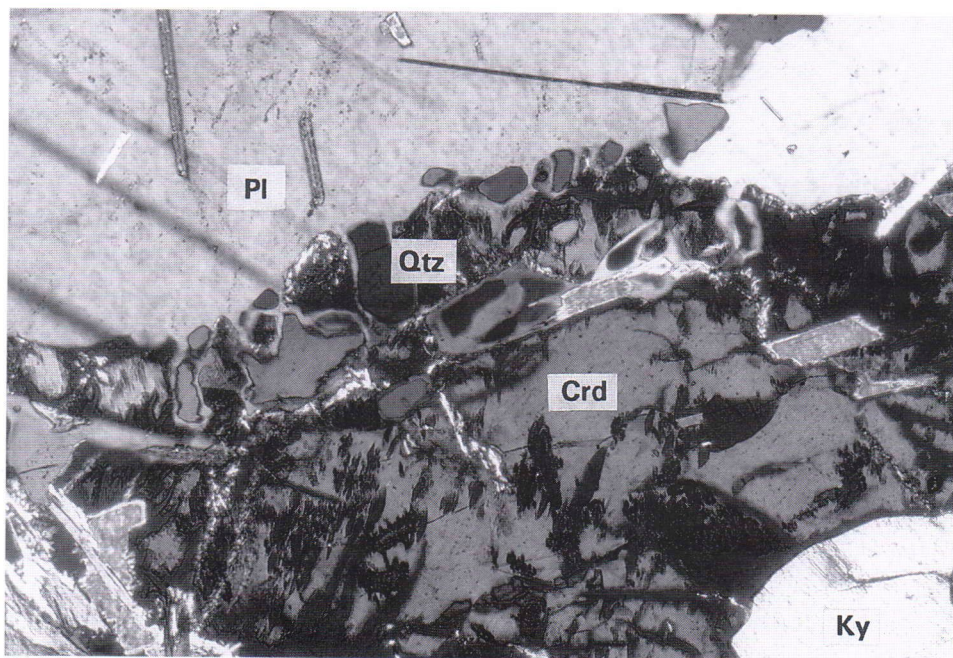
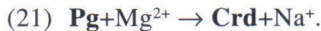
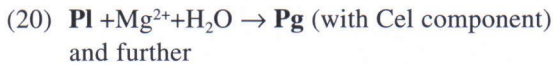


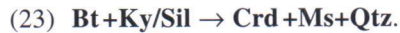
Fig. 28. Microstructure produced by metasomatic breakdown reaction of plagioclase with Mg-rich fluid to cordierite and quartz. Field of view c. 2 mm wide. Crossed nicols. Photo by M. Pajunen.



Formation of cordierite through a mica phase is also postulated by the chloritic alteration rim in the cordieritization front, as exemplified at Tuomaanvaara (Fig. 16). A distinctive cordierite-forming reaction is the decomposition of biotite with kyanite in the reaction



Potassium was expelled from the system in all breakdown reactions of biotite and was deposited in the coarse-grained, randomly oriented biotite aggregates characteristic of the targets with abundant cordierite. Exceptionally, at Tetrilampi, muscovite crystallized in a cordierite-producing biotite-breakdown reaction, which may be formulated as isochemical



The isochemical chlorite breakdown reaction (24) was locally an important cordierite-forming reaction, too.



At Hiltuspuro, the orthoamphibole-cordierite assemblage replaces biotite and chlorite. The prograde, possibly isochemical, decomposition of quartz and chlorite produced orthoamphibole in the reaction



and locally also cordierite in the reaction



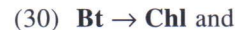
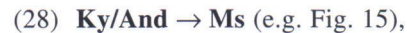
Orthoamphibole is anthophyllitic in composition except in reaction (26), which also produced concurrent gedrite in fibrous aggregates (Fig. 29). Anthophyllite replaces biotite in the metasomatic reaction



Note that cordierite- and anthophyllite-bearing rock is a real metasomatic rock with a tonalitic precursor preserved as a relic in outcrops. A similar example of magnesia metasomatism of meta-diorite to cordierite-anthophyllite rock has been described from Hirvas, northern Finland, by Härme and Perttunen (1971).

Cooling stage

In general, progressive metasomatic-metamorphic assemblages undergo only weak alterations in late retrogression. Reactions such as



are related to late hydration and carbonization processes during the cooling stage. Weak retrogression is a strong indication of quick termination of fluidization and rapid cooling. Secondary fluid inclusions in kyanite and cordierite record late mobility of both CO_2 - and H_2O -bearing fluids. Sericitization also indicates an increase in the activity of potassium in fluid during retrogression.

METAMORPHIC HISTORY

Regional metamorphism

The main features of the Archaean metamorphic evolution were described in section "Geological outline" (pp. 76–77). To summarize, the regional metamorphic peak conditions of amphibolite to granulite facies were attained in the TTG areas, but only greenschist to amphibolite facies conditions in the greenstone belts. The peak metamorphic parageneses are overprinted by epidote-amphibolite or greenschist facies retrogression. Ac-

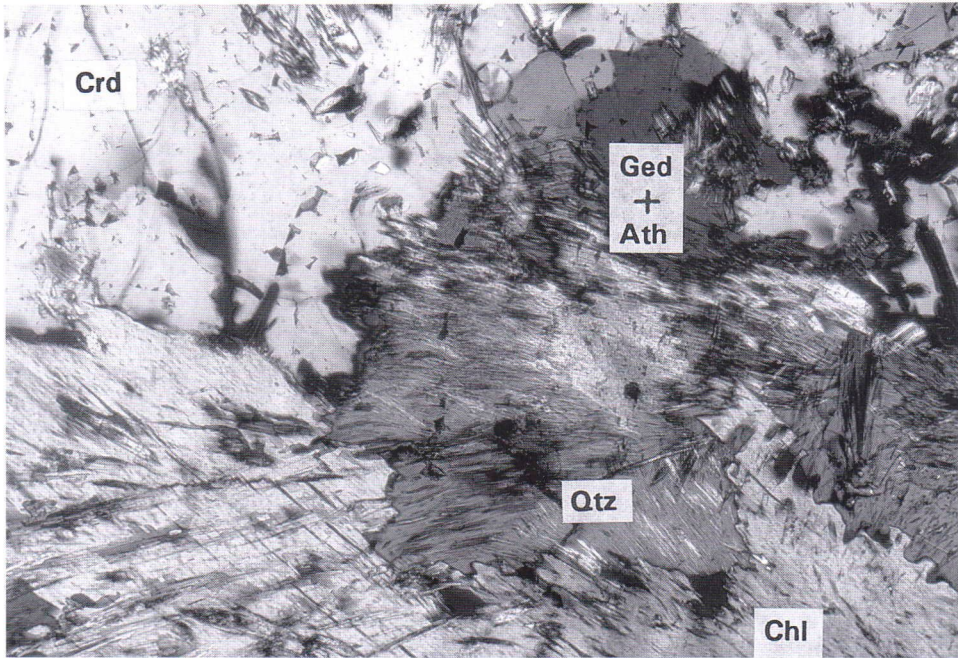


Fig. 29. Chlorite-quartz breakdown reaction has produced anthophyllite, gedrite and cordierite at Hiltuspuro. Field of view c. 2 mm wide. Crossed nicols. Photo by M. Pajunen.

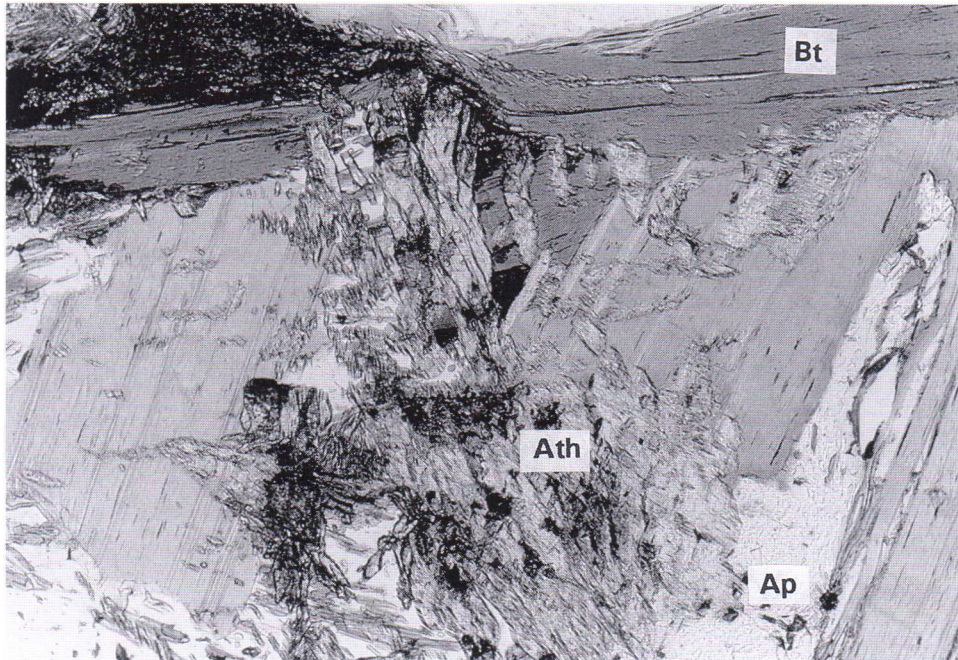


Fig. 30. Anthophyllite replaces biotite at Hiltuspuro. Field of view c. 2 mm wide. Plane polarized light. Photo by M. Pajunen.

cording to Luukkonen (1992), the crust had largely been cratonized before the Neoproterozoic deformation events, D₄, D₅ and D₆. Cooling had advanced to a low temperature and crust rigidity was high. Low-temperature epidote-filled fractures are cross-cut by Palaeoproterozoic diabase dykes in several places. The kyanite-bearing mineral assemblages penetrate the stabilized Archaean structures. Similar structures with metasomatic alteration also cut the amphibolite-facies metamorphic fabrics in the Palaeoproterozoic metadiabase dykes. Thus, the generation of kyanite rocks represents a Palaeoproterozoic reactivation event in the Archaean crust of eastern Finland.

Early-stage P-T conditions

The peak P-T conditions of the early stage are constrained by stabilization of the kyanite-staurolite assemblages. The increase in temperature is confirmed by reactions from Ms-Chl-Qtz to St-Ky. The minimum pressure of kyanite-staurolite stabilization is about 4.5–5 kbar on the basis of the andalusite-kyanite stabilities of Holland and Powell (1990) and the staurolite-in reaction of Winkler (1979). The mineral assemblages at Havukkalammit thought to represent early-stage conditions were tested with TWEEQU software (Berman 1991) using the thermodynamic dataset of Holland and Powell (1990). The assemblages did not, however, show equilibrium conditions, probably due to the late-stage reorganization of components.

The isochore for the primary fluid inclusions in kyanite is located in the stability field of andalusite-sillimanite (Fig. 31). This may indicate that fluid pressure was lower than lithostatic pressure (Walther 1990) during the entrapment or later re-equilibration of the inclusions. At Levävaara, andalusite and kyanite crystallized simultaneously, implying that kyanite crystallized under conditions close to those of the kyanite-andalusite reaction boundary. In contrast, at Turkkivaara and east Havukkalammit, andalusite postdates kyanite. The dissimilar crystallization sequences of aluminium silicates in various targets reflect slight differences in crystallization pressures between targets. It is possible that at Turkkivaara and east Havukkalam-

mit, andalusite was not stabilized until the late stage, in equilibrium with cordierite. The upper temperature limit during the early stage can be established from the breakdown reactions, St+Qtz and Chl+Qtz, and the polymorphic change of kyanite to sillimanite at about 600°C (Fig. 31).

Late-stage P-T conditions

The reaction history of kyanite rocks demonstrates that metasomatism occurred during the progression from greenschist to amphibolite facies conditions. The increase in temperature is well documented by prograde reactions from kyanite and andalusite stability fields to the sillimanite stability field (Figs. 8 and 27).

Decomposition of staurolite and quartz to cordierite and sillimanite is reliable evidence of an increase in temperature. Reaction (16) was experimentally studied by Richardson (1968) for the Fe-Al-Si-O-H system. In a Mg-free system the reaction proceeds at low pressures (2–2.5 kbar/600°C), but Richardson (op. cit.) expects the stability field of Mg-bearing staurolite with quartz to be wider in temperature and, especially, to shift towards higher pressure. Here, the reaction was studied as an isochemical one (cf. p. 103) with TWEEQU software (Berman 1991) using the thermodynamic dataset of Holland and Powell (1990). The result (reaction A in Fig. 31) shows that the pressure estimate at 600°C coincides well with the other data. $X_{\text{H}_2\text{O}}$ is estimated to be 1.0 in all TWEEQU calculations. It is probable that the actual value was somewhat lower, but its effect on geological interpretation is small. The uncertainties in estimations are discussed in Holland and Powell (1990) and Berman (1991).

The chlorite breakdown reaction with quartz (26) produced anthophyllite-gedrite fibroblasts (Fig. 29) in which gedrite and anthophyllite occur as separate grains. The stability field of the Chl-Qtz assemblage was studied by Fleming and Fawcett (1976). They found that, for a Mg-rich composition, the pair is stable up to the kyanite-sillimanite reaction boundary at a pressure of about 4 kbar and is thus stable at the temperature achieved during the early stage. A crest in the

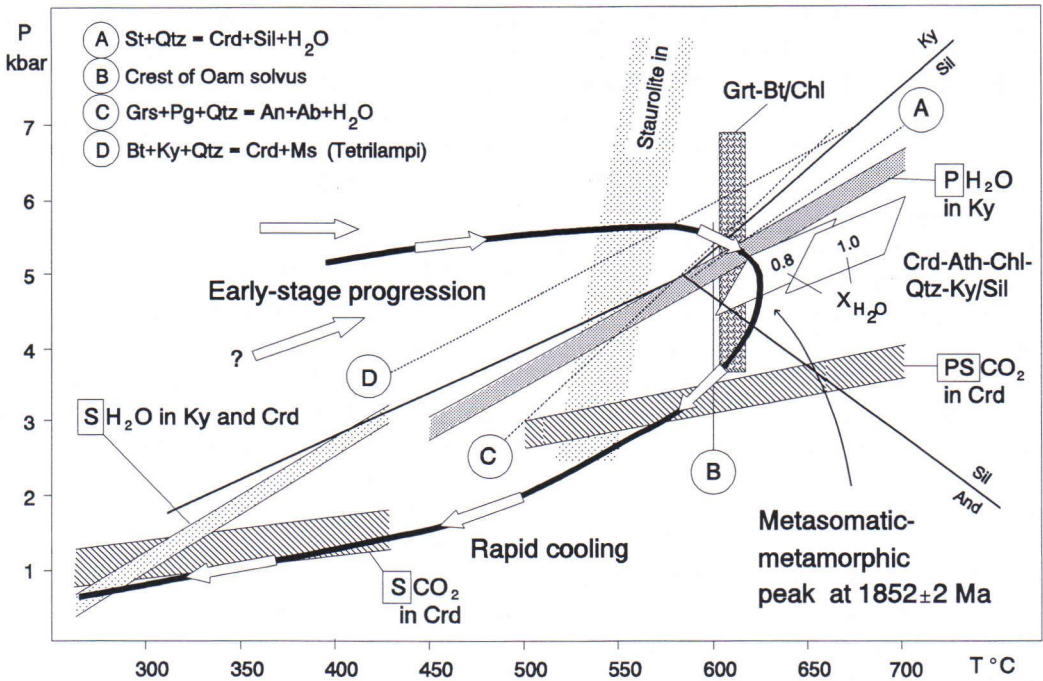


Fig. 31. Palaeoproterozoic P-T evolution of kyanite rocks at Hiltuspuro and Tetrilampi. The path is based on temperature determinations (Grt-Bt/Chl; Table 3), on TWEEQU analysis of assemblage Crd-Ath-Chl-Qtz-Ky/Sil and reactions A-D (see text), and on fluid inclusion data (P = primary inclusion, PS = pseudosecondary inclusion and S = secondary inclusion; Table 1). Aluminium silicate stabilities are from Holland and Powell (1990) and staurolite stability from Winkler (1979).

miscibility gap between the anthophyllite and gedrite series (Robinson et al. 1982) is estimated to lie at about 600°C in samples with a bulk X_{Mg} of 0.6 (Spear 1980). The pressure dependence of the solvus has not been established, but the critical curve is suggested to have a positive dP/dT (Crowley & Spear 1981). On the other hand, the production of two orthoamphibole generations in one reaction and the number of reactions with only one phase imply that the reaction took place close to the temperature of the solid solution gap. The outcome of the TWEEQU calculation of the Mg-rich assemblage, Ath-Crd-Am-Ky/Sil-Qtz, is presented in Fig. 31 with estimated X_{H_2O} values 1.0 and 0.8. The variation in values, c. 610–650°C/4.5–5.0 kbar, is small and mainly in temperature. At the temperature given by the garnet-biotite/chlorite thermometer, the calculated value of X_{H_2O} is approximately 0.7–0.8. The effect of the varia-

tion in X_{H_2O} on pressure estimation is insignificant for geological interpretations.

The garnet-quartz rock at northwest Hiltuspuro enables us to calculate temperature by thermometry based on Mg-Fe exchange in the mineral pairs chlorite-garnet and biotite-garnet. The analyses were made on a garnet partly replaced by chlorite and on a portion of a younger garnet generation rimming the chloritized part of the grain (Fig. 32). We attribute the growth of the garnet rims to the increase in temperature during late-stage alteration – late-stage parageneses are well developed in adjacent outcrops. The most reliable estimates were obtained with the consistent program GEOPATH (Gerya & Perchuk 1992) (Table 3). The garnet core gives only an indicative average temperature of 638°C (sx = 14.6°C), maximum 652°C. The rim garnet compositions give an average T of 602°C (sx = 11.6°C), maximum

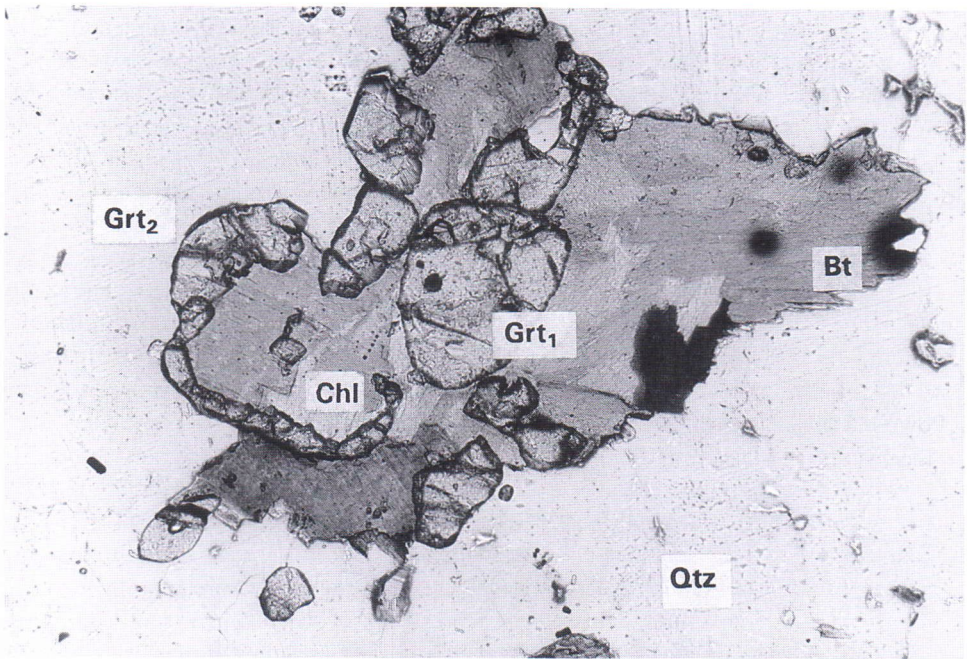


Fig. 32. Garnet-chlorite-biotite assemblage in garnet-quartz rock at Hiltuspuro. Garnet (Grt_1) is replaced by chlorite, which is rimmed by later garnet (Grt_2). Field of view c. 4 mm wide. Plane polarized light. Photo by M. Pajunen.

Table 3. Garnet-biotite and garnet-chlorite temperature estimates (G&P; Gerya & Perchuk 1992) of garnet-quartz rock at Hiltuspuro.

Grt-Bt	Analysis no. (*)	19&78	20&78	22&78	20&79	21&79	22&79
	Analysis point (**)	R-R	C-R	R-R	C-R	R-R	R-R
Grt	X_{Alm}	0.615	0.595	0.604	0.595	0.610	0.604
Grt	X_{Prp}	0.073	0.086	0.074	0.086	0.072	0.074
Grt	X_{Sps}	0.226	0.211	0.225	0.211	0.218	0.225
Grt	X_{Grs}	0.087	0.108	0.098	0.108	0.100	0.098
Bi	X_{Mg}	0.317	0.317	0.317	0.355	0.355	0.355
T°C	G&P	610	651	615	616	579	583
Grt-Chl	Analysis no. (*)	20&91	22&91	20&92	22&92	20&93	22&93
	Analysis point (**)	C-R	R-R	C-R	R-R	C-R	R-R
Grt	X_{Alm}	0.595	0.604	0.595	0.604	0.595	0.604
Grt	X_{Prp}	0.086	0.074	0.086	0.074	0.086	0.074
Grt	X_{Sps}	0.211	0.225	0.211	0.225	0.211	0.225
Grt	X_{Grs}	0.108	0.098	0.108	0.098	0.108	0.098
Chl	X_{Mg}	0.355	0.355	0.338	0.338	0.354	0.354
T°C	G&P	637	603	652	617	638	603

(*) analysis numbers in Appendices 5, 8 and 9.

(**) R = rim and C = core

617°C. Pressure was estimated to be 5 kbar and $X_{\text{H}_2\text{O}}$ 1.0 in both calculations. The P-dependence of temperature is restricted and the estimated pressure coincides well with other observations, e.g. the kyanite-sillimanite transformation. The rim of a large garnet generation portion coexists with Ms-P1-Qtz. The stability of the reaction



was calculated with TWEEQU (Berman 1990, 1991), using the thermodynamic dataset of Holland and Powell (1990). Reaction C (Fig. 31) runs very near the kyanite-sillimanite reaction boundary.

The late-stage structures are due to the pronounced effect of fluid – static replacement reactions along microfractures in grain boundaries, for instance. The pseudosecondary fluid inclusions in cordierite record c. 4 kbar pressure at the peak temperature; this is about 1 kbar lower than suggested by the kyanite-sillimanite transformation and reactions A, C and D (Fig. 31).

At the upper crustal levels of brittle behaviour, fluid pressure is hydrostatic, $P_f = P_h$, but at greater depth it approaches lithostatic pressure, P_l , that is suprahydrostatic fluid pressure or fluid overpressure, because of decreasing porosity (e.g. Gavrilenko & Gueguen 1993). At great depths, beneath the level of brittle-ductile transition of the crust, fluid pressure is proposed to be lithostatic, $P_f = P_l$ (Walther 1990). Thus, a layered division of crustal fluid convection and P_f regime is suggested (e.g. Etheridge et al. 1983, Oliver et al. 1990, Ivanov & Ivanov 1993). Supralithostatic fluid pressures, $P_f > P_l$, may be maintained only briefly and locally (see Sibson 1992, Gavrilenko & Gueguen 1993), because of the tensile fracturing that may occur when P_f exceeds the minimum principal compressional stress, σ_3 , of the rock (e.g. Etheridge et al. 1983).

It is unlikely that the medium-pressure assemblages in the kyanite rocks were formed due to high fluid pressure caused by fluid entrapment, because there are no signs of such a widespread trap system in the Nurmes–Sotkamo area. Moreover, the high density contrast between the fluid

and tonalitic country rock forces the hot fluid to upwell at P_f lower than P_l (cf. Lister & Kerr 1991). The high temperature supercritical fluids have very low viscosities and therefore also high mobilities (Wickham 1992). Some structures, such as microfracturing and subsequent metasomatism along grain boundaries, suggest fluid agility in places, but high fluid overpressures causing a systematic metasomatic-metamorphic reaction series such as that in kyanite rocks is not plausible. The early-stage structures are well preserved from the later violent brecciation that could be expected to form if high fluid pressures should relax. Thus, as we see it, the pressure obtained, 4–5 kbar, is really lithostatic, and it is even possible that fluid pressure followed its own path at lower pressure. This interpretation is supported by metamorphic assemblages suggesting corresponding crystallization pressures in the neighbouring Palaeoproterozoic North Karelia Schist Belt (Koistinen 1981, Treloar et al. 1981, Halden & Bowes 1984) and Kainuu Schist Belt (Tuisku & Laajoki 1990, Tuisku 1991). Because all the reactions described (e.g. A, C and D in Fig. 31) are to some extent dependent on pressure and because the lower pressure assemblages have a clear tendency to stabilization, some exhumation must have occurred between the early and late stages. The pressure estimate implies that, during the late stage, the Nurmes–Sotkamo area was thickly covered by Archaean ± Palaeoproterozoic crust. The calculated depth ($P = \rho * h * g$, where ρ = density, h = height and g = gravitational acceleration) is about 15.7–19.6 km on the basis of the average density of rocks, 2600 kg/m³, in the Nurmes–Sotkamo area (see Yliniemi et al. 1993), or about 11.7 km on the basis of fluid inclusion isochores and assuming that the pressure of inclusions represents lithostatic pressure.

The mineral assemblages of metasomatic rocks imply an overall increase in metamorphic grade southwards. Thus, the late thermal event, characterized by CO₂-rich fluid, was more pronounced in the south, but was not absent from the north either, e.g. Tuomaanvaara, Turkkivaara and east Havukkalammit. According to the microstructure it is possible that andalusite stabilized with cordierite at east Havukkalammit and Turkkivaara

during the late stage. At Turkkivaara, the temperature continued to rise in the sillimanite field, but at east Havukkalammit the thermal peak was achieved under andalusite field conditions, suggesting a slight difference in peak temperatures between occurrences.

ISOTOPE GEOLOGY

Radioactive mineral inclusions causing a yellow halo in cordierite are typical of the cordierite-bearing samples (Fig. 33). A coarse-grained kyanite-chlorite-cordierite rock sample (A1298) from southeast Hiltuspuro (see Figs. 2b, 3 and 5) was separated for isotopic study. Xenotime, which becomes enriched in the heavy, $>4.3 \text{ g/cm}^3$, 1.4 A, magnetic Franz fraction, occurred as fresh, yellowish or greenish grains with few crystal faces. The length/width ratio of the crystals, 70–160 μm in diameter, was close to 1. The majority of the grains were translucent, but cloudy, poikiloblastic grains also occurred.

Two U-Pb analyses (Table 4) were made in the Isotopic Laboratory of the Geological Survey of Finland in Espoo. Concordant analyses gave a very accurate age of $1852 \pm 2 \text{ Ma}$ (Fig. 34). A very high U content and low common lead content are characteristic of the analyses.

The crystallization of the cordierite-sillimanite paragenesis represents metamorphic peak conditions of kyanite rocks at about 600–620°C/4–5 kbar. Xenotime is intimately associated with these highest grade phases, indicating that the radioactive elements, and REE and the closely related yttrium, were mobilized under approximately such conditions. Enrichment of the radioactive components, U and Th, in shear zones has been observed by some workers, e.g. Kerrich et al. (1991). According to Aleinikoff and Grauch (1990), REE transport in fluid occurs in carbonate, phosphate or sulphate complexes or in fluorine-rich fluids. During late-stage alteration, the fluid was rich in CO_2 , and phosphates, apatite and xenotime are fairly common minerals. Transport of REE as carbonate and phosphate complexes is

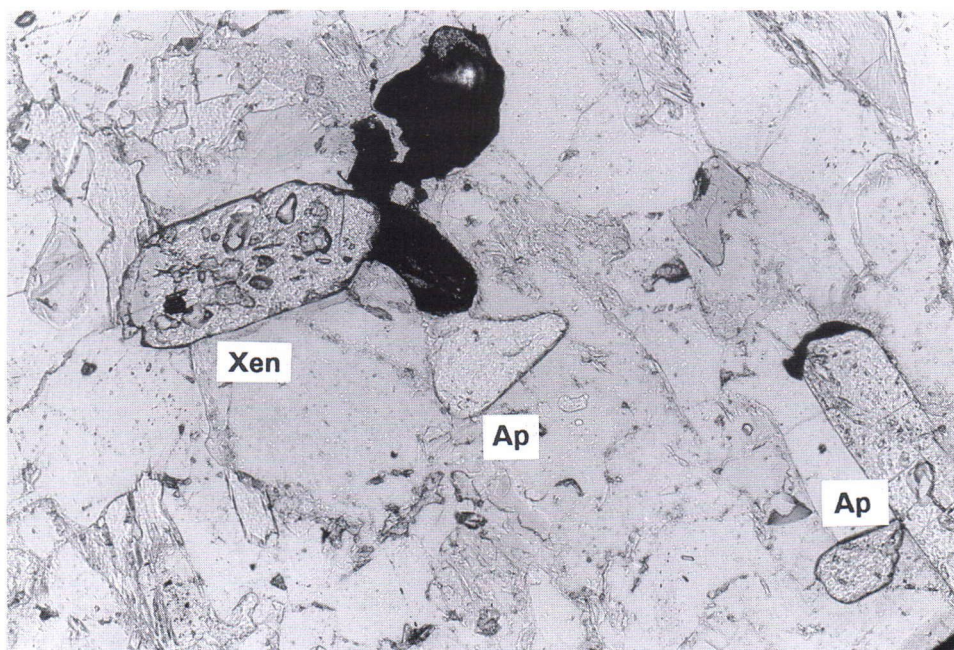


Fig. 33. Xenotime and apatite in cordierite-rich assemblage at Hiltuspuro. Field of view c. 2 mm wide. Plane polarized light. Photo by M. Pajunen.

Table 4. U-Pb data on xenotime of kyanite-chlorite-cordierite rock (sample A1298) at Hiltuspuro (x=7070.51 and y=4485.25).

Sample	density / size (g/cm ³) (μm)	²³⁸ U (ppm)	²⁰⁶ Pb (ppm)	Measured		1)	1)	2)	2)	Age (Ma)	
				²⁰⁶ Pb/ ²⁰⁴ Pb	²⁰⁷ Pb/ ²⁰⁶ Pb	²⁰⁸ Pb/ ²⁰⁶ Pb	²⁰⁶ Pb/ ²³⁸ U	²⁰⁷ Pb/ ²³⁵ U	²⁰⁶ Pb/ ²³⁸ U	²⁰⁷ Pb/ ²³⁵ U	²⁰⁷ Pb/ ²⁰⁶ Pb
A1298A	>4.3 / >70	9483	2653	90608	.1134	.1046	.32331	5.0504	1805	1827	1853
A1298B	>4.3 / >70	10748	3069	75066	.1133	.1209	.33000	5.1519	1838	1844	1852

1) Corrected for blank (0.5 ng Pb).
 2) Corrected for blank and common lead (Stacey & Kramers 1975).

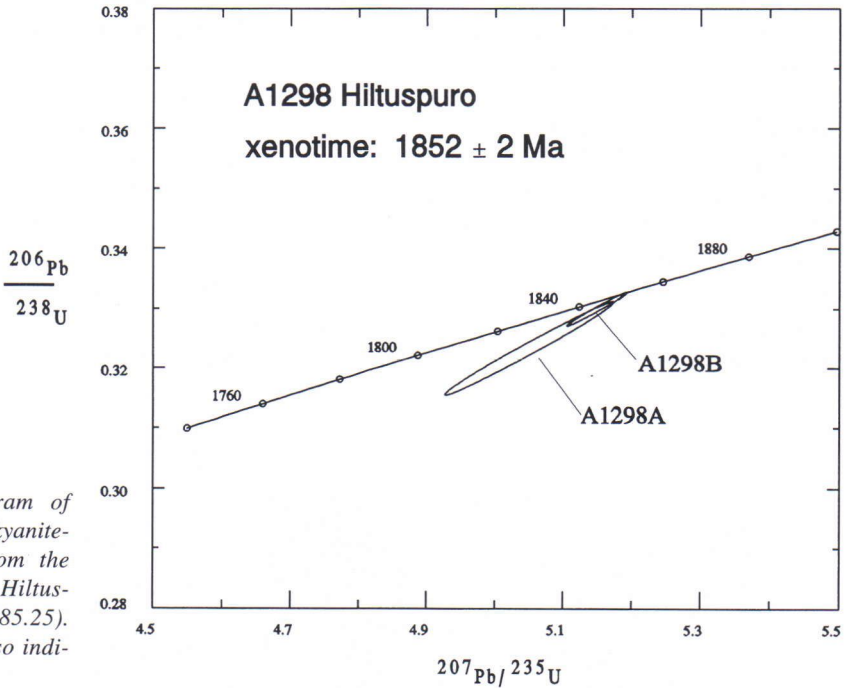


Fig. 34. Concordia diagram of xenotime of coarse-grained kyanite-chlorite-cordierite rock from the outcrop shown in Fig. 3 at Hiltuspuro (x=7070.51, y=4485.25). Sample site (A1298A–B) also indicated in Figs. 2b and 5.

thus possible. For the Hiltuspuro carbonate minerals, this would imply precipitation of carbonate complexes; these are, however, rare. Instead, the abundant phosphates suggest that phosphate complexes were the most probable media of transport and deposition. Even slight changes in pH result in phosphate destabilization and deposition (Mineyev 1963).

Schärer et al. (1990) reported xenotime and monazite ages on a leucogranitic intrusion in the Ailao Shan-Red River shear zone in China. They found no significant differences between the dates

and concluded that the U-Pb closure in xenotime corresponds to that of monazite. Monazite closure temperature estimates vary between 530°C (Wagner et al. 1977) and 720–750°C (Copeland et al. 1988). Observations of Smith and Barreiro (1990) suggest that monazite is immune to lead loss and resetting of the U-Pb clock at or below upper sillimanite grade metamorphism. Thus, the closure temperature of xenotime is thought to be close to the temperature obtained from Hiltuspuro. Smith and Barreiro (1990) found that metamorphic monazite (xenotime?) may even crystallize under stau-

rolite-grade conditions, at above $525 \pm 25^\circ\text{C}$ and 3.1 ± 0.5 kbar. The faint signs of retrograde processes after the peak conditions, at Hiltuspuro in particular, mean that the fluid activity and crustal cooling, and, thus, the U-Pb blocking of xenotime, terminated rather rapidly. Therefore, the age 1852 ± 2 Ma refers reasonably well to the time of the thermal peak.

DISCUSSION

Confirming the actual metasomatic nature of a rock without studying the relation of the metasomatic process to tectonic structures is often difficult; in other words, we have to verify that the alteration overprints an earlier tectonic-metamorphic feature. It is important to distinguish between metasomatism and syngenetic alteration, especially, when interpreting genetic features of ores. The diverse theories formulated on the genesis of cordierite-anthophyllite rocks and the base metal sulphide ores related to them or in their vicinity are a good example.

Structural and metamorphic studies show that the Archaean crust was largely cratonized and that cooling was far advanced during the last Neoproterozoic tectonic events. As illustrated by Figs. 4, 9, 12 and 16, the kyanite rocks crosscut the regional metamorphic structures in the Archaean tonalitic rocks. Thus, their formation represents a new tectonic, metamorphic and metasomatic episode and reactivation of the Archaean crust.

The assemblages in kyanite rocks show metasomatism under prograde metamorphic conditions, from Chl-Ms-Qtz to Ky-St and further to Crd-Sil stabilities. The earliest assemblages of kyanite rocks represent lower-grade metamorphic conditions than do those in their host rocks. The differences in metasomatic mineral growth successions in various locations indicate fluctuations in metasomatic-metamorphic conditions. The differences are clearest in Al-silicate crystallization sequences: Ky (Kallioniemi, Kauhealampi and Korpilampi), Ky-Ky (Havukkalammit), Ky-And (east Havukkalammit), Ky-And-Sil (Turkkivaara), Ky/

And-Sil (Levävaara) and Ky-Sil (Hiltuspuro, Teljo and Tetrilampi) (Fig. 35). It is obvious that in shear, fault and fracture zones metasomatic-metamorphic reactions proceed to completion in some parts of the zone whereas in others the rock may be totally unaffected. The progression of reactions also depends on the structural state of the reactive zone, i.e. on the openness of the zone for fluids. Besides, it is unlikely that analogous reactions always took place simultaneously in different zones. Even if no mineral reactions can be detected, phases may be restabilized by exchange reactions. The P-T paths of the zones studied cannot be directly correlated with each other, and yet their similar clockwise forms suggest that the metamorphic succession of the zones and crustal evolution of the areas were similar.

Fluid composition

The fluid inclusion data on Hiltuspuro are informative about the fluid composition during metasomatism. The primary fluid inclusions in early kyanite are dense and saline (11–17% weight equivalent NaCl) H_2O (Table 1), and represent a fluid that was trapped during kyanite growth. Very high salinity fluids (up to 40% weight equivalent of NaCl from minerals) have been described from deep-penetrating shear zones in Alpine areas (personal communication of S. Tempest reported in McCaigh 1989). More normal values are about 20–25 wt% dissolved salts. The salinity of groundwater, which increases with depth in the Canadian Shield, is postulated to be caused by rock-fluid interaction at greater depth (Frape & Fritz 1987, Frape et al. 1984). Isotopic studies suggest that meteoric water may even reach depths as great as 20 km (see Nur & Walder 1990). The early-stage fluid in kyanite rocks may have been expelled from an overthrust Palaeoproterozoic sequence soon after its collision. This meteoric water percolated deeper into the crust. The high salinity of these fluids is hard to explain without fluid-rock interaction.

During the late stage, the existence of a greater proportion of CO_2 in fluid phase is demonstrated by the pseudosecondary fluid inclusions in

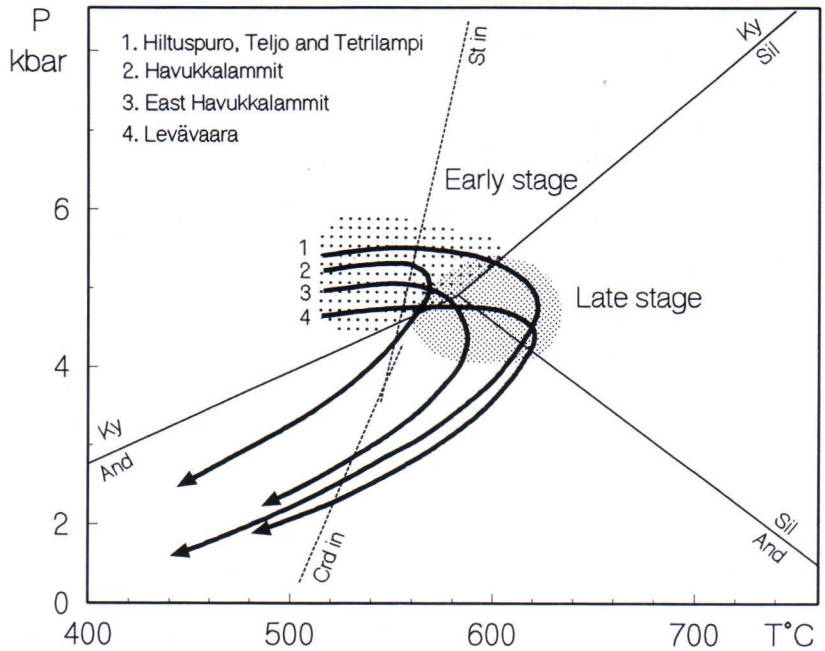


Fig. 35. Palaeoproterozoic P-T paths of kyanite rock showing variation in aluminium silicate crystallization history. Stabilities of aluminium silicates and staurolite as in Fig. 31. Cordierite stability is from Winkler (1979).

cordierite. As no carbonates were formed in this high temperature process, opportunities for estimating fluid composition by physico-chemical methods are limited. H₂O-rich fluids in the deep crust, at above 650°C, dissolve in silicate melts (e.g. Fyfe 1973, Newton 1990). An increase in migmatization with a concomitant increase in CO₂ in fluid inclusions has been shown to have occurred in the low-pressure Svecofennian metamorphic belt in southern Finland by Poutiainen (1990). CO₂ infiltration is a major factor in granulitization of the lower crust (e.g. Newton et al. 1980, Harris 1989). These fluids may derive from mantle degassing processes or magmatic production of CO₂ (Vry et al. 1988). Observations of CO₂-bearing fluid causing late metamorphism have been reported by Gruau et al. (1992) from the southern part of the Archaean Kuhmo Greenstone Belt. Cordierite-sillimanite metamorphism is pronounced in the southern targets, but cordierite patches very similar to those at Hiltuspuro also exist in the northernmost target, Tuomaanvaara. We assume that cordieritization – Mg-metasomatism and CO₂-rich fluidization – was, indeed, very far-reaching and also suspect that the CO₂-rich

fluid of the late stage had a deep-seated origin – e.g. mantle degassing or magmatic CO₂ – over a wide area.

The Palaeoproterozoic fluid compositions at Hiltuspuro differ markedly from the fluid inclusions in quartz veins in the Archaean Moukkorinaho Au mineralization in the Suomussalmi Greenstone Belt (north of the area shown in Fig. 1); there the mineralizing fluids were low-saline complex H₂O-CO₂ mixtures (Luukkonen et al. 1992, Poutiainen & Luukkonen 1994). The ore mineral contents of the kyanite rocks in the Nurmes-Sotkamo area are very low and the metasomatic processes described may well have depleted, not enriched, the system in ore constituents.

Tectonic-metamorphic correlation

Early stage

The early-stage kyanite-staurolite metasomatism-metamorphism has not been dated. According to structural observations on the western occurrences, the kyanite-staurolite assemblage was formed by the immediate static state rise in temperature af-

Table 5. Correlation scheme of tectonic-metamorphic successions between the Palaeoproterozoic North Karelia

North Karelia Schist Belt						Major tectonics
Koistinen (1981), Outokumpu area			Campbell et al. (1979), Heinävaara area			
Deformation and trend	Mineral growth	P-T and timing	Deformation	Mineral growth	P-T	
D1 NNE-NE tectonic transport	early - pre-D1 Bt S1: Bt schistosity post-D1 Grt	greenschist facies Bt grade	D1	S1: mica schistosity stubby mica		thrust tectonics
D2 NNE-NE tectonic transport	S2: dominant Bt-Ms schistosity/crenulation post-D2 Bt growth	temperature increases	D2	S2: mica schistosity Bt and Ms, strain-free	temperature increases	
D3 (D2c)* NW-SE, rare NNE-SSW	S3: spaced Bt schistosity/crenulation post-D3 St Ky juxtaposed with St	middle amphibolite facies about 1860 Ma ago	not present	post-D2 St pre-D4 Grt	metamorphic peak : T = 675 ± 25 °C	transition
D4 (D3) 145-185 °	S4: crenulation St rim on S4 some new Bt St inclusions in And - stage ?	Treolar et al. 1981: T = 600 ± 50 °C P = 3.5 ± 1 kbar	D4 (D3)	S4: zonal crenulation syn-D4 Grt syn/post-D4 Ms and Bt Sil on F4 fold hinges	P = 5 ± 0.25 kbar PH ₂ O = 0.6 P _{tot}	strike slip and transform fault tectonics
D5 (D4) 225-245 °	S5: weak cleavage late Chl - stage ?	retrograde	D5 (D4)	S5: fracture cleavage Ms and Chl growth	retrograde	
D6 (D5) 080-100 °	S6: fracture or healed cleavage	metamorphism	D6 (D5)	S6: fracture cleavage Chl and Ms growth	metamorphism	
D7(D6) 000-015 °	S7: fracture cleavage Chl, pseudotachylites					

* Deformation names used by the referred authors are in parantheses

ter the early shearing that generated the foliated chlorite-muscovite-quartz assemblages. The present data do not exclude the possibility that, in some places, the earliest alteration is a product of a Neoproterozoic or pre-collisional Palaeoproterozoic (e.g. related to diabase evolution) event. However, the successive series of metasomatic-metamorphic reactions in kyanite rocks and the structural relationships between kyanite rocks and metadiabase dykes, e.g. at Levävaara, confirm that they belong to the same Barrovian-type progression.

Correlation of the metamorphic succession of kyanite rocks to that of the Palaeoproterozoic metasedimentary sequences in the Kainuu and

North Karelia Schist Belts gives an idea of its date (cf. Campbell et al. 1979, Koistinen 1981, Tuisku & Laajoki 1990, Tuisku 1991); the main structural and metamorphic stages in the schist belts are summarized in Table 5. The first deformation phases, D₁ and D₂, were formed by extended thrusting of the allochthonous Palaeoproterozoic slices over the Archaean craton and autochthonous sequences (see Koistinen 1981, Tuisku 1991). The dominant mica schistosity in metasediments was formed. D₃ represents the transitional stage from thrust to transform fault tectonics. Regional metamorphic peak conditions were achieved in both areas after D₃, at about 1870–1860 Ma ago. At that time deformation was characterized by strike-slip

and Kainuu Schist Belts and kyanite rocks in the Archaean Nurmes–Sotkamo area.

Kainuu Schist Belt			Major tectonics	Archaean Nurmes–Sotkamo area				
<i>Tuisku (1991), Puolankajärvi area</i>				<i>This study</i>				
Deformation and trend	Mineral growth	P-T and timing	thrust tectonics transition strike slip and transform fault tectonics	Deformation and trend	Mineral growth	P-T and timing		
D1 NE tectonic transport	S1: segregation layering syn-D1 Grt paragenesis: Grt-Chl-Bt	T = c. 400°C temperature increases		thrust tectonics	Collision (not identified in this study)	Park 1988 and Park and Bowes 1983: shearing in major D2 zones	Vaasjoki and Sakko 1988: about 1.9–1.875 Ga ago	
D2 E tectonic transport					DP1	metamorphism and deformation of diabases	timing unknown (pre- or syn-collisional ?)	
D3	S3: crenulation or segregation segregation cleavage paragenesis: Grt-Bt-St. last regional metam. assemblage	T = 535°C and following isothermic decompression		transition	Early stage NW-SE	ductile shearing mobile brecciation Ms-Chl-Qtz static Ky-St ±And, Crn	temperature increases T = 550–600°C P = about or in excess of 5 kbar	
D4 NE-SW	S4: mica schistosity paragenesis: Grt-Als-Bt-St Ky earlier than Sil Crd+And during or after D4	metamorphic peak: T = 550–580°C P = 4–6 kbar c. 1870 Ma ago decompressional			strike slip and transform fault tectonics	Late stage DP2 NW-SE rare N-S or NE-SW	semi-brittle fracturing static growth Crd-Sil±And Oam	peak metamorphism T = 600–620°C P = 4–5 kbar 1852±2 Ma ago
D5 N-S	S5: crenulation cleavage syn-D4 or later Crd-And	cooling to T = 500–530°C P = 2.5–3.5 kbar					Cooling stage	late fractures Chl, Ms, Crb
D6 E-W	S6: fracture cleavage							

or transform fault tectonics. The shear zones that formed during these later stages, e.g. the Auh shear zone, crosscut the Archaean rocks (Tuisku 1991). Staurolite crystallized during static heating after D₃, and in North Karelia the staurolite rim grew on S₄ schistosity (Koistinen 1981). Kyanite and sillimanite were stabilized: in the Kainuu Schist Belt kyanite preceded sillimanite (Tuisku 1991), and in the North Karelia Schist Belt kyanite crystallization was juxtaposed to staurolite growth (Koistinen 1981). Metamorphism was due to isothermal decompression between D₃ and D₄. Both schist belts show andalusite and/or cordierite growth after staurolite and, according to Tuisku (1991), their stabilization represents decompress-

sional cooling after D₄. Later deformation phases record retrograde conditions, as evidenced by chlorite and muscovite overgrowth on the peak metamorphic assemblages in late shear or fracture zones.

Although structural correlation between the Palaeoproterozoic and Archaean Nurmes–Sotkamo areas is not straightforward, their metamorphic P-T successions were very similar (Table 5). The early shearing observed in kyanite rocks may be correlated to D_{3/4} shear zones in the Palaeoproterozoic areas, but we have insufficient data to confirm this. Our interpretation is that the early-stage kyanite-staurolite metamorphism in the Archaean area largely corresponds to the Palaeoproterozoic

ic, post-D₃ or D₄, kyanite-staurolite metamorphism in the Kainuu and North Karelia Schist Belts and, thus, was formed during the post-tectonic stage with respect to the Palaeoproterozoic collision and crustal thickening. Similar metamorphism in the eastern Archaean area in Russia is also interpreted as Proterozoic in age (e.g. Belyaev et al. 1993, Petrov 1993). The pressure obtained here, ≥ 5 kbar, is lithostatic, meaning that this crustal level was overlain by a thick pile of Archaean and/or Palaeoproterozoic rocks.

The Palaeoproterozoic metadiabase dykes are often undeformed and carry only static metamorphic assemblages recording amphibolite and epidote-amphibolite facies conditions. Some more strained dykes show well-developed metamorphic foliation. At Hiltuspuro and Levävaara, the amphibolite-facies metadiabase dykes are foliated, and have a steep southwesterly to westerly dip. The foliation of metadiabases can sometimes be traced into the tonalitic host rock, but correlation further away from the contact zone is uncertain. The signatures of shearing and schistosity development that are visible in some dykes but not in others demonstrate that Palaeoproterozoic deformation, although still operational rather far east in the Archaean area, was there restricted in zones. The timing of the amphibolite-facies foliation in metadiabase dykes has, however, still to be established. Clearly the dykes were affected by two separate epidote-amphibolite to amphibolite facies events: the earlier penetrative and the later zonal with metasomatism. Whether the earlier event is connected to the early extension of the Archaean "supercontinent" (Lahtinen 1994) or to the Svecofennian collision is not known.

Late stage

In the Palaeoproterozoic Kainuu Schist Belt the cordierite- and andalusite-bearing assemblages were stabilized during the post-D₄ and D₅ stages (Table 5). There are very similar metamorphic assemblages in some western kyanite rocks. According to Tuisku (1991), they indicate decompressional cooling, whereas our observations of kyanite rocks show that the late cordierite-silli-

manite/andalusite paragenesis represents the thermal peak during decompressional heating, suggesting an extensional stage (cf. Platt & England 1993).

Before our study, no age determinations had been conducted on an approximately 1850-Ma-old process that is, furthermore, exactly linked to tectonic-metamorphic structures in the Archaean area. On the other hand, comprehensive age data on the Palaeoproterozoic area show that only a small proportion of post-tectonic magmatism happened between 1880 Ma and 1850 Ma (Huhma 1986, Vaasjoki & Sakko 1988). The nearest rocks dated to that age group are in the North Karelia Schist Belt – the post-tectonic Maarianvaara granodiorite (Fig. 1), which is 1857 ± 8 Ma old (Huhma 1986) and in the Kainuu Schist Belt – the Ristijärvi granodiorite, which is 1859 ± 8 Ma old (Kontinen & Meriläinen 1993). Granitic intrusions of this kind are rather common to the west of the study area, in a north–south-trending zone near the Archaean-Palaeoproterozoic boundary. According to the Sm-Nd isotopic composition, these magmas represent a mixture of Archaean and Palaeoproterozoic material (Huhma 1986). Granodiorite of similar age, 1.853 ± 8 Ga (Vaasjoki & Sakko 1988), has been described also further west in Svecofennian terrain. The existence of these granitoids is an evidence of marked thermal input into the lower crust at about 1.850 Ga ago.

Huhma (1981) described microtonalitic dykes crosscutting the Maarianvaara granodiorite. Microtonalites are widely distributed in the North Karelia Schist Belt. He interpreted their sphene U-Pb age, 1850 Ma, as metamorphic, but crosscutting relations place their age between 1857 ± 8 Ma (Maarianvaara) and 1830 Ma, which is the age of local lamprophyre dykes (Huhma 1981). It is interesting that the lamprophyre dykes are characterized by high apatite and LREE contents (Laukkanen 1987) – geochemical features that seem to be characteristic of late-stage kyanite rocks, too. These widespread thermal and magmatic events are of the same age as the metamorphic peak in kyanite rocks, suggesting the same energy source for the processes.

Resetting of the K-Ar isotopic compositions of

biotite and hornblende in the Archaean TTG-granitoids indicates an increase in temperature during the Palaeoproterozoic era (Kontinen et al. 1992, O'Brien et al. 1993). Palaeoproterozoic reheating is also postulated by Gruau et al. (1992) and Karhu et al. (1993).

Post-tectonic magmatism in Karelian terrain shows that the Palaeoproterozoic+Archaean crust underwent some kind of disturbance between 1860 and 1830 Ma ago. It is possible that reworking and melting in the lower crust and upper lithosphere (cf. Fountain 1989) were then more pronounced than can be inferred from the current erosion level. The event may be connected with post-collisional extension of the upper crust (cf. Gaudemer et al. 1988), as suggested by dilatational structures and the decrease in pressure in kyanite rocks and also by the decompressional heating history. The process produced enough CO₂-rich fluid and energy for the heating and metasomatism detected. Extension and upwelling of the crust by this deep-crustal process caused rapid tectonic and/or erosional exhumation, termination of fluid action and crustal cooling. The crust, especially the high-velocity layer of the lower crust, of eastern Finland is exceptionally thick (Yliniemi et al. 1993, Korja et al. 1993). Korja et al. (op. cit.) attribute this to Palaeoproterozoic reworking of the lower crust and the Moho. The results of our study support this concept. The thermal event and the characteristics of the metasomatism are interpreted to be connected with magmatic underplating that transformed the lower crust up to the Kuhmo Greenstone Belt in the east during Palaeoproterozoic time.

Because the Palaeoproterozoic structures identified in the eastern part of the Archaean area are zonal and rather limited, the old stabilized crust must have behaved very competently and in large coherent slices. The impact of metamorphism on these slices and blocks was slight and static in type, because the TTG crust was cool and dry. The energy that would have been needed for large-scale penetrative metamorphism was apparently not available. The most intense Palaeoproterozoic metasomatic and metamorphic overprints are therefore visible along the zones of weakness, which were open for an intense fluid flow capa-

ble of transporting sufficient heat to produce the features seen in kyanite rocks.

CONCLUSIONS

The main conclusions drawn from *this study* are:

1. Palaeoproterozoic deformation zones crosscutting the Archaean crust in eastern Finland show a change in deformation style from early-stage ductile to late-stage semi-brittle, and have been affected by strong metasomatism.
2. The early-stage metasomatic-metamorphic event shows progression from Chl-Ms-Qtz to Ky/And-St stability of Barrovian-type assemblages, presumably related to crustal thickening during the Svecofennian orogeny and to the temperature increase soon thereafter. Metasomatism was induced by a saline H₂O fluid.
3. The late-stage semi-brittle event exhibits dilatational features. Mg metasomatism at increasing temperature and CO₂-rich fluidization produced cordierite-rich assemblages in the sillimanite or andalusite stability field under maximum P-T conditions of about 600–620°C/4–5 kbar. This peak metamorphism is dated to 1852±2 Ma.
4. The metamorphic assemblages in the metasomatic zones indicate small pressure differences in the Nurmes–Sotkamo area, i.e. in the thickness of the column of overlying Palaeoproterozoic±Archaean rocks, about 1850 Ma ago. The thickness of the exhumed slice was about 15–20 km. The pressure decrease indicates slight exhumation between the early and late stages, and the late-stage heating was decompressional. The dilatational structures and decompressional thermal evolution indicate extensional evolution during the late stage.
5. The thermal event at 1850 Ma is a distal reflection of high overall thermal activity in the Palaeoproterozoic Svecofennian area in the west but, here, in the Archaean craton, it was restricted to fracture zones and was connected to the evolution of the lower crust with a thick high-velocity layer. Thermal input is interpreted to be a result of magmatic underplating.

ACKNOWLEDGEMENTS. *This investigation is a contribution to the regional metamorphic studies conducted in eastern Finland for the "Global Geoscience Transects" project by the Geological Survey of Finland. Dr Kalevi Korsman supervised the study throughout. Several discussions with him and his comments on the manuscript were important for the final form of the paper. Discussions with Professor Heikki Papunen and his critical comments likewise improved the paper. Dr Erkki Luukkonen opened our eyes to the problems of Archaean geology. Without his guidance the tectonic features of the area would have been difficult to unravel. He, too, proposed many valuable corrections to the manuscript. Drs Tapio Koistinen, Jarmo Kohonen and Pentti Hölttä read earlier versions of the paper. Their interest was of great value.*

The minerals were dated in the Unit for Isotope Geology by Drs Hannu Huhma and Matti Sakko and the mineral compositions were analysed by Lassi Pakkanen and Bo Johanson at the Geological Survey of Finland in Espoo. Minerals were separated and X-ray studies were made at the Geological Survey's Mineralogical Laboratory in Espoo by Mirja Saarinen, Leena Järvinen, Anneli Lindh and Matti Karhunen. Thin sections were prepared by Andrej Wennström, Jouko Pääkkönen and Pekka Wasenius. Maps were drawn in final form by Elsa Järvinen and Ritva Forsman. The English was corrected by Gillian Häkli.

We express our cordial thanks to the editors, to all the persons named and to all those not mentioned here, but who were involved in the study in different ways.

REFERENCES

Äikäs, O. 1989. Uraanitukimukset Nurmeksen Levävaarassa 1982–85. Geological Survey of Finland, unpublished report M 19/4324/–89/2/60. 19 p. (in Finnish).

Alapieti, T.T. & Lahtinen, J.J. 1989. Early Proterozoic layered intrusions in the northeastern part of Fennoscandian Shield. Geological Survey of Finland, Guide 29, 3–41.

Aleinikoff, J.N. & Grauch, R.I. 1990. U-Pb geochronologic

constraints on the origin of a unique monazite-xenotime gneiss, Hudson Highlands, New York. *American Journal of Science* 290, 522–546.

Anderson, G.M. & Burnham, C.W. 1983. Feldspar solubility and the transport of aluminum under metamorphic conditions. *American Journal of Science* 283-A, 283–297.

Aro, K. & Laitakari, I. (eds.) 1987. Suomen diabaasit ja muut juonikivet. Geological Survey of Finland, Report of Investigation 76. 254 p. (in Finnish with English summaries).

Belyaev, O.A., Bushmin, S.A., Voinov, A.S., Volodichev, O.I., Glebovitsky, V.A., Ivliyev, A.I., Klein, V.A., Kuleshevich, L.V., Petrov, B.V., Petrov, V.P., Polekhovskiy, Yu.S. & Puura, V.A. 1991. Map of mineral facies of metamorphic rocks in the Eastern Baltic Shield, Scale 1:500,000. St.Petersburg: Russian Academy of Sciences, Institute of Precambrian Geology and Geochronology.

Belyaev, O.A., Mitrofanov, F.P. & Petrov, P.P. 1993. Geological-petrological model of the Baltic Shield, metamorphic structure development. Symposium on "The Svecofennian Domain", geological/geophysical aspects of continental crust and annual meeting of IGCP-275, in Turku, Finland, August 23–25, 1993, Abstracts, p. 12.

Berman, R.G. 1990. Mixing properties of Ca-Mg-Fe-Mn garnets. *American Mineralogist* 75, 328–344.

Berman, R.G. 1991. Thermobarometry using multiequilibrium calculations: a new technique with petrologic applications. *Canadian Mineralogist* 29, 833–855.

Blais, S. & Auvray, B. 1990. Serpentinization in the Archean komatiitic rocks of the Kuhmo greenstone belt, Eastern Finland. *Canadian Mineralogist* 28, 55–66.

Bottinga, Y. & Richet, P. 1981. High pressure and temperature equation of state and calculation of the thermodynamic properties of gaseous carbon dioxide. *American Journal of Science* 281, 615–660.

Brown, P.E. 1989. FLINCOR: A microcomputer program for the reduction and investigation of fluid inclusion data. *American Mineralogist* 74, 1390–1393.

Brown, P.E. & Lamb, W.M. 1989. P-V-T properties of fluids in the system H₂O-CO₂-NaCl: New graphical presentations and implications for fluid inclusion studies. *Geochimica et Cosmochimica Acta* 53, 1209–1221.

Campbell, D.S., Treolar, P.J. & Bowes, D.R. 1979. Metamorphic history of staurolite-bearing schists from the Svecokarelides, near Heinävaara, eastern Finland. *Geologiska Föreningens i Stocholm Förhandlingar* 101, 105–118.

Copeland, P., Parrish, R.R. & Harrison, T.M. 1988. Identification of inherited radiogenic Pb in monazite and its implications for U-Pb systematics. *Nature* 333, 760–763.

Crowley, P.D. & Spear, F.S. 1981. The orthoamphibole solvus: P, T, X (Fe-Mg) relations. Geological Society of America, Abstracts with Program, 13, p. 435.

Etheridge, M.A., Wall, V.J. & Vernon, R.H. 1983. The role of the fluid phase during regional metamorphism and deformation. *Journal of Metamorphic Geology* 1, 205–226.

- Fleming, P.D. & Fawcett, J.J. 1976. Upper stability of chlorite+quartz in the system MgO-FeO-Al₂O₃-SiO₂-H₂O at 2 kbar water pressure. *American Mineralogist* 61, 1175–1193.
- Fountain, D.M. 1989. Growth and modification of lower continental crust in extended terrains: the role of extension and magmatic underplating. In: Mereu, R.F., Muller, S. & Fountain, D.M. (eds.) *Properties and Processes of the Earth's Lower Crust*. Geophysical Monograph 51, 287–299.
- Frape, S.K. & Fritz, P. 1987. Chemical trends for groundwaters from the Canadian Shield. In: Fritz, P. & Frape, K.S. (eds.) *Saline Water and Gases in Crystalline rocks*. Geological Association of Canada, Special Paper 33, 19–38.
- Frape, S.K., Fritz, P. & McNutt, R.H. 1984. The role of water-rock interaction in chemical evolution of groundwaters from the Canadian Shield. *Geochimica et Cosmochimica Acta* 48, 1617–1627.
- Fyfe, W.S. 1973. The granulite facies, partial melting, and the Archaean crust. *Philosophical Transactions of the Royal Society of London, Series A* 273, 456–461.
- Gaudemer, Y., Jaupart, C. & Tapponnier, P. 1988. Thermal control on post-orogenic extension in collision belts. *Earth and Planetary Science Letters* 89, 48–62.
- Gavrilenko, P. & Gueguen, Y. 1993. Fluid overpressures and pressure solution in the crust. *Tectonophysics* 217, 91–110.
- Gerya, T.V. & Perchuk, L.L. 1992. GEOPATH – a thermodynamic database for geothermobarometry and related calculations with the IBM PC AT/XT computer. 29th International Geological Congress, Kyoto, V.2, p. 1026.
- Grant, J.A. 1986. The isocon diagram – a simple solution to Gresens' equation for metasomatic alteration. *Economic Geology* 81, 1976–1982.
- Gresens, R.L. 1967. Composition-volume relationships on metasomatism. *Chemical Geology* 2, 47–65.
- Gruau, G., Tourpin, S., Fourcade, S. & Blais, S. 1992. Loss of isotopic (Nd, O) and chemical (REE) memory during metamorphism of komatiites: new evidence from eastern Finland. *Contributions to Mineralogy and Petrology* 112, 66–82.
- Halden, N.M. & Bowes, D.R. 1984. Metamorphic development of cordierite-bearing layered schist and mica schist in the vicinity of Savonranta, eastern Finland. *Bulletin of the Geological Society of Finland* 56, 3–23.
- Härme, M. & Perttunen, V. 1971. Magnesia metasomatism at Hirvas, northern Finland. *Geological Survey of Finland, Bulletin* 250, 28 p.
- Harris, N. 1989. Carbon dioxide in the deep crust. *Nature* 340, 347–348.
- Holland, T.J.B. & Powell, R. 1990. An enlarged and updated internally consistent thermodynamic dataset with uncertainties and corrections: the system K₂O-Na₂O-CaO-MgO-MnO-FeO-Fe₂O₃-Al₂O₃-TiO₂-SiO₂-C-H₂-O₂. *Journal of Metamorphic Geology* 8, 89–124.
- Hölttä, P. & Paavola, J. 1989. Kornerupine-bearing granulites and evidence of uplift in the Archaean Varpaisjärvi area, Central Finland. *Geological Survey of Finland, Special Paper* 10, 11–17.
- Horneman, R. 1990. Arkeaiset granitoidit Tipasjärven ympäristössä. English summary: Archaean granitoids surrounding the Tipasjärvi schist belt, eastern Finland. Pohjois-Karjalan malmiprojekti, Raportti 1990, University of Oulu, 87 p.
- Horneman, R. & Hyvärinen, T. 1987. Haukkalammin kya-niittiesiintymä. Arkeisten alueiden malmiprojekti, Raportti 2, University of Oulu, 22 p. (in Finnish).
- Horneman, R. & Hyvärinen, T. 1989. Puukarin karttalehden tutkimustilanne 1988. Arkeisten granitoidien malmiprojekti, Raportti 6, University of Oulu, 123 p. (in Finnish).
- Huhma, A. 1981. Youngest Precambrian dyke rocks in North Karelia, East Finland. *Bulletin of the Geological Society of Finland* 53, 67–82.
- Huhma, H. 1986. Sm-Nd, U-Pb and Pb-Pb isotopic evidence for the origin of the early Proterozoic Svecokarelian crust in Finland. *Geological Survey of Finland, Bulletin* 337, 52 p.
- Ivanov, S.N. & Ivanov, K.S. 1993. Hydrodynamic zoning of the Earth's crust and its significance. *Journal of Geodynamics* 17, 155–180.
- Jegouzo, P. & Blais, S. 1993. Évidences structurales pour une reprise karélienne de la croûte archéenne de Finlande orientale. *Comptes Rendus de l'Académie des Sciences, Paris, t. 316, Série II*, 1297–1301.
- Karhu, J.A., Nurmi, P.A. & O'Brien, H.E. 1993. Carbon and oxygen isotope ratios of hydrothermal carbonates associated with gold mineralization in the late Archaean Hattu schist belt, Ilomantsi, eastern Finland. *Geological Survey of Finland, Special Paper* 17, 307–316.
- Kerrich, R., La Tour, T.E. & Willmore, L. 1991. Fluid participation in deep fault zones: Evidence from geological, geochemical, and ¹⁸O/¹⁶O relations. *Journal of Geophysical Research* 89, 4331–4343.
- Kohonen, J. 1995. From continental rifting to collisional crustal shortening – Paleoproterozoic Kaleva sediments of the Höytiäinen area in North Karelia, Finland. *Geological Survey of Finland, Bulletin* 380, 79 p.
- Kohonen, J., Luukkonen, E. & Sorjonen-Ward, P. 1991. Nunnanlahti and Holinmäki shear zones in North Karelia: Evidence for major Early Proterozoic ductile deformation of Archaean basement and further discussion of regional kinematic evolution. *Geological Survey of Finland, Special Paper* 12, 11–16.
- Koistinen, T.J. 1981. Structural evolution of an early Proterozoic strata-bound Cu-Co-Zn deposit, Outokumpu, Finland. *Transactions of the Royal Society of Edinburgh: Earth Sciences* 72, 115–158.
- Kontinen, A. 1991. Evidence for significant paragneiss component within the Late Archaean Nurmes gneiss complex, eastern Finland. *Geological Survey of Finland, Special Paper* 12, 17–19.
- Kontinen, A. & Meriläinen, K. 1993. Paltamo. *Geological Map of Finland 1:100 000, Pre-Quaternary Rocks, Sheet 3434*. Geological Survey of Finland.

- Kontinen, A. & Paavola, J. 1996. Svecofennian (Palaeoproterozoic) tectono-thermal effect on the Archaean bedrock of North Karelia, eastern Finland. In: Ekdahl, E. & Autio, S. (eds.) *Global Geoscience Transect/SVEKA – Proceedings of the Kuopio Seminar, Finland 25.–26.11.1993*. Geological Survey of Finland, Report of Investigation 136, 7–8.
- Kontinen, A., Paavola, J. & Lukkarinen, H. 1992. K-Ar ages of hornblende and biotite from Late Archaean rocks of eastern Finland – interpretation and discussion of tectonic implications. *Geological Survey of Finland, Bulletin* 365, 31 p.
- Korja, A., Korja, T., Luosto, U. & Heikkinen, P. 1993. Seismic and geoelectric evidence for collisional and extensional events in the Fennoscandian Shield – implications for Precambrian crustal evolution. In: Green, A. G., Kröner, A., Götze, H.-J. & Pavlenkova, N. (eds.) *Plate Tectonic Signatures in Continental Lithosphere*. Tectonophysics 219, 129–152.
- Korja, T., Luosto, U., Korsman, K. & Pajunen, M. 1994. Geophysical and metamorphic features of Palaeoproterozoic Svecofennian orogeny and Palaeoproterozoic overprinting on Archaean crust. *Geological Survey of Finland, Guide* 37, 11–20.
- Korsman, K. 1982. Metamorfoositutkimuksen merkityksestä. In: Laajoki, K., Paakkola, J. & Tuisku, P. (eds.) *Suomen kallioperän ja malmien metamorfoosi ja deformaatio*. Res Terrae, Serie B 5, 36–40. (in Finnish).
- Korzhinskii, D.S. 1964. An outline of metasomatic processes (Part 2 of 3). *International Geological Review* 6, 1920–1952.
- Korzhinskii, D.S. 1970. *Theory of metasomatic zoning*. Oxford: Clarendon Press. 162 p.
- Kozhevnikov, V.N., Chukhonin, A.P. & Shulesko, I.K. 1987. Asynchronous high-temperature metamorphism of oldest rocks in Western Karelia. *Transactions (Doklady) of the USSR Academy of Sciences, Earth Science Sections*, 292, (6), 1441–1445.
- Lahtinen, R. 1994. Crustal evolution of the Svecofennian and Karelian domains during 2.1–1.79 Ga, with special emphasis on the geochemistry and origin of 1.93–1.91 Ga gneissic tonalites and associated supracrustal rocks in the Rautalampi area, central Finland. *Geological Survey of Finland, Bulletin* 378, 128 p.
- Laukkanen, J. 1987. Väli-Suomen lamprofyrijuonet. English abstract: The lamprophyres of Middle Finland. *Geological Survey of Finland, Report of Investigation* 76, 91–98.
- Leake, B.E. 1978. Nomenclature of amphiboles. *American Mineralogist* 63, 1023–1053.
- Lister, J.R. & Kerr, R.C. 1991. Fluid-mechanical models of crack propagation and their application to magma transport in dykes. *Journal of Geophysical Research* 96, 10049–10077.
- Luukkonen E. 1985. Structural and U-Pb isotopic study of late Archaean migmatitic gneisses of the Presvecofennides, Lylyvaara, eastern Finland. *Transactions of the Royal Society of Edinburgh: Earth Sciences* 76, 401–410.
- Luukkonen E. 1988. The structure and stratigraphy of the northern part of the late Archaean Kuhmo greenstone belt, eastern Finland. *Geological Survey of Finland, Special Paper* 4, 71–96.
- Luukkonen, E.J. 1989a. The early Proterozoic Saari-Kieikki greenstone belt: A representative of Sariola Group at Kuhmo, eastern Finland. *Bulletin of the Geological Society of Finland* 61, 161–187.
- Luukkonen, E. 1989b. Geology of the Moisiovaara area. In: Gaál, G. (ed.) *Archaean granitoids and associated Mo, W and Au mineralization in eastern Finland*. Geological Survey of Finland, Guide 25, 7–15.
- Luukkonen, E.J. 1992. Late Archaean and early Proterozoic structural evolution in the Kuhmo–Suomussalmi terrain, eastern Finland. *Turun yliopiston julkaisuja – Annales Universitatis Turkuensis. Sarja-Ser. A. II. Biologica-Geographica-Geologica* 78, 37 p.
- Luukkonen, E.J., Pajunen, M. & Poutiainen M. 1992. Kuhmo–Suomussalmen alueen arkeisen kallioperän rakenne- ja evoluutio ja Au-aiheet. In: Ekdahl, E. (ed.) *Suomen kallioperän kehitys ja raaka-ainevarat, Symposio Oulussa 1.–2.10.1992*, Vuorimiesyhdistys, Sarja B 51, 11–12. (in Finnish).
- McCaigh, A.M. 1989. Fluid flow through fault zones. *Nature* 340, p. 600.
- McCaigh, A.M. & Knipe, R.J. 1990. Mass-transport mechanisms in deforming rocks: Recognition using microstructural and microchemical criteria. *Geology* 18, 824–827.
- Mineyev, D.A. 1963. Geochemical differentiation of the rare earths. *Geochemistry* 12, 1129–1149.
- Newton, R.C. 1990. Fluids and shear zones in the deep crust. *Tectonophysics* 182, 21–37.
- Newton, R.C., Smith, J.V. & Windley, B.F. 1980. Carbonic metamorphism, granulites, and crustal growth. *Nature* 288, 45–50.
- Nur, A. & Walder, J. 1990. Time-dependent hydraulics of the Earth's crust. In: *Studies in Geophysics, The role of fluids in crustal processes*. Washington, D.C.: National Academy Press, 113–127.
- O'Brien, H.E., Nurmi, P.A. & Karhu, J.A. 1993. Oxygen, hydrogen and strontium isotopic compositions of gold mineralization in the late Archaean Hattu schist belt, Ilomantsi, eastern Finland. *Geological Survey of Finland, Special Paper* 17, 291–306.
- Oliver, N.H.S., Valenta, R.K. & Wall, V.J. 1990. The effect of heterogeneous stress and strain on metamorphic fluid flow, Mary Kathleen, Australia, and a model for large-scale fluid circulation. *Journal of Metamorphic Geology* 8, 311–331.
- Paavola, J. 1984. On the Archaean high-grade metamorphic rocks in the Varpaisjärvi area, Central Finland. *Geological Survey of Finland, Bulletin* 327, 33 p.
- Paavola, J. 1986. A communication on the U-Pb and K-Ar age relations of the Archaean basement in the Lapinlahti–Varpaisjärvi area, central Finland. *Geological Survey of Finland, Bulletin* 339, 7–15.
- Park, A.F. 1988. A new section through the sub-Karelian

- unconformity at Niinivaara, Savo, eastern Finland. Bulletin of the Geological Society of Finland 60, 67–73.
- Park, A.F. & Bowes, D.R. 1983. Basement-cover relationships during polyphase deformation in the Svecokareliides of the Kaavi district, eastern Finland. Transactions of the Royal Society of Edinburgh: Earth Sciences 74, 95–118.
- Pekkala, Y. 1982. Kyanitiitin esiintyminen Suomen kallioperässä. English abstract: Kyanite occurrences in Finland. In: Laajoki, K., Paakkola, J. & Tuisku, P. (eds.) Suomen kallioperän ja malmien metamorfoosi ja deformaatio. Res Terrae, Serie B 5, 179–193.
- Petrov, V.P. 1993. Svecofennian tectono-metamorphic evolution of the north-eastern Baltic Shield. Symposium on "The Svecofennian Domain", geological/geophysical aspects of continental crust and annual meeting of IGCP-275, in Turku, Finland, August 23–25, 1993, Abstracts, p. 47.
- Platt, J.P. & England, P.C. 1993. Convective removal of lithosphere beneath mountain belts: thermal and mechanical consequences. American Journal of Sciences 293, 307–336.
- Poutiainen, M. & Luukkonen, E. 1994. The geology and fluid inclusion studies of some epigenetic gold deposits in the Archaean Kuhmo and Suomussalmi greenstone belts, eastern Finland. Fifth Biennial Pan-American Conference on Research on Fluid Inclusions (PACROFI V) Cuernavaca, Morelos, Mexico, May 19–21, 1994, Abstracts, 77–78.
- Poutiainen, M. 1990. Evolution of a metamorphic fluid during progressive metamorphism in the Joroinen-Sulkava area, southeastern Finland, as indicated by fluid inclusions. Mineralogical Magazine 54, 207–218.
- Rask, M. 1979. Kyaniittitutkimukset Nurmeksessa 1.6.–30.9.1978. Geological Survey of Finland, unpublished report, Markku Rask 23.5.1979. 6 p. (in Finnish).
- Richardson, S.W. 1968. Staurolite stability in part of the system Fe-Al-Si-O-H. Journal of Petrology 9, 467–488.
- Robinson, P., Spear, F.S., Schumacher, J.C., Laird, J., Klein, C., Evans, B.W. & Doolan, B.L. 1982. Phase relations of metamorphic amphiboles: Natural occurrence and theory. Mineralogical Society of America, Reviews in Mineralogy 9B, 1–211.
- Roedder, E. 1984. Fluid inclusions. Mineralogical Society of America, Reviews in Mineralogy 12. 644 p.
- Russian Academy of Science, Institute of Geology, Karelian Research Center 1993. Kyanite. In: Precambrian industrial minerals of Karelia, (Russia). International Conference "The Industrial Minerals of the Baltic / Fennoscandian Shield and New Technologies" in Petrozavsk, September 7–14, 1993, 32–35.
- Schärer, U., Tapponnier, P., Lacassin, R., Leloup, P.H., Dalai, Z. & Shaocheng, J. 1990. Intraplate tectonics in Asia: a precise age for large-scale Miocene movement along the Ailao Shan-Red River shear zone, China. Earth and Planetary Science Letters 97, 65–77.
- Selverstone, J., Morteani, G. & Staude, J.-M. 1991. Fluid channelling during ductile shearing: transformation of granodiorite into aluminous schist in the Tauern Window, Eastern Alps. Journal of Metamorphic Geology 9, 419–431.
- Shepherd T., Rankin A.H. & Alderton, D.H.M. 1985. A practical guide to fluid inclusion studies. Glasgow: Blackie. 239 p.
- Sibson R.H. 1992. Implications of fault-valve behavior for rupture nucleation and recurrence. Tectonophysics 211, 283–293.
- Simonen, A. 1980. The Precambrian in Finland. Geological Survey of Finland, Bulletin 304. 58 p.
- Smith, H.A. & Barreiro, B. 1990. Monazite U-Pb dating of staurolite grade metamorphism in pelitic schists. Contributions to Mineralogy and Petrology 105, 602–615.
- Sorjonen-Ward, P. & Clauoué-Long, J. 1993. Preliminary note on ion probe results for zircons from the Silvevaara granodiorite, Ilomantsi, Eastern Finland. Geological Survey of Finland, Special Paper 18, 25–29.
- Sorokin, V.I. and Dadze, T.P. 1995. Solubility and complex formation in systems Hg-H₂O, S-H₂O, SiO₂-H₂O and SnO₂-H₂O. In: Shmulovich, K.I., Yardley, B.W.D. & Gonchar, G.G. (eds.) Fluids in the crust, equilibrium and transport properties. London: Chapman & Hall, 57–93.
- Spear, F.S. 1980. The gedrite-anthophyllite solvus and the composition limits of orthoamphibole from the Post Pond Volcanics, Vermont. American Mineralogist 65, 1103–1118.
- Stacey, J.S. & Kramers, J.D. 1975. Approximation of terrestrial lead isotope evolution by a two-stage model. Earth and Planetary Science Letters 26, 207–221.
- Sterner, S.M. & Bodnar, R.J. 1984. Synthetic fluid inclusions in natural quartz. I. Compositional types synthesized and applications to experimental geochemistry. *Ceochimica et Cosmochimica Acta* 48, 2659–2668.
- Taipale, K. 1982. Kuhmon arkeeminen vihreäkivi-granitoidialue. Osa I. Tipasjärvi–Hietajärvi. Raportti 4, Arkeisten alueiden malmiprojekti. 143 p. (in Finnish with English summary).
- Thompson, A.B. 1988. Fluids and rock deformation. Rendiconti Della Società Italiana di Mineralogia e Petrologia 43, 61–64.
- Treloar, P.J., Koistinen, T.J. & Bowes, D.R. 1981. Metamorphic development of cordierite-amphibole rocks and mica schists in the vicinity of the Outokumpu ore deposit, Finland. Transactions of the Royal Society of Edinburgh: Earth Sciences 72, 201–215.
- Tuisku, P. 1991. Metamorphism and structural evolution of the early Proterozoic Puolankajärvi Formation, Finland. Res Terrae, Serie A, 4. 47 p.
- Tuisku, P. & Laajoki, K. 1990. Metamorphic and structural evolution of the Early Proterozoic Puolankajärvi formation, Finland – II. The pressure-temperature-deformation-composition path. Journal of Metamorphic Geology 8, 375–391.
- Tuisku, P. & Sivonen, S. 1984. Paine- ja lämpötilaolosuhteet Kuhmon vihreäkivivyöhykkeen metamorfoosissa. English summary: Geothermometry and geobarometry in the Archaean Kuhmo – Suomussalmi greenstone belt,

- Eastern Finland. Arkeisten alueiden malmiprojekti, Raportti 19, University of Oulu. 65 p.
- Vaasjoki, M. & Sakko, M. 1988. The evolution of the Raahe-Ladoga zone in Finland: isotopic constraints. Geological Survey of Finland, Bulletin 343, 7–32.
- Väyrynen, H. 1939. On the geology and tectonics of the Outokumpu ore field and region. Bulletin de la Commission géologique de Finlande 124. 91 p.
- Vry, J., Brown, P.E., Valley, J.W. & Morrison, J. 1988. Constraints on granulite genesis from carbon isotope compositions of cordierite and graphite. Nature 332, 66–68.
- Vuollo, J. 1994. Palaeoproterozoic basic igneous events in Eastern Fennoscandian Shield between 2.45 Ga and 1.97 Ga, studied by means of mafic dyke swarms and ophiolites in Finland. Acta Universitatis Ouluensis A 250. 47 p.
- Wagner, G.A., Reimer, G.M. & Jäger, E. 1977. Cooling ages derived by apatite fission track mica Rb-Sr and K-Ar dating, the uplift and cooling history of the Central Alps. Memorie degli Istituti di Geologia e Mineralogia, University Padova, 30, 1–27.
- Walther, J.V. 1990. Fluid dynamics during progressive regional metamorphism. In: Studies in Geophysics, The role of fluids in crustal processes. Washington, D.C.: National Academy Press. 64–71.
- Ward, P. 1993. An overview of structural evolution and lithic units within and intruding the late Archean Hattus schist belt, Ilomantsi, eastern Finland. Geological Survey of Finland, Special Paper 17, 9–102.
- Wegmann, C.E. 1928. Über die Tektonik der jüngeren Faltung in Ostfinnland. Fennia 50, 1–22.
- Winkler, H.G.F. 1979. Petrogenesis of Metamorphic Rocks. New York: Springer-Verlag. 348 p.
- Wickham, S.M. 1992. Fluids in the deep crust – Petrological and isotopic evidence. In: Fountain, D.M., Arculus, R. & Kay, R.W. (eds.) Continental crust. Developments in Geotectonics 23. Amsterdam: Elsevier, 391–421.
- Yardley, B.W.D. & Shmulovich, K.I. 1995. An introduction to crustal fluids. In: Shmulovich, K.I., Yardley, B.W.D. & Gonchar, G.G. (eds.) Fluids in the crust, equilibrium and transport properties. London: Chapman & Hall, 1–12.
- Yliniemi, J., Jokinen, M. & Luukkonen, E.J. 1993. Deep structure of the Earth along the SVEKA extension to northwest. GGT/SVEKA, Työkokous Kuopiossa 25.–26.11.1993. Ohjelma ja esitysten lyhenteet ja osanottajaluettelo. (in Finnish)

Appendix 1. Mineral abbreviations used in text.

Ab = albite	Ksf = potassium feldspar
Alm = almandine	Ky = kyanite
Aln = allanite	Mag = magnetite
Am = amesite	Ms = muscovite
An = anorthite	Oam = orthoamphibole
And = andalusite	Olg = oligoclase
Ap = apatite	Pg = paragonite
Ath = anthophyllite	Pl = plagioclase
Bt = biotite	Prp = pyrope
Cam = clinoamphibole	Py = pyrite
Cel = celadonite	Pyh = pyrrhotite
Chl = chlorite	Qtz = quartz
Crb = carbonate	Rt = rutile
Crd = cordierite	Sil = sillimanite
Crn = corundum	Sph = sulphide
Ep = epidote	Spn = sphene
Ged = gedrite	Sps = spessartine
Grs = grossularite	St = staurolite
Grt = garnet	Tou = tourmaline
Hbl = hornblende	Xen = xenotime + unidentified radioactive mineral
Ilm = ilmenite	Zrn = zircon

Appendix 2. Mineral assemblages of the rock types studied. Intensity of metasomatism is classified as none = unaltered, weak = weakly altered, but primary structure well preserved, strong = penetratively altered, but primary structure still identifiable and penetrative = old phases occur only as relics in totally recrystallized and neomineralized rock. X = major mineral, o = minor mineral and + = accessory mineral. Pz = Palaeoproterozoic.

Northwestern occurrences		Mineral abbreviations are listed in Appendix 1.																									
Occurrence (in Fig.1)/rock type	Alteration	Qtz	Pl	Kfs	Bt	Chl	Ms	Cam	Oam	Crd	St	Ky	Sil	And	Ep	Aln	Spn	Zrn	Xen*	Ap	Tou	Rt	Mag	Ilm	Sph	Crb	
Tuomaanvaara (1)																											
Tonalite	weak	X	X		X	o										+		+		+							
Chl-Qtz rock	penetrative	X			o	X																					
Bt rock	penetrative	+			X	+																					
Crd-Chl-Bt rock	penetrative	o	o		o	o	+			X						+		+		+							
Turkkivaara (2)																											
Bt-Pl-And rock	penetrative		X		X	+	+							+	X				+								
And-Ky-Crd rock	penetrative	X			o	o				X			o	+	X				+							+	
Bt-Crd rock	penetrative				X		o			X									+	+							
Bt-Crd-St rock	penetrative				X	+				X	o		o						+	+	+		+		+		
Kallioniemi (3)																											
Tonalite	none	X	X		X	+													+		+						
Ky-bearing tonalite	strong	X	X		X	o	o						+						+		+		+				
Chl-Ms-Ky rock	penetrative	X	o			X	X						o						+		+		+				
Varpuniemi (4)																											
St-Chl-Pl rock	penetrative	+	X		+	X	o				X		o						+		+		+				
Korpilampi (5)																											
Ky-Bt-Pl rock	penetrative	o	X		X	o							o						+		+		+				
Kauhealampi (6)																											
Ky-Chl-Ms rock	penetrative	X	X			X	X						o						+		+		+				
Havukkalammit (7)																											
Mag tonalite	strong		X		X	o										+			+		+				X		
Ep rock	penetrative	o			o			o								X								+	o		
Ky-Pl rock, coarse	penetrative	X			X	o	+						X						+		+						+
East Havukkalammit (7)																											
Crd-Bt-Pl rock	penetrative	o	X		X	o	+			o									+		+						
Crd-Ky-And rock	penetrative				X	o	o			X			X	X					+		+		+				
Matovaara (8)																											
Oam-mica rock	strong	o	X		X	+	+	X											+		+						+

* and unidentified radiogenic minerals

Appendix 2. cont.

Southeastern occurrences		Mineral abbreviations are listed in Appendix 1.																													
Occurrence (in Fig.1)/rock type	Alteration	Qtz	Pl	Kfs	Bt	Chl	Ms	Cam	Oam	Crd	St	Grt	Ky	Sil	And	Crm	Ep	Aln	Spn	Zrn	Xen*	Ap	Tou	Rt	Mag	Ilm	Sph	Crb			
Levävaara (9)																															
Metadiabase, Pz	none	o	X						X														+					o			
Tonalite	weak	o	X			X	o	+													+	o	+		o						
Tonalite	strong	o	X			o	X	+													+	o			o	o					
Tonalite, mylonitic	weak	X	X			o	o	+													+				o						
Bt-Chl rock, foliated	penetrative		+			X	X														+	+		o	o			o			
Tur-Chl-Pl rock, coarse	penetrative		X			X															+	+		o							
Chl-Pl-Ms rock, coarse	penetrative	+	X			X	X														+	+		o	o						
Ky-Chl-Ms rock, coarse	penetrative	+	o			X	X						X								+	+			o						
Chl-Pl rock, coarse	penetrative	o	X			+	X	+													+	o			o						
And-Ky-Chl rock, coarse	penetrative	o	X			X	X						o		X						+	+			o						
Crm-Bt-Chl rock, coarse	penetrative	o	o			X	X	o					o			o					+	+			o				+		
Ky-Crd-Chl rock, coarse	penetrative		X			X	X	o			o	o	X	o							+	o	o		o						
Ky-Chl-Pl rock, coarse	penetrative		X			+	X	o			o		o								+	o			o						
Hiltuspuro (10)																															
D3 Hbl-tonalite	none	X	X		X			X										+	+	o			+						+		
D3 Bt-tonalite	none	X	X	o	X	o		o										o		+	+		+						+		
Leucotonalite	weak	X	X		X	o															+		+		+				+		
Tonalitic migmatite	weak	X	X		X	o															+		+		+			+			
Metadiabase, Pz	none	+	X		+			X													+	o		+				o			
Metadiabase, Pz	none	o	X		o			X													+	o		+							
Metadiabase, Pz, zone	strong	o	X					+	X									o	+				o				o				
Ky-Crd rock, zone	strong	X	X		X	o	+			o			o	+							+				+						
Ky-Crd-St rock, zone	strong	X	X		X	+	+			X	o		o								+	o	+								
Crd-rock, spot	penetrative	X	o		o	o	+			X	o		o								+	+		+				o			
Crd-Oam rock, spot	penetrative	X	+		o	X	+		X	X		o									+	+		o			+				
Kya-Crd-St rock, spot	penetrative	o			X	+	+			X	X		X	+							+	o	o	+		+	+	o			
Crd-Oam rock, spot	penetrative	X	o		o	o	+		X	X		o											+		o						
Crd-Oam rock, spot	penetrative	X			+	+	+		o	X												+	+		o						
Ky-Crd-Chl-Pl rock, coarse	penetrative		X		o	X	+			X			X	+							+	o	o		o						
Ky-Crd-Chl rock, coarse	penetrative	o	o			X	o			X			X								+	o	o		o						
Crd-Chl-Pl rock, coarse	penetrative		X		o	X	o			X											+	+			o						
Bt-Chl rock, coarse	penetrative					X	X	+		X			o	+							+			+							
Teljo (11)																															
Tonalitic gneiss	none	X	X		X	+	+											+			+		+								
D3 tonalite	weak	X	X		X	+															+	+	+		+						
Ky-Crd rock, zone	strong	o	X		X	o	+			X			X	o							+		+		o						
Ky-Crd rock, spot	strong	X	X		X	o	o			X			X	o							+	+			o						
Ky-Crd rock, spot	penetrative	X	X		o	+	+			X			X	+							+				o						
Egyptinkorpi (12)																															
Kya-Pl rock	penetrative	X	X		+	+	+						X	o											+				+		
Tettilammit (13)																															
Tonalite with Sil-zone	weak	X	X		X	+	o							X							+		+		+						
Ky-Crd rock, zone	strong	X	X		X	+	o			X			X								+	+									
Ky-Crd rock, zone	strong	X	X		o	+	o			X			o	o							+	o			o						
Ky-Crd-Sil rock, zone	strong	X	X		o	+	o			X			X	X							+		+		o						

* and unidentified radiogenic minerals

Appendix 3. Chemical compositions of cordierites.

Analysis no. Occurrence Sample/ring n	Hiltuspuro:												Tetrilampi:	
	1	2	3	4	5	6	7	8	9	10	11	12	13	14
	1A1/1	1A1/2	1A1/2	1A1/3	1A2/1	1A2/2	1A2/3	10A/1	10A/2	10C	12A	12C1	15B2/1	15B2/2
	5	1	1	2	1	1	2	1	1	1	2	2	3	2
SiO ₂	49.16	49.49	49.16	49.05	49.15	47.95	48.69	48.22	48.81	47.89	49.52	47.94	50.15	50.64
TiO ₂	0.01	0.00	0.01	0.01	0.00	0.01	0.02	0.00	0.01	0.01	0.00	0.01	0.00	0.01
Al ₂ O ₃	33.57	34.59	33.96	33.41	33.73	33.50	32.90	33.34	34.10	33.65	33.36	32.85	33.61	34.54
FeO	3.96	4.05	4.21	4.07	3.86	4.38	3.86	4.75	4.81	5.17	3.56	3.68	3.85	3.61
MnO	0.15	0.08	0.17	0.13	0.09	0.17	0.10	0.24	0.15	0.12	0.22	0.17	n.a.	n.a.
MgO	10.84	11.25	11.14	11.01	11.07	10.57	10.85	10.29	10.24	10.06	10.95	10.99	11.08	11.02
CaO	0.01	0.01	0.00	0.01	0.02	0.03	0.02	0.00	0.01	0.02	0.01	0.01	0.01	0.03
Na ₂ O	0.20	0.19	0.24	0.22	0.21	0.23	0.22	0.27	0.32	0.21	0.39	0.54	0.22	0.19
K ₂ O	0.01	0.01	0.01	0.03	0.00	0.02	0.02	0.00	0.01	0.03	0.03	0.02	0.02	0.02
Cr ₂ O ₃	0.01	0.02	0.00	0.01	0.00	0.00	0.00	0.00	0.01	0.00	0.02	0.00	n.a.	n.a.
Total	97.89	99.69	98.90	97.93	98.13	96.86	96.66	97.11	98.47	97.16	98.04	96.19	98.94	100.05
Si	4.986	4.933	4.947	4.979	4.971	4.933	5.000	4.955	4.945	4.927	5.010	4.957	5.024	5.007
Ti	0.001	0.000	0.001	0.000	0.000	0.001	0.002	0.000	0.001	0.001	0.000	0.001	0.000	0.001
Al	4.012	4.064	4.027	3.996	4.021	4.062	3.981	4.038	4.072	4.080	3.977	4.003	3.968	4.026
Fe ²⁺	0.336	0.338	0.354	0.345	0.327	0.377	0.331	0.408	0.408	0.445	0.301	0.318	0.323	0.298
Mn	0.013	0.007	0.014	0.011	0.008	0.015	0.009	0.021	0.013	0.010	0.018	0.015	n.a.	n.a.
Mg	1.638	1.672	1.671	1.666	1.669	1.621	1.661	1.576	1.547	1.543	1.652	1.693	1.655	1.625
Ca	0.001	0.001	0.000	0.001	0.002	0.003	0.002	0.000	0.001	0.002	0.001	0.001	0.001	0.003
Na	0.038	0.037	0.047	0.043	0.041	0.046	0.044	0.054	0.063	0.042	0.077	0.107	0.042	0.036
K	0.001	0.001	0.001	0.003	0.000	0.003	0.003	0.000	0.001	0.004	0.004	0.002	0.003	0.003
Cr	0.000	0.002	0.000	0.000	0.000	0.000	0.000	0.000	0.001	0.000	0.001	0.000	n.a.	n.a.
Total	11.027	11.053	11.063	11.046	11.039	11.060	11.031	11.053	11.050	11.055	11.041	11.096	11.015	10.998
Al(T2)	0.014	0.067	0.053	0.021	0.029	0.067	0.000	0.045	0.055	0.073	0.000	0.043	0.000	0.000
Al(T1)	3.998	3.997	3.974	3.975	3.992	3.995	3.981	3.993	3.998	3.999	3.977	3.959	3.968	3.999
Fe(T1)	0.001	0.002	0.025	0.024	0.008	0.005	0.018	0.007	0.000	0.000	0.021	0.040	0.032	0.000
Al(M)	0.000	0.000	0.000	0.000	0.000	0.000	0.000	0.000	0.018	0.008	0.000	0.000	0.000	0.026
Fe(M)	0.335	0.336	0.329	0.321	0.319	0.372	0.314	0.402	0.408	0.445	0.279	0.278	0.291	0.298
X _{Mg}	0.824	0.829	0.820	0.824	0.833	0.805	0.830	0.786	0.786	0.772	0.838	0.836	0.837	0.845

n = number of analyses

n.a. = not analysed

mineral formula based on 36 charges or 18 oxygens

Assemblages:

Oam-Crd-Ky rock (zone)

1. Crd-Ky-Qtz-Pl-Bt-Chl-Ath
2. Crd-Chl-Ged-Ath-Qtz-Bt
3. Crd-Bt-Ath
4. Crd-Ath-Pl-Chl-Qtz
5. Crd-Ath-Bt-Qtz-Chl-Pl
6. Crd-Bt-Qtz
7. Crd-Ath-Qtz

Ky-St-Crd rock (zone)

8. Crd-St-Ky-Sil-Pl-Qtz
9. Crd-St-Bt-Ilm
10. Crd-St-Pl-Qtz-Bt

Ky-Chl-Crd rock (coarse-grained)

11. Crd-Ky-Bt-Chl-Pl-Qtz
12. Crd-Ky-Bt-Chl

Ky-Crd-Sil rock (zone)

13. Crd-Ky-Sil-Bt-Ms-Pl-Qtz
14. Crd-Ky-Sil-Bt-Ms-Pl-Qtz

Appendix 4. Chemical compositions of staurolites.

Analysis no.	15	16	17	18
Occurrence	Hiltuspuro:			
Sample/ring n	10A/1 1	10A/1 1	10A/2 2	10C 1
SiO ₂	27.79	27.36	27.50	27.28
TiO ₂	0.43	0.37	0.62	0.59
Al ₂ O ₃	54.31	53.46	52.85	52.25
FeO	12.89	12.13	13.16	13.32
MnO	0.33	0.31	0.30	0.26
MgO	2.55	2.71	2.92	2.87
CaO	0.00	0.00	0.01	0.01
Na ₂ O	0.00	0.04	0.02	0.02
K ₂ O	0.00	0.01	0.01	0.03
Cr ₂ O ₃	0.13	0.02	0.05	0.01
Total	98.43	96.38	97.43	96.62
Si	3.905	3.914	3.915	3.921
Ti	0.045	0.039	0.067	0.064
Al	8.993	9.013	8.868	8.851
Fe ²⁺	1.515	1.451	1.567	1.601
Mn	0.039	0.038	0.036	0.032
Mg	0.534	0.577	0.620	0.615
Ca	0.000	0.000	0.001	0.001
Na	0.000	0.011	0.006	0.004
K	0.000	0.002	0.002	0.005
Cr	0.014	0.002	0.005	0.001
Total	15.046	15.046	15.086	15.094
Al(T)	0.095	0.086	0.085	0.079
Al(M6)	8.898	8.927	8.782	8.772
Al(M4+M6)	0.000	0.000	0.000	0.000
Fe(M6)	0.087	0.071	0.212	0.227
Fe(M4+M6)	1.427	1.379	1.355	1.374
X _{Mg}	0.256	0.279	0.279	0.274

n = number of analyses

mineral formula based on 47 charges or 23.5 oxygens

Assemblages:**Ky-St-Crd rock (zone)**

15. St-Crd-Ky-Sil-Pl-Qtz
 16. St-Crd-Ky-Sil-Pl-Qtz
 17. St-Crd-Bt-Ilm
 18. St-Crd-Pl-Qtz-Bt

Appendix 5. Chemical compositions of garnets.

Analysis no.	19	20	21	22	23	24	25
Occurrence	Hiltuspuro:						
Sample/ring	48B1/1	48B1/1	48B1/1	48B1/1	48B1/6	48B1/6	48B2/1
SiO ₂	36.83	36.90	36.67	36.94	36.40	36.13	35.91
TiO ₂	0.00	0.01	0.00	0.03	0.01	0.04	0.01
Al ₂ O ₃	20.63	20.58	20.35	20.53	20.70	20.34	20.59
FeO	27.39	26.88	27.08	27.18	35.31	33.51	36.27
MnO	9.93	9.42	9.56	10.00	5.05	5.63	4.17
MgO	1.83	2.17	1.80	1.87	0.90	1.54	1.17
CaO	3.01	3.82	3.48	3.43	1.13	1.19	1.14
Cr ₂ O ₃	0.04	0.03	0.04	0.02	0.00	0.00	0.00
Total	99.66	99.80	98.97	100.00	99.49	98.37	99.25
Si	2.997	2.992	3.003	2.997	2.997	2.998	2.971
Ti	0.000	0.000	0.000	0.002	0.000	0.002	0.000
Al	1.979	1.966	1.965	1.963	2.008	1.989	2.008
Fe ²⁺	1.864	1.823	1.855	1.845	2.431	2.325	2.510
Mn	0.685	0.647	0.663	0.687	0.352	0.395	0.292
Mg	0.222	0.263	0.219	0.226	0.110	0.191	0.144
Ca	0.263	0.332	0.305	0.298	0.100	0.106	0.101
Cr	0.002	0.002	0.002	0.001	0.000	0.000	0.000
Total	8.012	8.024	8.013	8.019	7.999	8.006	8.025
Alm	0.615	0.595	0.610	0.604	0.812	0.771	0.824
Sps	0.226	0.211	0.218	0.225	0.118	0.131	0.096
Prp	0.073	0.086	0.072	0.074	0.037	0.063	0.047
Grs	0.087	0.108	0.100	0.098	0.033	0.035	0.033

mineral formula based on 24 charges or 12 oxygens

Assemblages:**Grt-Qtz rock**

19. rim, Grt-Bt-Chl-Qtz
 20. core, Grt-Bt-Chl-Qtz
 21. rim, Grt-Bt-Chl-Qtz
 22. rim, Grt-Bt-Chl-Qtz
 23. rim, Grt-Ms-Pl-Qts
 24. core, Grt-Ms-Pl-Qts
 25. core, Grt-Ms-Pl-Qtz

Appendix 6. Chemical compositions of orthoamphiboles.

Analysis no.	26	27	28	29	30	31	32	33	34
Occurrence	Hiltuspuro:								
Sample/ring	1A1/1	1A1/2	1A1/2	1A1/2	1A1/2	1A1/3	1A2/3	1A2/3	1A2/3
SiO₂	53.47	46.00	53.99	55.33	56.05	54.43	54.88	54.60	54.88
TiO₂	0.03	0.26	0.04	0.06	0.03	0.04	0.00	0.03	0.02
Al₂O₃	3.69	13.43	3.25	2.88	2.38	3.00	2.67	2.18	1.43
FeO	18.57	19.36	19.47	18.11	19.02	19.55	19.58	17.76	17.73
MnO	0.65	0.61	0.60	0.59	0.59	0.54	0.59	0.62	0.69
MgO	21.95	16.74	20.11	22.01	22.33	22.03	22.15	21.81	22.08
CaO	0.13	0.13	0.07	0.10	0.06	0.08	0.09	0.09	0.04
Na₂O	0.21	1.55	0.25	0.23	0.16	0.17	0.22	0.19	0.06
K₂O	0.00	0.02	0.02	0.01	0.00	0.01	0.01	0.01	0.00
Total	98.70	98.10	97.80	99.32	100.62	99.85	100.19	97.29	96.93
Si	7.561	6.635	7.718	7.730	7.754	7.627	7.664	7.787	7.852
Ti	0.003	0.028	0.004	0.006	0.003	0.004	0.000	0.003	0.002
Al	0.615	2.283	0.548	0.474	0.388	0.495	0.439	0.366	0.241
Fe²⁺	2.196	2.335	2.328	2.116	2.200	2.291	2.287	2.118	2.122
Mn	0.078	0.075	0.073	0.070	0.069	0.064	0.070	0.075	0.084
Mg	4.627	3.600	4.286	4.584	4.605	4.602	4.611	4.637	4.710
Ca	0.020	0.020	0.011	0.015	0.009	0.012	0.013	0.014	0.006
Na	0.058	0.433	0.069	0.062	0.043	0.046	0.060	0.053	0.017
K	0.000	0.004	0.004	0.002	0.000	0.002	0.002	0.002	0.000
Total	15.157	15.414	15.040	15.059	15.071	15.145	15.147	15.054	15.033
Al(T1)	0.439	1.365	0.282	0.270	0.246	0.373	0.336	0.213	0.148
Al(M2)	0.176	0.918	0.266	0.204	0.142	0.123	0.104	0.153	0.093
Ti(M2)	0.003	0.028	0.004	0.006	0.003	0.004	0.000	0.003	0.002
Fe(M2)	0.586	0.414	0.609	0.565	0.600	0.622	0.629	0.578	0.591
Mg(M2)	1.235	0.639	1.121	1.225	1.255	1.250	1.268	1.266	1.313
Fe(M1+M3)	0.966	1.180	1.056	0.947	0.970	0.997	0.995	0.941	0.932
Mg(M1+M3)	2.034	1.820	1.944	2.053	2.030	2.003	2.005	2.059	2.068
Fe(M4)	0.644	0.740	0.663	0.603	0.630	0.672	0.664	0.599	0.598
Mg(M4)	1.358	1.141	1.221	1.307	1.319	1.349	1.338	1.312	1.328
Mn(M4)	0.078	0.075	0.073	0.070	0.069	0.064	0.070	0.075	0.084
Ca(M4)	0.020	0.020	0.011	0.015	0.009	0.012	0.013	0.014	0.006
Na(M4)	0.000	0.023	0.031	0.005	0.000	0.000	0.000	0.000	0.000
K(M4)	0.000	0.000	0.001	0.000	0.000	0.000	0.000	0.000	0.000
Na(A)	0.058	0.410	0.038	0.057	0.043	0.046	0.060	0.052	0.017
K(A)	0.000	0.003	0.003	0.002	0.000	0.002	0.002	0.002	0.000
Vac(A)	0.942	0.586	0.959	0.941	0.957	0.952	0.939	0.946	0.983
X_{Mg}	0.678	0.607	0.648	0.684	0.677	0.668	0.668	0.686	0.689

mineral formula based on 46 charges or 23 oxygens; 15 cations, all Fe as Fe²⁺.

Assemblages:**Oam-Crd-Ky rock (zone)**

26. Ath-Crd-Ky-Qtz-Pl-Bt-Chl
 27. Ged-Ath-Crd-Chl-Qtz-Bt
 28. Ath-Ged-Crd-Chl-Qtz-Bt
 29. Ath-Crd-Bt
 30. Ath-Crd-Bt

31. Ath-Crd-Pl-Chl-Qtz
 32. Ath-Crd-Qtz
 33. Ath-Crd-Qtz
 34. Ath-Crd-Qtz

Appendix 7. Chemical compositions of plagioclases.

Analysis no. Occurrence Sample/ring n	35						41						45						50					
	Havukkalammit:						Hiltuspuro:						Tettilampi:											
	25A1/2	25B/1	25B/2	25B/3	25B/3	25B/5	1A1/1	1A1/3	1A2/1	3	10A/1	10C	12A	48B1/6	48B2/1	15B2/1								
1	1	1	1	1	1	1	2	3	2	3	2	2	1	1	1									
SiO ₂	54.14	46.71	46.76	54.02	51.60	49.82	67.95	66.21	65.78	65.56	66.20	65.34	67.11	65.98	63.81	64.89								
TiO ₂	0.02	0.00	0.01	0.00	0.00	0.00	0.00	0.00	0.04	0.00	0.02	0.01	0.00	0.00	0.00	0.03								
Al ₂ O ₃	29.68	34.73	35.14	30.41	30.02	33.27	20.56	21.91	20.33	21.32	20.69	21.87	20.69	22.27	23.06	19.48								
FeO	0.03	0.02	0.06	0.04	0.03	0.05	0.00	0.04	0.21	0.01	0.03	0.05	0.02	0.09	0.07	0.00								
MnO	n.a.	n.a.	n.a.	n.a.	n.a.	n.a.	n.a.	n.a.	n.a.	n.a.	n.a.	n.a.	n.a.	0.00	n.a.	n.a.								
MgO	0.03	0.00	0.00	0.00	0.00	0.00	0.01	0.00	0.01	0.00	0.02	0.02	0.01	0.00	0.00	0.00								
CaO	11.20	15.51	17.37	11.95	12.83	14.65	0.83	2.06	0.45	2.29	1.69	1.87	1.30	2.09	3.56	0.51								
Na ₂ O	4.65	1.77	1.56	4.54	4.13	2.70	11.07	9.74	11.22	10.67	10.95	10.43	10.76	9.94	9.40	11.59								
K ₂ O	0.03	0.01	0.03	0.03	0.06	0.00	0.03	0.01	0.06	0.04	0.03	0.10	0.03	0.05	0.07	0.04								
Total	99.78	98.75	100.93	100.99	98.67	100.49	100.45	99.97	98.10	99.89	99.64	99.66	99.91	100.42	99.97	96.54								
Si	2.442	2.158	2.127	2.414	2.371	2.254	2.956	2.897	2.937	2.887	2.918	2.879	2.939	2.879	2.814	2.948								
Ti	0.001	0.000	0.000	0.000	0.000	0.000	0.000	0.000	0.001	0.000	0.001	0.000	0.000	0.000	0.000	0.001								
Al	1.578	1.891	1.884	1.601	1.626	1.774	1.054	1.130	1.070	1.107	1.075	1.135	1.068	1.146	1.198	1.043								
Fe ²⁺	0.001	0.001	0.002	0.001	0.001	0.002	0.000	0.001	0.008	0.000	0.001	0.002	0.001	0.003	0.003	0.000								
Mn	n.a.	n.a.	n.a.	n.a.	n.a.	n.a.	n.a.	n.a.	n.a.	n.a.	n.a.	n.a.	n.a.	0.000	n.a.	n.a.								
Mg	0.002	0.000	0.000	0.000	0.000	0.000	0.001	0.000	0.001	0.000	0.001	0.001	0.001	0.000	0.000	0.000								
Ca	0.541	0.768	0.847	0.572	0.632	0.710	0.039	0.097	0.022	0.108	0.080	0.088	0.061	0.098	0.168	0.025								
Na	0.407	0.159	0.138	0.393	0.368	0.237	0.934	0.826	0.971	0.911	0.935	0.891	0.913	0.841	0.804	1.021								
K	0.002	0.001	0.002	0.002	0.004	0.000	0.002	0.001	0.003	0.002	0.002	0.005	0.002	0.003	0.004	0.002								
Total	4.973	4.976	5.000	4.983	5.002	4.977	4.985	4.952	5.014	5.016	5.013	5.001	4.984	4.970	4.991	5.041								
An	0.570	0.828	0.859	0.592	0.630	0.750	0.040	0.105	0.022	0.106	0.079	0.089	0.063	0.104	0.172	0.024								
Ab	0.428	0.171	0.140	0.407	0.367	0.250	0.959	0.895	0.975	0.892	0.920	0.905	0.936	0.893	0.824	0.974								
Or	0.002	0.001	0.002	0.002	0.004	0.000	0.002	0.001	0.003	0.002	0.002	0.005	0.002	0.003	0.004	0.002								

n = number of analyses

n.a. = not analysed

mineral formula based on 16 charges or 8 oxygens

Assemblages:

Ky-Bt-Pl rock (coarsed grained)

- 35. Pl-Bt-Ky (earlier phase)
- 36. Pl-Bt (earlier phase)
- 37. Pl-Bt (earlier phase)
- 38. Pl-Bt-Ky (later phase)
- 39. Pl-Bt-Ky (later phase)
- 40. Pl-Bt-Ky (later phase)

Oam-Crd-Ky rock (zone)

- 41. Pl-Crd-Ky-Ath-Bt-Chl-Qtz
- 42. Pl-Crd-Ath-Chl-Qtz
- 43. Pl-Cdr-Ath-Bt-Chl-Qtz
- Leucotonalite
- 44. Pl-Bt-Qtz

Ky-St-Crd rock (zone)

- 45. Pl-Crd-St-Ky-Sil-Qtz
- 46. Pl-Crd-St-Bt-Qtz

Ky-Chl-Crd rock (coarse grained)

- 47. Pl-Crd-Ky-Bt-Chl-Qtz

Grt-Qtz rock

- 48. Pl-Grt-Ms-Qtz
- 49. Pl-Grt-Ms-Qtz

Ky-Crd-Sil rock (zone)

- 50. Pl-Crd-Ky-Sil-Bt-Ms-Qtz

Appendix 8. Chemical compositions of biotites.

Analysis no.	51	52	53	54	55	56	57	58	59	60	61	62
Occurrence	Havukkalammit:								Tettilampi:			
Sample/ring n	25A1/1	25A1/2	25B/1	25B/2	25B/3	25B/3	25B/4	25B/5	15B2/1	15B2/1	15B2/2	15B2/2
	1	1	1	1	1	1	1	1	1	1	1	1
SiO ₂	38.73	37.31	36.38	36.56	37.34	37.31	36.97	37.06	38.16	38.43	38.29	37.72
TiO ₂	0.58	0.53	0.59	0.52	0.47	0.64	0.96	0.56	1.21	1.08	1.10	1.12
Al ₂ O ₃	20.77	19.19	20.77	19.65	20.95	20.91	20.33	20.62	20.23	20.57	20.47	21.21
FeO	11.66	11.98	13.76	13.28	12.33	12.78	13.23	13.16	10.82	10.79	10.51	11.02
MnO	0.11	0.16	0.20	0.17	0.13	0.15	0.14	0.15	0.04	0.13	0.07	0.14
MgO	17.11	17.20	15.60	15.29	15.49	15.31	15.79	15.68	17.03	17.21	17.43	16.44
CaO	0.04	0.00	0.15	0.04	0.01	0.03	0.03	0.05	0.00	0.00	0.00	0.03
Na ₂ O	0.34	0.21	0.27	0.31	0.47	0.39	0.22	0.37	0.32	0.36	0.37	0.30
K ₂ O	8.80	9.02	8.38	8.95	8.62	9.16	9.32	8.72	8.82	8.70	8.53	8.61
Total	98.15	95.58	96.10	94.76	95.81	96.67	96.98	96.38	96.63	97.28	96.77	96.60
Si	2.724	2.717	2.649	2.704	2.704	2.692	2.671	2.684	2.720	2.717	2.716	2.689
Ti	0.030	0.029	0.032	0.029	0.026	0.035	0.052	0.031	0.065	0.058	0.059	0.060
Al	1.722	1.646	1.783	1.713	1.788	1.778	1.731	1.760	1.700	1.715	1.711	1.782
Fe ²⁺	0.686	0.729	0.838	0.822	0.747	0.771	0.799	0.797	0.645	0.638	0.624	0.657
Mn	0.007	0.010	0.012	0.010	0.008	0.009	0.008	0.009	0.003	0.008	0.004	0.008
Mg	1.794	1.866	1.693	1.685	1.672	1.647	1.701	1.693	1.810	1.815	1.843	1.748
Ca	0.003	0.000	0.011	0.003	0.001	0.002	0.002	0.004	0.000	0.000	0.000	0.003
Na	0.047	0.029	0.039	0.044	0.066	0.055	0.031	0.052	0.044	0.050	0.050	0.042
K	0.790	0.838	0.778	0.844	0.797	0.843	0.859	0.806	0.802	0.785	0.772	0.783
Total	7.803	7.864	7.836	7.855	7.808	7.832	7.856	7.834	7.788	7.785	7.781	7.772
Si(T2)	0.724	0.717	0.649	0.704	0.704	0.692	0.671	0.684	0.720	0.717	0.716	0.689
Al(T2)	1.276	1.283	1.351	1.296	1.296	1.308	1.329	1.316	1.280	1.283	1.284	1.311
Al(M2)	0.446	0.363	0.432	0.417	0.492	0.471	0.403	0.444	0.420	0.432	0.428	0.472
Fe(M2)	0.420	0.449	0.504	0.506	0.455	0.474	0.491	0.485	0.397	0.391	0.382	0.399
Mg(M2)	1.097	1.149	1.019	1.038	1.019	1.012	1.046	1.031	1.115	1.112	1.128	1.061
Fe(M1)	0.266	0.280	0.333	0.316	0.291	0.297	0.308	0.311	0.247	0.247	0.242	0.258
Mg(M1)	0.697	0.717	0.674	0.648	0.653	0.635	0.656	0.662	0.695	0.703	0.716	0.686
Vac(A)	0.257	0.191	0.261	0.200	0.269	0.212	0.172	0.246	0.242	0.265	0.278	0.259
X _{Mg}	0.721	0.716	0.666	0.669	0.689	0.679	0.678	0.677	0.736	0.738	0.746	0.724

n = number of analyses

mineral formula based on 22 charges or 11 oxygens

Assemblages:**Ky-Bt-Pl rock (coarse grained)**

- 51. Bt-Pl-Ky-Ms-Chl
- 52. Bt-Pl-Ky
- 53. Bt-Pl
- 54. Bt-Pl
- 55. Bt-Pl-Ky
- 56. Bt-Pl-Ky
- 57. Bt-Chl-Ky-Pl
- 58. Bt-Pl-Ky

Ky-Crd-Sil rock (zone)

- 59. Bt-Crd-Ky-Sil-Ms-Pl-Qtz
- 60. Bt-Crd-Ky-Sil-Ms-Pl-Qtz
- 61. Bt-Crd-Ky-Sil-Ms-Pl-Qtz
- 62. Bt-Crd-Ky-Sil-Ms-Pl-Qtz

Appendix 8. cont.

Analysis no.	63	64	65	66	67	68	69	70	71	72	73	74	75	76	77	78	79
Occurrence	Hiltuspuro:																
Sample/ring n	1A1/1 1	1A1/2 1	1A1/2 2	1A2/2 2	1A2/4 1	1A2/4 1	3 1	10A/1 2	10A/2 1	10A/2 2	10C 2	10C 1	12A 2	12A 1	12C1 4	48B1/1 1	48B1/1 1
SiO ₂	39.02	39.47	39.35	38.26	38.55	38.50	37.53	36.70	37.40	37.39	36.88	35.95	37.93	38.48	38.45	35.65	35.29
TiO ₂	1.17	1.19	1.24	1.13	1.06	1.04	1.12	1.08	1.17	0.99	1.25	1.04	1.32	0.96	1.20	1.13	0.90
Al ₂ O ₃	18.31	17.69	17.06	17.13	18.20	17.45	19.25	18.97	18.32	18.35	18.59	18.96	18.06	19.09	19.34	19.20	19.24
FeO	12.04	12.70	11.43	11.82	12.13	12.47	13.32	14.93	16.28	15.15	16.58	16.03	11.68	11.01	9.58	24.81	22.30
MnO	0.01	0.03	0.04	0.04	0.02	0.00	0.07	0.06	0.09	0.09	0.04	0.03	0.13	0.09	0.07	0.81	0.78
MgO	16.68	17.83	16.98	17.91	17.42	17.52	15.53	14.63	14.47	14.46	14.13	13.59	17.64	17.43	16.66	6.68	7.13
CaO	0.02	0.02	0.04	0.02	0.00	0.00	0.01	0.17	0.01	0.00	0.01	0.03	0.02	0.01	0.01	0.00	0.01
Na ₂ O	0.37	0.29	0.44	0.48	0.75	0.54	0.28	0.46	0.45	0.39	0.21	0.29	0.34	0.38	0.35	0.13	0.10
K ₂ O	8.32	8.37	8.29	8.32	8.18	8.21	9.22	8.28	8.66	8.81	9.08	8.89	8.65	8.44	9.29	9.09	9.25
Total	95.94	97.59	94.85	95.08	96.31	95.73	96.33	95.25	96.85	95.62	96.76	94.81	95.74	95.89	94.94	97.52	94.99
Si	2.809	2.803	2.859	2.789	2.773	2.791	2.729	2.713	2.739	2.760	2.714	2.696	2.749	2.763	2.782	2.718	2.736
Ti	0.063	0.064	0.068	0.062	0.057	0.057	0.061	0.060	0.064	0.055	0.069	0.059	0.072	0.052	0.065	0.065	0.052
Al	1.554	1.481	1.461	1.472	1.543	1.491	1.650	1.653	1.581	1.596	1.613	1.676	1.542	1.616	1.648	1.725	1.758
Fe ²⁺	0.725	0.754	0.695	0.721	0.730	0.756	0.810	0.923	0.997	0.935	1.021	1.005	0.708	0.661	0.579	1.582	1.446
Mn	0.001	0.002	0.002	0.002	0.001	0.000	0.004	0.003	0.006	0.006	0.002	0.002	0.008	0.005	0.004	0.052	0.051
Mg	1.790	1.888	1.840	1.946	1.868	1.894	1.683	1.612	1.580	1.591	1.550	1.520	1.905	1.866	1.797	0.759	0.824
Ca	0.002	0.002	0.003	0.001	0.000	0.000	0.001	0.013	0.001	0.000	0.001	0.002	0.001	0.001	0.001	0.000	0.001
Na	0.052	0.040	0.061	0.068	0.105	0.076	0.039	0.066	0.064	0.056	0.030	0.042	0.047	0.053	0.049	0.020	0.015
K	0.764	0.758	0.769	0.773	0.751	0.759	0.855	0.780	0.809	0.829	0.852	0.851	0.800	0.773	0.857	0.884	0.915
Total	7.759	7.792	7.757	7.834	7.826	7.824	7.833	7.824	7.842	7.829	7.852	7.853	7.832	7.790	7.782	7.806	7.798
Si(T2)	0.809	0.803	0.859	0.789	0.773	0.791	0.729	0.713	0.739	0.760	0.714	0.696	0.749	0.763	0.782	0.718	0.736
Al(T2)	1.191	1.197	1.141	1.211	1.227	1.209	1.271	1.287	1.261	1.240	1.286	1.304	1.251	1.237	1.218	1.282	1.264
Al(M2)	0.363	0.284	0.320	0.261	0.315	0.282	0.378	0.366	0.321	0.357	0.327	0.372	0.291	0.379	0.430	0.443	0.494
Fe(M2)	0.454	0.471	0.441	0.453	0.457	0.474	0.506	0.572	0.623	0.586	0.636	0.624	0.441	0.409	0.366	0.972	0.893
Mg(M2)	1.120	1.179	1.168	1.222	1.169	1.187	1.051	0.999	0.986	0.997	0.966	0.943	1.188	1.155	1.135	0.467	0.510
Fe(M1)	0.271	0.283	0.253	0.268	0.273	0.282	0.304	0.351	0.375	0.349	0.385	0.382	0.267	0.252	0.213	0.610	0.552
Mg(M1)	0.670	0.709	0.671	0.724	0.698	0.707	0.633	0.613	0.594	0.595	0.584	0.577	0.717	0.711	0.662	0.293	0.315
Vac(A)	0.288	0.282	0.292	0.295	0.354	0.317	0.184	0.286	0.255	0.227	0.178	0.191	0.247	0.280	0.192	0.136	0.100
X _{Mg}	0.711	0.714	0.725	0.729	0.719	0.715	0.674	0.635	0.612	0.628	0.602	0.602	0.727	0.737	0.755	0.317	0.355

n = number of analyses

mineral formula based on 22 charges or 11 oxygens

Assemblages:

Oam-Crd-Ky rock (zone)

- 63. Bt-Crd-Ky-Chl-Ath-Pl-Qtz
- 64. Bt-Crd-Ath
- 65. Bt-Crd-Ath
- 66. Bt-Crd-Ath
- 67. Bt-Pl-Crd
- 68. Bt-Pl-Crd

Leucotonalite

- 69. Bt-Pl-Qtz

Ky-St-Crd rock (zone)

- 70. Bt-Crd-St-Ky-Sil-Pl-Qtz
- 71. Bt-Crd-St-Ilm
- 72. Bt-Crd-St-Ilm
- 73. Bt-Crd-St-Pl-Qtz
- 74. Bt-Crd-St-Pl-Qtz

Ky-Chl-Crd rock (coarse grained)

- 75. Bt-Crd-Ky-Chl-Pl-Qtz
- 76. Bt-Crd-Ky-Chl-Pl-Qtz
- 77. Bt-Crd-Ky-Chl

Grt-Qtz rock

- 78. Bt-Grt-Chl-Qtz
- 79. Bt-Grt-Chl-Qtz

Appendix 9. Chemical compositions of chlorites.

Analysis no. Occurrence Sample/ring n	80	81	82	83	84	85	86	87	88	89	90	91	92	93
	Havukkalammit:			Hiltuspuro:										
	25A1/1	25A1/1	25B/4	1A1/1	1A1/1	1A1/2	1A1/2	1A1/3	12A	12A	12C1	48B1/1	48B1/1	48B1/1
	1	1	1	1	1	2	2	1	3	2	2	1	1	1
SiO ₂	26.71	26.47	25.78	26.14	26.93	27.43	27.13	27.31	25.76	26.40	27.40	24.85	23.97	24.52
TiO ₂	0.00	0.01	0.02	0.05	0.07	0.10	0.06	0.04	0.07	0.06	0.09	0.08	0.04	0.01
Al ₂ O ₃	25.97	26.15	23.50	23.59	23.22	22.87	23.90	22.58	23.55	23.74	23.74	22.05	23.31	23.19
FeO	14.04	16.32	15.14	13.14	13.09	12.48	12.84	13.31	13.67	13.88	10.91	31.37	31.58	32.78
MnO	0.18	0.28	0.22	0.03	0.09	0.05	0.06	0.08	0.14	0.10	0.18	0.59	0.87	0.99
MgO	23.99	21.46	22.83	24.01	23.70	23.22	23.78	22.28	24.94	24.42	24.67	9.86	9.31	10.39
CaO	0.01	0.06	0.02	0.00	0.02	0.01	0.02	0.03	0.01	0.02	0.01	0.00	0.00	0.00
Na ₂ O	0.02	0.01	0.00	0.03	0.03	0.02	0.01	0.03	0.04	0.02	0.03	0.05	0.11	0.02
K ₂ O	0.04	0.04	0.03	0.03	0.01	0.08	0.04	0.04	0.02	0.03	0.04	0.02	0.13	0.02
Total	90.95	90.81	87.54	87.02	87.16	86.26	87.83	85.70	88.19	88.65	87.04	88.87	89.32	91.91
Si	2.543	2.553	2.577	2.597	2.666	2.731	2.658	2.749	2.539	2.584	2.682	2.670	2.573	2.565
Ti	0.000	0.001	0.002	0.004	0.005	0.007	0.004	0.003	0.005	0.004	0.007	0.006	0.003	0.001
Al	2.914	2.972	2.769	2.762	2.709	2.684	2.760	2.678	2.735	2.739	2.739	2.792	2.949	2.859
Fe ²⁺	1.118	1.316	1.266	1.092	1.084	1.039	1.052	1.120	1.127	1.136	0.893	2.819	2.835	2.868
Mn	0.015	0.023	0.019	0.003	0.008	0.004	0.005	0.007	0.012	0.008	0.015	0.054	0.079	0.088
Mg	3.405	3.085	3.402	3.556	3.497	3.446	3.473	3.343	3.664	3.564	3.600	1.579	1.490	1.620
Ca	0.001	0.006	0.002	0.000	0.002	0.001	0.002	0.003	0.001	0.002	0.001	0.000	0.000	0.000
Na	0.004	0.002	0.000	0.006	0.006	0.004	0.002	0.006	0.008	0.004	0.006	0.010	0.023	0.004
K	0.005	0.005	0.004	0.004	0.001	0.010	0.005	0.005	0.003	0.004	0.005	0.003	0.018	0.003
Total	10.004	9.964	10.039	10.023	9.978	9.927	9.961	9.915	10.093	10.046	9.947	9.934	9.970	10.008
Si(T2)	0.543	0.553	0.577	0.597	0.666	0.731	0.658	0.749	0.539	0.584	0.682	0.670	0.573	0.565
Al(T2)	1.457	1.446	1.422	1.399	1.329	1.262	1.338	1.248	1.456	1.411	1.311	1.323	1.424	1.434
Al(M2)	1.457	1.526	1.347	1.363	1.380	1.422	1.422	1.430	1.279	1.328	1.427	1.469	1.525	1.425
Fe(M2)	0.134	0.141	0.176	0.150	0.146	0.134	0.134	0.143	0.169	0.162	0.113	0.336	0.306	0.360
Mg(M2)	0.407	0.331	0.474	0.487	0.472	0.444	0.443	0.426	0.550	0.509	0.457	0.188	0.161	0.204
Mn(M2)	0.002	0.002	0.003	0.000	0.001	0.001	0.001	0.001	0.002	0.001	0.002	0.006	0.009	0.011
Fe(M1)	0.984	1.175	1.089	0.942	0.937	0.905	0.918	0.978	0.958	0.974	0.780	2.483	2.529	2.508
Mg(M1)	2.998	2.755	2.928	3.069	3.025	3.003	3.030	2.917	3.115	3.055	3.143	1.391	1.329	1.417
Mn(M1)	0.013	0.020	0.016	0.002	0.007	0.004	0.004	0.006	0.010	0.007	0.013	0.047	0.071	0.077
X _{Mg}	0.750	0.697	0.726	0.765	0.762	0.768	0.767	0.748	0.763	0.757	0.799	0.355	0.338	0.354

n = number of analyses

mineral formula based on 28 charges or 14 oxygens

Assemblages:

Ky-Bt-Pl rock (coarse grained)

- 80. Chl-Ky-Bt-Ms-Pl
- 81. Chl-Ky-Bt-Ms-Pl
- 82. Chl-Bt-Ky-Pl

Ky-Chl-Crd rock (coarse grained)

- 88. Chl-Crd-Ky-Bt-Pl-Qtz
- 89. Chl-Crd-Ky-Bt-Pl-Qtz
- 90. Chl-Crd-Ky-Bt

Oam-Crd-Ky rock (zone)

- 83. Chl-Crd-Ky-Bt-Ath-Pl-Qtz
- 84. Chl-Crd-Ky-Bt-Ath-Pl-Qtz
- 85. Chl-Crd-Ged-Ath-Qtz-Bt
- 86. Chl-Crd-Ged-Ath-Qtz-Bt
- 87. Chl-Crd-Ath-Pl-Qtz

Grt-Qtz rock

- 91. Chl-Grt-Bt-Qtz
- 92. Chl-Grt-Bt-Qtz
- 93. Chl-Grt-Bt-Qtz

Appendix 10. Chemical compositions of white micas.

Analysis no.	94	95	96	97	98	99	100	101	102	103
Occurrence	Havukkalammit:		Hiltuspuro:			Tettilampi:				
Sample/ring n	25A1/1	25A1/1	1A2/4	1A2/4	48B1/6	15B2/1	15B2/1	15B2/1	15B2/2	15B2/2
	1	1	1	1	8	1	1	1	1	1
SiO₂	45.38	45.91	47.33	48.98	46.36	45.60	46.71	45.05	46.74	46.82
TiO₂	0.05	0.18	0.00	0.01	0.19	0.48	0.61	0.48	0.70	0.63
Al₂O₃	35.95	36.86	37.59	32.42	37.91	35.80	35.90	36.66	35.61	36.16
FeO	2.18	2.36	0.85	1.60	1.21	1.73	2.06	2.00	2.00	1.91
MnO	0.00	0.00	0.04	0.00	0.00	0.00	0.00	0.00	0.00	0.00
MgO	0.45	0.38	1.50	6.00	0.28	0.55	0.58	0.55	0.68	0.78
CaO	0.05	0.06	0.04	0.04	0.01	0.02	0.00	0.02	0.01	0.00
Na₂O	1.31	1.34	6.02	4.49	0.92	1.83	1.80	2.14	1.90	1.65
K₂O	8.85	8.40	1.26	1.20	9.62	7.95	8.09	7.97	7.75	7.46
Total	94.41	95.49	94.63	94.74	96.49	94.16	95.85	95.02	95.68	95.75
Si	3.046	3.033	3.049	3.156	3.027	3.052	3.071	2.998	3.079	3.072
Ti	0.002	0.009	0.000	0.000	0.009	0.024	0.030	0.024	0.035	0.031
Al	2.845	2.870	2.854	2.462	2.917	2.824	2.782	2.875	2.765	2.797
Fe²⁺	0.122	0.130	0.046	0.086	0.066	0.097	0.113	0.111	0.110	0.105
Mn	0.000	0.000	0.002	0.000	0.000	0.000	0.000	0.000	0.000	0.000
Mg	0.045	0.037	0.144	0.576	0.027	0.055	0.057	0.055	0.067	0.077
Ca	0.004	0.004	0.003	0.003	0.001	0.002	0.000	0.001	0.001	0.000
Na	0.171	0.171	0.752	0.561	0.117	0.237	0.230	0.276	0.243	0.210
K	0.758	0.708	0.104	0.099	0.801	0.679	0.679	0.677	0.651	0.624
Total	6.993	6.963	6.952	6.943	6.964	6.970	6.962	7.017	6.951	6.916
Si(T2)	1.046	1.033	1.049	1.156	1.027	1.052	1.071	0.998	1.079	1.072
Al(T2)	0.954	0.967	0.951	0.844	0.973	0.948	0.929	1.002	0.921	0.928
Al(M2)	1.891	1.903	1.902	1.617	1.943	1.876	1.853	1.873	1.844	1.869
Vac(A)	0.067	0.117	0.141	0.337	0.316	0.082	0.091	0.046	0.105	0.166
X_{Na}	0.184	0.194	0.879	0.850	0.127	0.259	0.253	0.290	0.272	0.252

mineral formula based on 22 charges or 11 oxygens
n = number of analyses

Assemblages:

Ky-Bt-Pl rock (coarse grained)

- 94. Ms-Ky-Bt-Chl-Pl
- 95. Ms-Ky-Bt-Chl-Pl

Oam-Crd-Ky rock (zone)

- 96. Pg-Crd-Pl
- 97. Pg-Crd-Pl

Grt-Qtz rock

- 98. Ms-Grt-Pl-Qtz

Ky-Crd-Sil rock (zone)

- 99. Ms-Crd-Bt-Ky-Sil-Pl-Qtz
- 100. Ms-Crd-Bt-Ky-Sil-Pl-Qtz
- 101. Ms-Crd-Bt-Ky-Sil-Pl-Qtz
- 102. Ms-Crd-Bt-Ky-Sil-Pl-Qtz
- 103. Ms-Crd-Bt-Ky-Sil-Pl-Qtz